Modification and Stabilization of MXene with Quaternary Ammonium-Containing Hyperbranched Polyethylene Ionomers for Electrochemical Energy Storage

Bahareh Raisi

A Thesis
in the Department of
Chemical and Materials Engineering

Presented in Partial Fulfillment of the Requirements
For the Degree of
Doctor of Philosophy (Chemical Engineering)

at Concordia University
Montréal, Québec, Canada

October 2023

CONCORDIA UNIVERSITY
SCHOOL OF GRADUATE STUDIES

This is to certify that the thesis prepared,

By: Bahareh Raisi

Entitled: Modification and Stabilization of MXene with Quaternary Ammonium - Containing Hyperbranched Polyethylene Ionomers for Electrochemical Energy Storage

and submitted in partial fulfillment of the requirements for the degree of

DOCTOR OF PHILOSOPHY (Chemical Engineering)

complies with the regulations of the University and meets the accepted standards with respect to originality and quality.

Signed by the final examining committee:

______________________________________ Chair
Dr. Pantcho Stoyanov

______________________________________ External Examiner
Dr. Yuning Li

______________________________________ Examiner
Dr. Sana Jahanshahi Anbuhi

______________________________________ Examiner
Dr. Jung Oh

______________________________________ Examiner
Dr. Xianming Zhang

______________________________________ Thesis Supervisor
Dr. Zhibin Ye

Approved by ______________________________________
Dr. Alex De Visscher, Chair

March 5, 2024 ______________________________________
Dr. Mourad Debbabi, Dean

Gina Cody School of Engineering and Computer Science

Abstract

Modification and Stabilization of MXene with Quaternary Ammonium-Containing Hyperbranched Polyethylene Ionomers for Electrochemical Energy Storage

Bahareh Raisi, Ph.D.

Concordia University, 2023

Nowadays, 2D MXene materials have attracted significant attention due to their unique structural, physical, and chemical properties. As a rising star within the 2D material family, MXenes exhibit a unique combination of multi-functional groups and possess a high surface area. Numerous investigations in recent years have shed light on the creation of MXene-polymer composites tailored for applications in the realm of energy storage. The particular significance is rechargeable batteries and supercapacitors, as they bear substantial promise for making substantial strides in the pursuit of sustainable energy solutions. However, the production of thoroughly exfoliated /delaminated 2D MXene nano-sheets is still a major challenge, limiting their potential for practical applications. Thus far, MXene flakes display colloidal stability only in a few polar solvents. Conversely, they are unstable in nonpolar or low polarity solvents, while critically important to significantly expand the spectrum of applications for MXenes. Furthermore, MXenes tend to get oxidized in the presence of oxygen and water during storage, handling, processing, delamination, and applications under ambient conditions.

In the present study, a self-assembly method to prepare ionomer-modified MXenes has been developed for the first time. Hyperbranched polyethylene ionomers containing quaternary ammonium ions are designed to prepare stable and highly concentrated modified $Ti_3C_2T_x$ MXene dispersions in various nonpolar and low-polarity organic solvents. As a result, the interlayer spacing of $Ti_3C_2T_x$ MXene is expanded to more than 5 nm (9.33 nm based on TEM results) with at least a 400% increase compared to the original spacing of 1 nm and can be delaminated to a few-layer or single-layer nano-flakes. The modification also markedly improves the oxidation stability of MXene sheets due to the presence of the tightly surface-bound hydrophobic hyperbranched polyethylene protecting layer.

Herein, an ionomer self-assembly strategy has been demonstrated to achieve high magnesium ion storage capability with pillar-structured $Ti_3C_2T_x$ MXene. With the expansion of interlayer spacing of $Ti_3C_2T_x$ MXene upon the ionomer intercalation and the affinity of the hyperbranched polyethylene-skeleton of the ionomers to THF-based electrolyte, the delaminated ionomer-modified MXene shows significantly improved electrochemical performance as a cathode material for Mg batteries. Subsequently, a symmetrical two-electrode supercapacitor exhibits a high capacitance in an ionic liquid electrolyte.

This thesis offers insights into the engineering of MXene electrode materials for applications in electrochemical energy storage.

***Keywords*:** *MXene, ionomer, hyperbranched polyethylene, modification, dispersions, antioxidation, rechargeable magnesium-ion batteries, supercapacitor.*

Acknowledgements

I would like to express my sincere acknowledgement and great gratitude to my supervisor, Prof. Zhibin Ye, who offered me such a great opportunity to continue my research at Concordia University and provided me with excellent support in experimental design and manuscript writing. He always encouraged me when I met challenges during my research and helped me solve the problems throughout my entire Ph.D. study. His continuous encouragement and invaluable instructions also support me during my career.

I would like to thank the Chemical and Materials Engineering Department lab technical supervisor, Ms. Harriet Laryea and chemical laboratory technician, Ms. Kerri Warbanski, for their support. They offered me tremendous help in training, installation, and maintenance of research equipment/setups in our labs. My research work could not have been smoothly finished without their kind help.

I would like to extend my gratitude to my colleagues, especially Xudong Liu, Lingqi Huang, Jalal Rahmatinejad, Ximeng Zhang, Xinling Wang and Liuqing Yang, for their assistance and encouragement during my research.

Finally, I would like to express my gratitude to my thesis committee members, Dr. Yuning Li, Dr. Sana Jahanshahi Anbuhi, Dr. Jung Oh, and Dr. Xianming Zhang, for their time, valuable suggestions, and constructive comments.

Last but certainly not least, my most heartfelt thanks go to my husband, Behzad, and my son, Arian, for supporting me with their patience and unconditional love and believing in me every single step of my journey. I am fortunate to be part of this great family. This accomplishment would not have been possible without their ever-lasting support and invaluable care.

Table of Contents

List of Figures

List of Tables

List of Abbreviations

2D	Two-Dimensional
$AETMA^+BF_4^-$	2-(acryloxy)ethyl]trimethylammonium tetrafluoroborate
AFM	Atomic Force Microscope
CNCs	Cellulose nanocrystals
CNFs	Cellulose nanofibers
CNTs	Carbon nanotubes
COFs	Covalent organic frameworks
CTAB	Cetyltrimethylammonium bromide
CV	Cyclic voltammetric
DCM	Dichloromethane
DFT	Density functional theory
DI	Deionized
DLS	Dynamic light scattering
DMF	N, N dimethylformamide
DMSO	Dimethyl sulfoxide
DOL	Dioxolane
ε	Extinction coefficient
EAC	Ethyl acetate
EDLC	Electric double-layer capacitance
EMI	Electro Magnetic Interface
$EMIMBF_4$	1-Ethyl-3-methylimidazolium tetrafluoroborate

EOC	Ethylene-olefin copolymer
FTIR	Fourier transform infrared
GCD	Galvanostatic charge-discharge
HBPE	Hyperbranched polyethylene
HF	Hydrofluoric acid
HCl	Hydrochloric acid
^{1}H NMR	^{1}H nuclear magnetic resonance
HPEIs	Hyperbranched polyethylene ionomers
HRTEM	High-resolution transmission electron microscopy
I	Ionomer
ILs	Ionic liquids
LIB	Lithium-Ion battery
LiF	Lithium Flouride
LiTFSI	Lithium bis(trifluoromethanesulfonyl)imide
LTM	Late transition metal
$MgCl_2$	Magnesium chloride
MIB	Magnesium-Ion battery
MILD	Minimally Intensive Layer Delamination
NaCl	Sodium chloride
NaOH	Sodium hydroxide
Na_2SO_4	Sodium sulfate
NIR	Near Infra Red

NLIB	Non-Lithium Ion Batteries
NMP	1-methyl-2-pyrrolidinone
NR	Natural rubber
PAM	Polyacrylamide
PANI	Polyaniline
PC	Propylene carbonate
PEI	Polyethylenimine
PO	Polyethyleoxide
PES	Polyethersulfone
PEDOT/PSS	Poly(3,4-ethylene dioxythiophene)/poly(styrene sulfonate)
PEG	Polyethylene glycol
Pd	Palladium
PDI	Polydispersity Index
PIL	Polyionic liquid
POM	Polyoxometalate
PPy	Polypyrrole
PSf	Polysulfone
PVA	Polyvinyl alcohol
PVDF	Polyvinylidene Fluoride
PVP	Polyvinylpyrrolidone
RMB	Rechargeable Magnesium Batteries
SAED	Selected area electron diffraction

SEM	Scanning electron microscopy
SiO_2	Silicon dioxide
TAEA	Tris(2-aminoethyl) amine
TBAOH	Tetrabutylammonium hydroxide
TEM	Transmission electron microscopy
TGA	Thermogravimetric analysis
THF	Tetrahydrofuran
TiO_2	Titanium dioxide
UHMWPE	Ultrahigh molecular weight polyethylene
UV-Vis	Ultraviolet-visible
XPS	X-ray photoelectron spectroscopy
XRD	X-ray Diffraction

Chapter 1. Introduction

1.1 Problem Statement

For more than one decade, two-dimensional (2D) layered nanomaterials have attracted enormous research interest due to their unique properties, including excellent thermal and electrical conductivity, charge carrier mobility, high mechanical flexibility, and desired optical and UV absorptions.[1] 2D materials are also considered as appropriate building blocks for a variety of nanostructures, membranes, and composites.[2] Amongst, numerous research studies on 2D nanomaterials have been focused on graphene, hexagonal boron nitride, MoS_2, phosphorene, and their derivatives.[3, 4] In 2011, a novel family of 2D transition metals hybridized with carbides, nitrides, and carbonitrides (MXenes) was introduced to the nanomaterials world.[5] MXenes are defined with the general formula $M_{n+1}X_nT_x$ where M covers groups 3 to 6 transition metals (such as Sc, Ti, Zr, Hf, V, Nb, Ta, Cr, Mo, *etc.*), X is carbon and/or nitrogen, and T corresponds to the surface termination moiety (e.g., OH, O or F).[6] MXenes are fabricated through a selective etching process by the elimination of ″A″ interlayer element (i.e., the element in groups 13 and 14 of the periodic table such as Al) from the MAX phase (ternary transition metal carbides and/or nitrides with a general formula $M_{n+1}AX_n$ (M = an early transition metal; X = C/N; and n = 1, 2, or 3).[5, 7] Thanks to their excellent electrical conductivity as well as high volumetric capacity, hydrophilicity and exceptional mechanical properties, MXenes have shown promising performance in a variety of applications such as water purification, catalysis, electromagnetic interference shielding,[8] optoelectronics, transparent conductive electrodes,[8-10] and, in particular, energy storage devices (*e.g.,* batteries and supercapacitors).[11]

The spectrum of MXene compositions containing all four components (M, X, T, n) of the MXene formula has been extended since 2019, expanding MXenes to new areas of research (Figure 1.1a).[12] Multiple strategies have been applied to introduce different small molecular species into the nano-scale interlayer spaces of MXene. Various procedures involve delamination/exfoliation techniques, ultra-sonication of MXene in organic solvents, utilization of liquid-phase surfactants, ionic liquids, and molten salts, as well as electrochemical treatment in different liquid media and shear techniques are used. These approaches have been employed to generate single-layer nanosheets, resulting in the emergence of novel properties and applications.[13] Alternatively, the incorporation of polymers into the MXene interlayers has been considered an innovative method for the additional improvement of their mechanical, physical, and electrochemical properties.[14] Since late 2018, the number of MXene publications has experienced an exponential increase (Figure 1.1b).[12] Seventy percent of published articles continue to be devoted to $Ti_3C_2T_x$ MXene (Figure 1.1c) due to the most effectively developed synthesis and processing protocol and the precursor's availability, among other factors. Titanium, carbon, and aluminum are readily available and cost-effective elements, offering the potential for practical products with no raw material restrictions. [12]

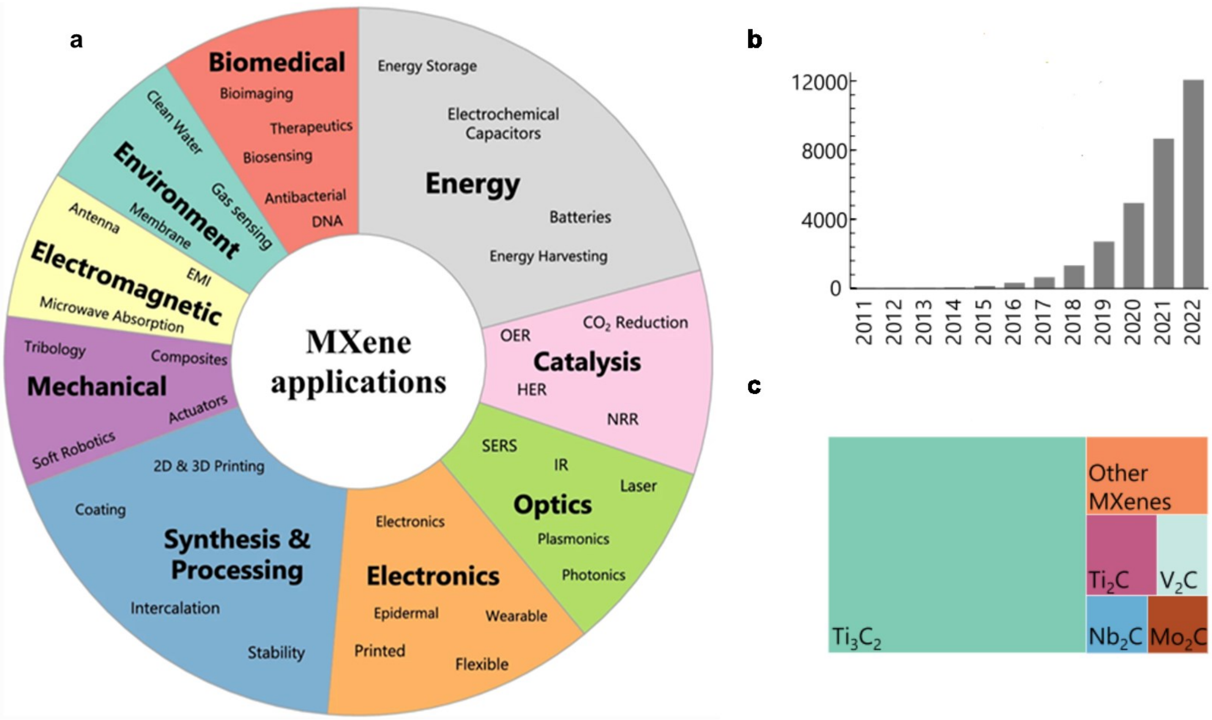

Figure 1.1 Examined applications and characteristics of MXenes thus far, (a) a representation of the distribution of publications across diverse MXene applications, relative to the overall volume of publications concerning MXenes; (b) the annual number of MXene publications; (c) a comparison of the total number of publications on various MXene. [12]

Nonetheless, MXenes, despite their prominent combination of properties, face several limitations that affect their practical use. These restrictions consist of weakness to environmental factors, such as humidity and oxidative exposure, resulting in diminished stability.[15] MXene oxidation in aqueous colloidal suspensions when stored in water at ambient conditions still remains a challenge.[16, 17] Additionally, MXenes often exhibit a propensity to aggregate in solutions, imposing impediments to their effective application. Furthermore, the processing of pure MXenes is often intricate due to their extensive surface area and proneness to aggregation. On the other hand, the dispersibility of MXene in solvents is only limited to a few cases, which were dedicated to the dispersion of MXene in aqueous solutions and a few polar organic solvents such as N,N dimethylformamide (DMF), N-methyl-2-pyrrolidone (NMP), dimethyl sulfoxide (DMSO) and propylene carbonate (PC).[18] Subsequently, MXene has presented its remarkable potential for producing highly conductive films and bulk materials; nevertheless, it still remains a significant challenge to fabricate extremely conductive, low-density, affordable nanocomposites with outstanding capacity performance in energy storage devices at minimal contents of MXenes.[3, 19] Hence, the development of new and stable energy storage nanocomposites possessing outstanding structural, physical, and chemical properties, high electronic and ionic conductivities, and suitable charge storage capacity is of great interest.

1.2 Research Objectives

In an effort to expand the scope of MXene applications and address the above-mentioned issues, surface modification of MXene via covalent and noncovalent approaches can be employed to affect their surface properties and endow them with the high dispersity in organic solvents (particularly nonpolar and low-polarity solvents) and hydrophobic polymer matrixes. Without suitable surface modification, the dispersion of MXene, with hydrophilic properties, in nonpolar solvents or hydrophobic polymers, such as polyolefins, will not be afforded. The crucial factor of intercalating polymer within MXenes nanosheets is the use of cationic-charged or hydrogen bond-containing polymers to induce strong interactions with negatively charged MXene surfaces possessing electronegative functional groups (e.g., -OH, -O, -F). Besides, solubility should be considered as another key factor along with the favourable interactions between polymer and MXene to achieve well-admixed MXene/polymer composites. To achieve the mentioned objectives, this study discloses a new ionomer modification methodology to construct fully delaminated MXene by intercalating quaternary-ammonium-containing hyperbranched polyethylene ionomers within the nanosheets. This new ionomer-modified MXene overcomes its inherent limitations and expands its applications in composites and energy storage. The specific research tasks and outcomes are listed as follows:

- Introducing polar functional groups into nonpolar polyethylene can improve their essential characteristics, such as toughness, adhesion, barrier, and surface properties.[20] As a result, polyolefins can find their way to entirely new areas of applications in which their intrinsic properties are combined with the new ones imposed by the incorporation of polar functionalized monomers. Direct copolymerization of olefins with polar vinyl monomers has been successfully performed by late transition metal (LTM) catalysts. On the other hand, ionomers are nanostructured materials similar to nanocomposites,[21] consisting of ionic aggregates dispersed within nonpolar polymer matrix property.[22] It is worth mentioning that a relatively small concentration of ionic functional groups (typically less than 10 mol%) covalently bonded to the polymer backbone induces substantial changes in the polymer's mechanical, physical, optical, and dielectric properties. The Pd─diimine catalyst, $[\mathrm{ArN = C(Me) - (Me)C = NAr]Pd(CH_3)(N \equiv C(Me)]^+SbF_6^-(Ar = 2{,}6 - (iPr)_2C_6H_3)}$, the acrylate-type ionic liquid comonomer, [2-(acryloxy)ethyl]trimethylammonium tetrafluoroborate ($\mathrm{AETMA^+BF_4^-}$) and quaternary ammonium-containing hyperbranched polyethylene ionomers with different ionic contents were synthesized by following the procedure reported in our group.
- The multi-layered MXene was synthesized from the MAX (Ti_3AlC_2) powder by using the minimally intensive layer delamination (MILD) method. A new strategy for intercalating macromolecules between MXene nanosheets has been developed. The positively charged quaternary ammonium ions tethered onto the nonpolar hyperbranched polyethylene skeleton bound with the negatively charged surfaces of MXene through the ionic interactions, rendering the modified functionalized MXene nanosheets and yielding the highly stable, hydrophobic and ordered stacking structure. The resulting modified MXenes were readily stably dispersible in a broad range of nonpolar or low-polarity organic solvents, including tetrahydrofuran (THF), chloroform, xylene, and toluene, at high concentrations (as high as 30 mg mL^{-1} in THF).
- The hydrophobic polyethylene umbrella protected MXene from non-desired oxidation and prolonged its shelf life. The ionomer-modified MXenes are stable in air-saturated water even for weeks with no/minimum oxidation.
- One of the most critical characteristics of 2D materials, in particular, MXene, is that the interlayer spacing can be directly affected through the intercalation of guest species during

the fabrication procedure; the 3D structure of ionomers with hyperbranched skeleton increased d-space layers dramatically. The interlayer spacing of $Ti_3C_2T_x$ MXene expanded to more than 5 nm with at least a 400% increase compared with the original spacing of 1 nm and delaminated to a few or single nano-flakes.

- Irreversible aggregation and restacking challenges with superior electrical properties are addressed by hydrophobe polymer in replacement of the incorporation of conductive hydrophilic polymers reported before. On the other hand, the use of MXenes in organic electrolytes and non-polar solvents was revealed to improve their performance in Mg batteries and supercapacitors. In Mg battery: Stable reversible capacities are achieved at each current, with the values of 213, 200, 195, 194, 186, 169, 140 and 110 mAh g^{-1} at 20, 40, 50, 80, 100, 200, 500 and 1000 mA g^{-1}, respectively. Moreover, a remarkable reversible higher capacity of ~ 250 mA h g^{-1} is maintained when the current density is switched back to 20 mA g^{-1}. It showed promising cycling stability with a capacity retention of 86% after 400 cycles and 71% after 1000 cycles at 200 mA g^{-1}. A symmetrical two-electrode supercapacitor made from modified Mxene suspension in THF exhibits a capacitance of 220 F g^{-1} at a scan rate of 2 mV s^{-1}.
- It is worth mentioning that ionomers have not been utilized for the intercalation, functionalization, and surface modification of MXene until now. To the best of our knowledge, it is the first work on polymer surfactants to modify and stabilize MXene. This work expands the opportunities for processing techniques to produce new nanocomposites and endows MXene nano-material with applications in electrochemical energy storage and nanocomposites.

1.3 Thesis Outline

The thesis is comprised of the following chapters.

Chapter 1 is a concise introduction to this thesis's problem statement and research objectives.

Chapter 2 is a comprehensive literature review. It includes principles and applications of MXene, their properties, synthesis and fabrication processes, intercalation/and delamination of MXene, MXene-polymer nanocomposites and their application in energy storages, especially in magnesium battery and supercapacitors, and major challenges. A brief introduction to Ionomers is included.

Chapter 3 reports the methodology to construct a multi-/few-layer of MXene by the intercalation of hyperbranched polyethylene ionomers containing quaternary ammonium ions. Quaternary ammonium-containing hyperbranched polyethylene ionomers enhance the MXene dispersion stability in various organic solvents as well as protect MXene from oxidation. Reinforcement properties of the ionomer-modified MXenes as nanofillers in ethylene-olefin copolymer matric are presented.

Chapter 4 demonstrates the use of ionomer-modified MXenes as the cathode materials for magnesium-ion batteries (MgIBs) and their distinct electrochemical performance properties for the storage of magnesium ions.

Chapter 5 reports the application of ionomer-modified MXenes as electrode materials for supercapacitors and their electrochemical performance properties.

Chapter 6 lists the main contributions and significance of this thesis research and some recommendations for further research.

Chapter 2 Literature Review

2.1 Introduction

This chapter is dedicated to a thorough review of MXene synthesis methodologies, modification, intercalation and delamination procedures, and the practical applications of polymer/MXene nanocomposites, with a specific focus on their critically significant role in energy storage systems. Drawing upon a meticulous analysis of state-of-the-art research, the review elucidates the strengths and limitations inherent in various MXene synthesis approaches. Additionally, it offers a nuanced exploration of the intricate intercalation and delamination techniques employed in the creation of polymer/MXene nanocomposites. The investigation delves into these nanocomposites' immense potential to significantly enhance the performance of electrochemical energy storage systems. Furthermore, the prominent challenges that characterize the field, including dispersion, stability, and the compatibility of MXenes with polymers, will be addressed.

2.2 Synthesis of MXene

The synthesis of MXenes typically involves three steps. First, layered MXene precursors are synthesized, which determines the crystal structure. Second, the "A" atomic layers are etched away, exfoliating weakly bonded MXene multilayers.[14] During the etching process, the relatively weaker M-A bonds are separated, resulting in the undercoordinated M metallic surfaces quickly re-saturated through reactions with Tx species in the etchant. Finally, the exfoliated MXene multilayers are delaminated to render single to few-layer MXene sheets. [23, 24, 25, 26, 27] Over the past decade, there has been a significant increase in the complexity of both the chemical composition and structural arrangements of synthesized MXenes. This expansion has led to the discovery of MXenes containing two or more transition metals.[25] Additionally, there has been considerable progress in achieving variety, uniformity, and control over the composition of surface termination groups (T_x) on MXenes. These surface groups play a crucial role in determining the behaviour and properties of MXenes. Previously limited to groups such as -O, -OH, and -F, the range of surface termination options now includes other halogens such as -Cl, -Br, -I, imido (-NH) groups, and termination-free surfaces.[26-29] The steady development of MXenes' bulk and surface chemistry is shown in Figure 2.1.

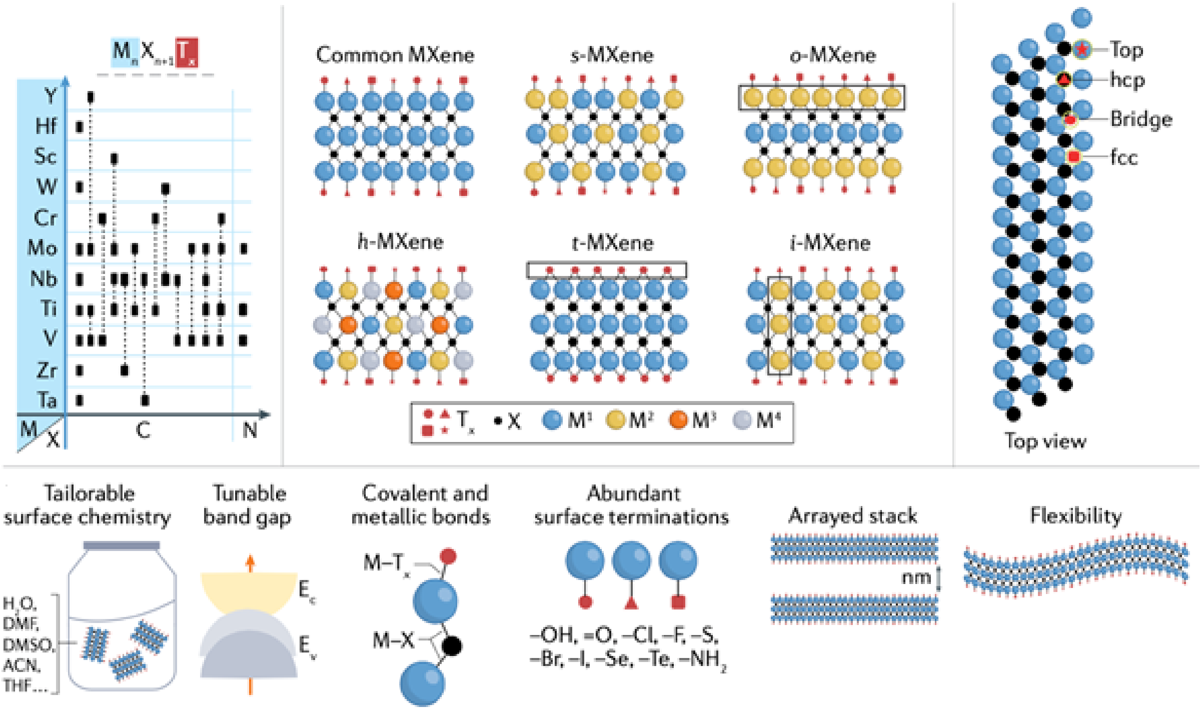

Figure 2.1 The steady development of MXenes' bulk and surface chemistry.[18]

2.2.1 MXene Precursors

Most MXenes are synthesized using top-down methods, developing their structure from bulk carbide and nitride precursors. Precursor chemistry, particularly the strength of M–X and M–A bonds, impacts exfoliation into MXenes.[27,30] Precursor composition (M, A, X elements) and bond chemistry affect MXene structure and properties. Nitrides have higher exfoliation energy than carbides due to weaker M–N bonds. Smaller M and A atoms with higher valence have stronger M–A bonds. Non-MAX phases can be compositionally tuned to produce challenging MXenes.[31]

Synthesizing precursor phases usually involves pressureless reactive sintering under an inert atmosphere. This results in porous sintered billets that can be processed into etchable powders. Elemental powder mixtures (e.g., Ti, Al, C) or carbide/nitride mixtures (e.g., Ti, TiC, Al) are commonly used for MAX phase synthesis. Metal hydrides, like titanium hydride, and molten salts are also employed. Different powder mixtures follow diverse formation pathways. Reactive sintering of elemental mixtures initially forms intermetallic M-A compounds, followed by the nucleation of binary carbide layers to create non-layered M-A-X phases.[27] MAX phase formation from carbide or nitride precursors relies on carbon- or nitrogen-vacancy-assisted diffusion.[32]

The choice of precursor powders and formation pathways influence MAX structure, including atomic-scale defects and variations in grain sizes and shapes.[31] For Ti_3AlC_2-derived $Ti_3C_2T_x$ MXene, different synthesis temperatures and carbon sources result in varying flake sizes and electrical conductivities. The carbon source affects the nucleation of Ti-Al intermetallics and elemental Ti layer growth, impacting grain sizes and electrical conductivity.[33] Sintering temperature also affects $Ti_3C_2T_x$ MXene properties, with lower temperatures leading to higher electrical conductivities (8000-15000 S/cm).[27,34]

2.2.2 MXene Synthesis Mechanism

MXene synthesis involves the etching and exfoliating of MAX phase precursors to obtain multilayer MXenes. The initial report used HF as an etchant to remove Al layers from Ti_3AlC_2, and subsequent protocols have been developed by using various etching methods, such as HF-based, electrochemical, alkaline, molten salt, and halogen etching.[32] The exfoliation process can further delaminate weakly bound multilayer MXenes into few- to single-layer 2D sheets. Understanding the details of MXene etching and delamination is crucial in determining the selectivity of different methods in producing specific MXenes and controlling their properties and surface chemistry. This section aims to highlight the trends in existing etching, exfoliation and intercalation-delamination methods.[27,35, 36]

a. Etching Methods

Etching methods involve selectively removing the A atomic layer from a precursor material. The etching process involves oxidizing the A atom, converting it to an oxidized species like Al^{3+}, as presented in equations (1) and (2).[27] The ability to remove the A element depends on the Gibbs free energy of the etching reaction, which is influenced by factors like the strength of the M-A bond and the formation of by-products. Exfoliation also relies on the oxidation of the A element and its conversion to soluble by-products that can be removed from the precursor. The etching solution should also eliminate the protective oxide layer on the MAX-phase.[27,30-32] Protons (H^+) act as the oxidizing agent, while F^- functions as the ligand solubilizing the by-product (Al^{3+}) in the case of etching Al-based MAX phases using HF-containing solutions. Other oxidizer-ligand pairs can be used for etching, such as OH^- in alkali-based routes or electrochemically coupled with OH^- and/or Cl^-. Similar principles apply to non-Al-based MAX phases, where additional oxidizers and ligands may be required.[27,37]

$Ti_3AlC_2(s) + 3H^+ (aq) \rightarrow Ti_3C_2(s) + Al\ (aq) + 3/2H_2\ (g)$ **(1)**

$Al_3^+(aq) + 3F^-(aq) \rightarrow AlF_3\ (aq)$ and $Al_3^+(aq) + 6F^-(aq) \rightarrow AlF_6^{3-}(aq)$ **(2)**

Different etching routes, such as halogen-based or molten salt routes, have gained popularity for producing MXenes with different surface termination functionalities beyond those achieved by HF-based etching. These routes offer the opportunity to explore MXene structures with unique properties that can be scalable and environmentally friendly. The surface chemistry of MXenes plays a crucial role in their properties, and different etching conditions can produce different surface terminations. Tuning the surface terminations can be achieved through covalent modification using reactions with chemically reactive groups like -OH, -F, -Cl, and –Br.[33, 35] Molecular dynamics simulations of Ti_3AlC_2 etching with HF have revealed that the initial adsorption of H and F weakens the Ti-Al bond, leading to the removal of Al as soluble AlF_3 and creating interlayer spaces for further HF and H_2O intercalation.[38] Experimental studies using cross-sections of Ti_3AlC_2 have shown that etching propagates stepwise, starting from the surface layers and progressing toward the center. Defects, particle size, and MXene layer thickness also influence the etching process.[39] Optimizing etching conditions for different MXene chemistries, considering factors like synthesis method, particle size, and protective oxide scale thickness, is crucial for improving our understanding of etching mechanisms and enhancing MXene quality, flake size, and properties. Additionally, studying etching kinetics can provide further insights into the etching mechanism for different MXenes. In general, hydrofluoric acid (HF)-based synthesis methods, mild condition, fluorine-free MXene synthesis, MXene etching in organic solvents, and MXene synthesis with uniform surface terminations are the main approaches here, which are presented in Figure 2.3.[37, 40]

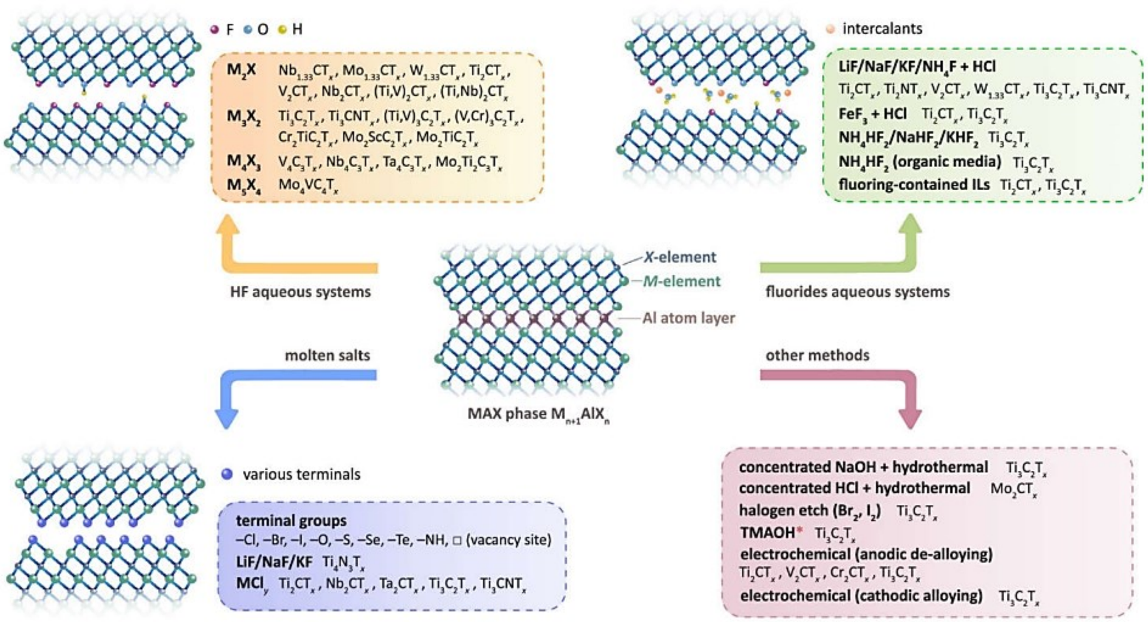

Figure 2.2 Synthesis pathways for MXene from $M_{n+1}AlX_n$ MAX phase. [38]

b. Hydrothermal and Solvothermal Synthesis

Employing high-temperature and high-pressure reactions, hydrothermal and solvothermal synthesis processes offer promising avenues for MXene synthesis. In these MAX phases, precursors are integrated with a suitable aqueous solution (in the case of hydrothermal) or non-aqueous solvents (for solvothermal processes).[41, 42] The resultant mixture is then introduced into an autoclave, where it is subjected to elevated temperatures and increased pressure to initiate a chemical reaction. These high-temperature, high-pressure conditions can prove to be more efficient in the selective removal of the 'A' layer from the MAX phases and the subsequent formation of MXenes. The choice of solvent is a pivotal aspect of these methods and requires consideration based on the desired MXene product and the specific MAX phase precursor.[41, 43]

The precision in controlling factors such as temperature, pressure, reaction time, and precursor compositions is essential to prevent the introduction of defects or the inadvertent destruction of the MXene structures.

c. Electrochemical Synthesis

In this process, a MAX phase, typically serving as the anode, is immersed in an electrochemical cell containing a suitable electrolyte solution. This setup plays a pivotal role in facilitating the controlled etching process that leads to the formation of MXene materials. [44-46]

d. Mechanical Exfoliation

Mechanical exfoliation stands as a prominent physical approach in the synthesis of MXene materials, where the aim is to effectively separate individual layers of MAX phases to yield the desired MXenes. This technique involves several methods, including manual exfoliation, sonication, and mechanical grinding.[47] While it may be a straightforward process, especially for initial laboratory-scale experiments, it's not well-suited for large-scale production due to its low efficiency and aggregation of MXene flakes.[48] The process's limitation becomes apparent when there's a need for substantial quantities of high-quality MXene materials, typically required for various applications.[49]

2.2.3 Surface Functionalization

Surface functionalization stands as a crucial strategy for the MXene adjustments surface properties, thereby strengthening their stability and rendering them versatile for applications in energy storage, energy conversion, sensors, and more. This multifaceted process introduces remarkable versatility in tailoring MXenes by enhancing reactivity, promoting compatibility with various media, and refining their performance attributes.

a. Polymerization and Small Molecule Addition

MXenes possess a unique advantage in terms of surface functionalization due to the presence of specific functional groups such as -OH and -F. These groups allow for the grafting of polymers in a range of modes, facilitating various applications.[50] Firstly, MXene-polymer composites are formed through ex-situ methods. These composites are known for their precise control over structure and tunable compositions. For instance, creating core-shell Ti_3C_2 MXene/polystyrene nanocomposites through hydrogen bonding leads to well-defined structures.[19] Additionally, Ti_3C_2 MXene can create a composite with poly(vinyl alcohol) through hydrogen bonding, showcasing hydrogel-based interactions. In-situ polymerization represents another avenue for covalent interactions between MXenes and specific polymers, such as pyrrole, facilitating a strong interplay between the materials. However, in the following, more discussion regarding the modification of the MXene surface with diverse polymers will be investigated. Moreover, the introduction of small molecules such as CTAB, DTAB, hexamethylene glycol mono dodecyl ether, diazonium salt, bismuth ferrite, and sodium aluminum hydride further enhances MXene stability.[51, 52]

b. Silylation and Covalent Bond Formation

Silylation reactions involving the use of amino silane coupling agents, like aminoethyl and aminopropyl trimethoxysilane, have gained prominence as effective surface functionalization strategies.[53-55] These reactions have the potential to transform the MXene surface into a functional platform, offering tailored functionalities for diverse applications.

c. Heteroatom and Metal Doping

It is essential to acknowledge that the pristine MXene surface may possess defects, which, albeit unintended, offer reactivity. By capitalizing on these surface defects, heteroatom and metal doping offer a significant pathway to enhance MXene's physical and chemical properties.[56] For example, nitrogen doping has been successfully introduced to MXene, resulting in enhanced electrochemical performance.[57] Particularly, nitrogen doping of carbide MXenes has garnered extensive attention for its role in shifting these materials from a semiconducting to a metallic state. Mo_2CT_x carbide MXenes, when subjected to substantial nitrogen doping, can be entirely transformed into 2D nitrides through ammoniation at 600 °C, representing an unconventional pathway to synthesize nitride-based MXenes.[58] One approach to nitrogen doping, as proposed by Yang *et al*., involves solvothermal treatment. This method utilizes a urea-saturated alcohol solution or monoethanolamine as a nitrogen source, facilitating the delamination of Ti_3C_2 (d-Ti_3C_2).[59]

An alternative nitrogen doping method involves heat treatment in an ammonia atmosphere, leading to the complete conversion of carbide MXenes into nitrides. Many works highlight this transformation for Mo_2C and V_2C carbide MXene precursors. Upon ammoniation at 600 °C, Mo_2N retains its layered MXene structure, while V_2N exhibits a layered structure comprising trigonal V_2N and cubic V_2N. This outcome underscores the selectivity of MXenes precursors in this unconventional synthesis.[57-59] In summary, the vast array of surface functionalization strategies empowers researchers to fine-tune the characteristics of MXenes for a myriad of applications, from sensors to energy storage systems, forging the way for enhanced performance and innovative applications.[60, 61]

2.3 Post-Synthesis Treatment

In the context of MXene research, post-synthesis treatments emerge as a crucial and multifaceted domain. This new section embarks on an exploration of the profound necessity underpinning post-synthesis treatments in MXenes. These treatments play a crucial role in the process of refining the material's properties, from its crystalline structure and electrical conductance to structural homogeneity. Additionally, they play an integral role in eliminating residual impurities or no useful agents, upholding the material's purity and functional competence. Notably, a pivotal focus of post-synthesis treatments is the tailored modification of MXenes' surface chemistry, rendering them highly adaptable for specific applications. This section delves into the intricate landscape of post-synthesis interventions, elucidating how they optimize MXenes, ultimately enhancing their versatility and efficacy across diverse domains. Herein, the most employed approaches are original/external termination changing and materials compounding.

2.3.1 Original Termination Changing

Modification of MXenes through termination regulation offers extensive opportunities for post-processing enhancement. Surface terminations, including -F, -O, and -OH, introduced during synthesis, play a pivotal role in shaping MXenes' properties.[50] The addition of external functional groups further broadens the versatility of MXenes, conferring unique hydrophobicity, positive surface potential, and heightened environmental sensitivity.[62] In the absence of an external functional group introduction, post-processing modifications aim to manipulate the composition of the intrinsic surface functional groups (primarily -F, -O, and -OH) acquired during synthesis. One prominent method for achieving this alteration is through heat treatment, a widely employed approach that can steer surface termination in various directions.[63, 64] It is noteworthy that the de-functionalization of high-electronegativity -F groups during heat treatment influences the band structure of MXenes, subsequently enhancing their electrical conductivity.[65]

Notably, a heat treatment in a reductive atmosphere and the inclusion of alkaline additives can influence the proportion of oxygen-containing terminations (-O and -OH) on MXenes' surfaces. Heat-treated $Ti_3C_2T_x$, which primarily featured -F and -O terminations, undergoes transformation into termination-free MXenes through reactions with hydrogen at elevated temperatures. This terminal-free form is expected to exhibit higher metallicity but requires passivation by other terminations.[64] In contrast, the addition of alkaline additives during heat treatment can enhance the -O termination content, leading to the transformation of $Ti_3C_2(OH)_x$ into oxygen-functionalized $Ti_3C_2O_x$. Although this work doesn't focus on the influence of terminal groups on MXenes' properties, other theoretical studies suggest that -F termination substitution enhances conductivity and the presence of numerous -OH terminations intensifies nanosheet hydrophilicity.[66] Throughout the heat treatment process, variations in surface functional group distribution on MXenes are primarily determined by temperature and atmosphere. Increasing treatment temperature results in the reduction of surface terminations in the order of -OH, -F, and -O, improving electrical conductivity and environmental stability. Therefore, this treatment is often used to enhance the conductivity of MXenes-based transparent conductive films. Nonetheless, the existence of a phase transition point in MXenes determines the upper limit of heat treatment.

Apart from heat treatment, several other post-processing methods aim to change MXenes' surface terminations. For example, plasma treatment in different atmospheres achieves reversible resistivity switching in $Ti_3C_2T_x$ films.[67] These methods provide options to precisely control the -O containing terminations of MXenes, allowing for reversible adjustments in their conductivity.

2.3.2 Materials Compounding

Compounding MXenes with other materials is a common post-processing method that significantly alters their properties. By incorporating materials like polyvinyl alcohol (PVA), natural rubber (NR), cellulose nanofibers (CNFs), poly(3,4-ethylenedioxythiophene)/poly(styrenesulfonate) (PEDOT/PSS), and polyaniline (PANI), the mechanical properties of MXene films are enhanced.[68] This mechanical improvement often comes at the expense of MXenes' conductivity. Moreover, MXenes' stability and hydrophilicity can be addressed through compounding. To protect against oxygen-induced degradation, a carbon nanoplating approach is used. Additionally, the hydrophilic nature of MXenes, due to the -OH termination introduced during synthesis, can be controlled by incorporating a cationic activator (e.g., cetyltrimethylammonium bromide (CTAB). The pH-sensitive interaction between CTAB and Ti_3C_2 allows for reversible transitions between hydrophilic and hydrophobic states.[69] When various materials are compounded with MXenes, the hybrid system leverages the strengths of each component but may experience property dilution due to the combination of different materials. Finding a balanced compromise between component properties is key.

2.4 Intercalation/Delamination of MXene

The delamination of MXenes into individual 2D sheets is a prerequisite for various applications. However, it is a challenging process due to the attractive forces that exist between MXene layers, Figure 2.3a.[27, 47, 70, 71] To address this challenge, delamination strategies have been explored.

The thicker $Ti_3C_2T_x$ MXene exhibits higher adhesion energy values compared to monolayer or thinner MXenes (Ti_2CT_x and Nb_2CT_x) due to its more decisive dipole moment and higher polarity, Figure 2.3b. These attributes pose obstacles to mechanical exfoliation, especially for manufacturing few-layer flakes. Instead, the typical approach involves intercalating various molecules and ions, followed by agitation or sonication, Figure 2.3c.[72] Intercalants expand the interlayer space and weaken interface interactions, facilitating successful delamination. Intercalation agents encompass solvents, organic molecules, and ions, each selected based on the specific MXene's surface chemistry. For -O, -OH, and -F terminated MXenes, polar solvents such as water, dimethylsulfoxide (DMSO), dimethylformamide (DMF), and N-methyl-2-pyrrolidone (NMP) are suitable choices. Various delamination agents have been employed successfully, including tetraalkylammonium hydroxide bases (e.g., TMAOH and TBAOH) and Li^+ ions, Figure 2.3d and e. However, delamination selectivity can be influenced by the MXene's etching method and surface terminations (see Figure 2.3f).[27, 72]

Intercalation and delamination processes lead to a significant increase in the c lattice parameter of multilayer MXenes. Water intercalation, particularly with Li^+ ions, also plays a crucial role in aqueous delamination. Interactions between intercalants and MXene surfaces persist even after delamination and washing, contributing to colloidal stability. These considerations introduce complexity to the development of new delamination approaches as they fine-tune intercalant-surface interactions, which are influenced by surface terminations and the MXene etching procedure. Osmotic swelling may offer the potential for delaminating MXenes beyond $Ti_3C_2T_x$ using inorganic intercalants. Furthermore, there is a need for more dedicated research into delaminating $Ti_3C_2T_x$, as current protocols involve challenging chemicals and/or extended sonication with limited yield.[27,73, 74] Addressing these challenges will expand the possibilities for MXene applications.

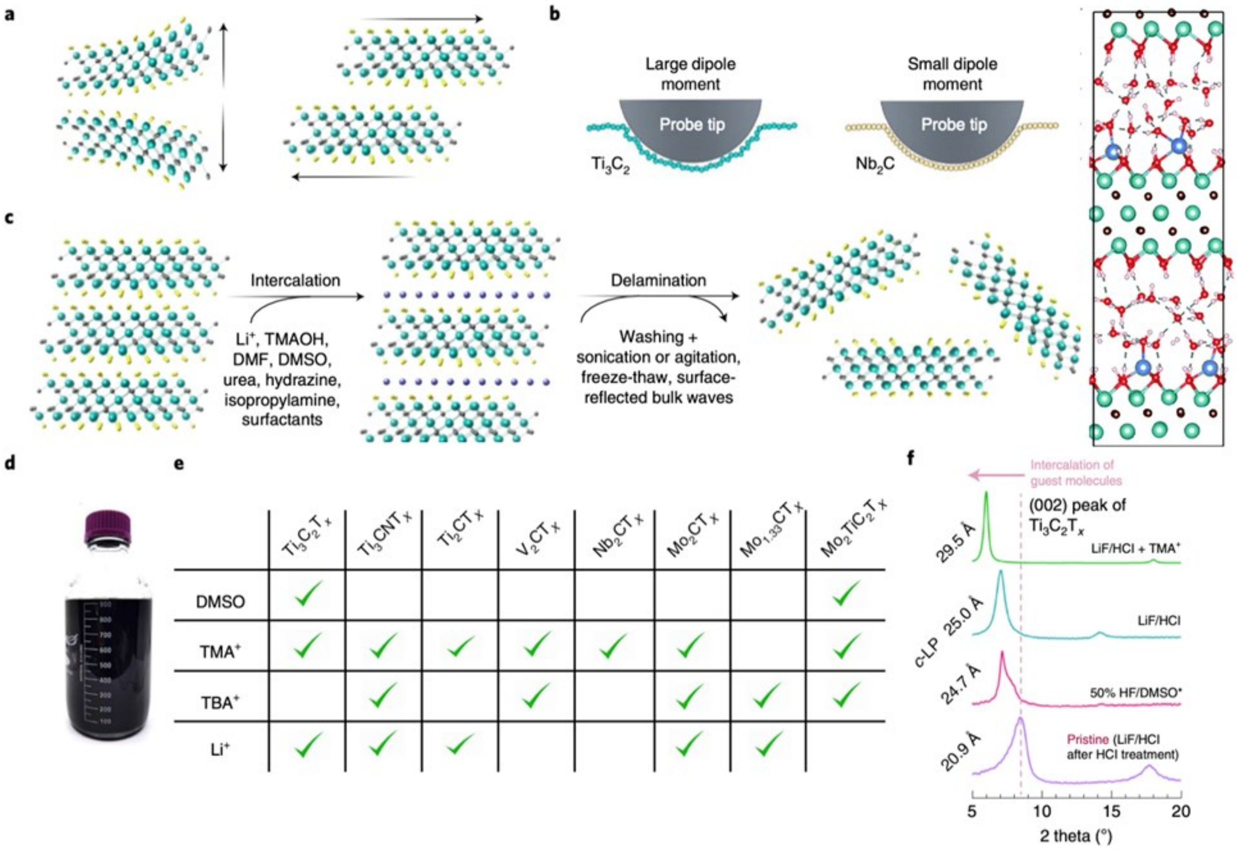

	$Ti_3C_2T_x$	Ti_3CNT_x	Ti_2CT_x	V_2CT_x	Nb_2CT_x	Mo_2CT_x	$Mo_{1.33}CT_x$	$Mo_2TiC_2T_x$
DMSO	✓							✓
TMA⁺	✓	✓	✓	✓	✓	✓		✓
TBA⁺		✓		✓		✓	✓	✓
Li⁺	✓	✓	✓			✓	✓	

Figure 2.3 Intercalation–Delamination mechanisms.[27]

On the other hand, polymers also can be utilized for MXene intercalation/delamination. Intercalation involves the insertion of polymer chains into the interlayer spaces of MXenes. This process significantly enhances the structural integrity and mechanical properties of MXenes while also providing opportunities for functionalization.[75] Polymers like polyethylene glycol (PEG), polyvinyl alcohol (PVA), and polyaniline (PANI) have been effectively intercalated into MXene layers. The insertion of polymer molecules between MXene sheets not only enhances the interaction between them but also prevents restacking, resulting in exfoliated and well-dispersed MXene-polymer composites.[76]

Moreover, polymers play a crucial role by promoting the separation of MXene layers. The polymer chains act as surfactants, reducing the interlayer adhesion forces, thus making it easier to split the MXene layers into a stable colloidal solution. Techniques such as sonication, agitation, and mechanical stirring in the presence of polymers facilitate the successful delamination of MXenes.

The integration of polymers with MXenes, a topic that is explored in the subsequent discussion, confers substantial benefits across diverse applications, encompassing energy storage systems, sensor technologies, and composite materials. The introduction of polymers into the MXene matrix results in augmented electrical conductivity, bolstered mechanical characteristics, and customizable surface chemistry. These enhancements culminate in improved performance and multifaceted utility, positioning MXene-polymer composites as a fertile terrain for advanced research and innovation.

2.4.1 Polymers/MXene Nanocomposites Applications

As previously delineated, MXene-polymer composites merge the advantageous characteristics of MXenes and polymers. This results in the augmented interlayer separation of MXene sheets, elevated mechanical robustness, and enhanced structural integrity. Consequently, MXene-polymer composites have the potential to manifest exceptional efficacy across diverse applications, with notable relevance in the domains of energy storage devices, EMI shielding, sensory functionalities, and photo-thermal conversion. In the ensuing section, we shall provide an overview of MXene-polymer composites applications.[71, 77]

The electrochemical performance of MXene-based electrode materials encounters a hindrance attributed to the undesired restacking of MXene sheets during the fabrication of freestanding films.[78] A noteworthy approach to surmount this restacking impediment involves the surface modification of MXene nanosheets with conducting polymers, enabling the construction of freestanding electrodes characterized by a highly accessible structure and specific surface area.[79] The utilization of conducting polymers in the development of MXene-polymer nanocomposite materials for electrochemical energy storage applications offers several notable advantages. These encompass cost-effectiveness, structural flexibility, non-toxicity, and the presence of pseudocapacitive properties. It is worth emphasizing that the emergence of conjugated polymers as electrochemically active materials with MXenes represents an intriguing concept. Conjugated polymers bestow a unique set of properties, including charge transport, variable band gap, water solubility, and the ability to be processed into diverse configurations.[80] Moreover, 2D MXene materials are characterized by high electrical conductivity coupled with reactive surface chemistry and hydrophilicity. These features render them an excellent foundation for synthesizing MXene/polymer hybrids. Such hybrids can be meticulously controlled in terms of their morphology, thickness, electrical conductivity, and mechanical properties.[78, 79]

In 2014, Ling *et al.* synthesized the first conductive and flexible freestanding $Ti_3C_2T_x$/polyvinyl alcohol (PVA) composite. [81] The PVA matrix showed strong interactions with the negatively charged surface of the $Ti_3C_2T_x$ nanosheets through hydrogen bonding. Besides, the fabricated materials were flexible and exhibited electrical conductivity as high as 2.2×10^4 and 2.4×10^5 S/m for $Ti_3C_2T_x$/PVA composite and pure MXene film, respectively. On the other hand, in 2015, Boota *et al.* fabricated a freestanding but brittle film of the self-assembled layered structure of MXene through the intercalation of polypyrrole (PPy) between the $Ti_3C_2T_x$ layers and utilized the obtained material as the electrode in supercapacitor.[82] The conductive property of PPy facilitates its intercalation between the $Ti_3C_2T_x$ layers, expanding the interlayer spaces for rapid and facile charge transport. Furthermore, to enhance the thermal and mechanical properties of polyethylene, in 2016, Zhang *et al.*[83] synthesized Ti_3C_2/UHMWPE (*i.e.,* ultrahigh molecular weight polyethylene) nanocomposite showed enhanced hardness, yield strength and creep resistance compared with pure UHMWPE. The anti-friction performance of the composite also decreased significantly. Also, Naguib *et al.*[84] prepared $Ti_3C_2T_x$/polyacrylamide (PAM) nanocomposites to obtain a highly conductive thin film by casting a well-admixed solution of $Ti_3C_2T_x$/PAM on a Teflon tray, followed by air-drying at room temperature over several days. Wu *et al.*[85] improved thermal, mechanical, and solvent-resistance properties of $Ti_3C_2T_x$-based nanocomposites through the incorporation of HF-etched DMSO-intercalated $Ti_3C_2T_x$ fillers into the hydrophilic polyethyleneimine (PEI) and successively, hydrophobic polydimethylsiloxane (PDMS) matrixes to prepare a highly active hybrid layer. In 2017, Cao *et al.* [86] delaminated MXene and prepared (Polyvinylidene fluoride) PVDF/MXene composites by solution blending method to boost the thermal conductivity of PVDF. Hence, the thermal conductivity of PVDF noticeably increased by loading five *wt*% of MXene. Furthermore, Han *et al.*[87]fabricated a composite membrane with excellent hydrophilicity, high flux, and efficient selectivity in the separation of dyes from salts through a simple filtration method on a polyethersulfone (PES) membrane utilizing etched and ultrasonicated Ti_3AlC_2.

In this regard, Boota *et al.*[80] conducted an investigation focused on the interactions between polar and nonpolar polyfluorane derivatives (PFDs) in conjunction with $Ti_3C_2T_x$ MXene. This study revealed that the strength of the interaction between MXene and polymers was notably influenced by the end functionalities present in the polymer structures. Consequently, the controlled synthesis of polymers with specific end functionalities holds promise for the production of MXene-polymer nanocomposites characterized by enhanced physicochemical and electrochemical attributes so that this nanocomposite displayed a 1.5 times higher capacitance density than the intrinsic MXene. Furthermore, the amalgamation of MXenes with polymers contributes to the enlargement of interfacial areas between the electrode and the electrolyte. This extension leads to improved electrochemical performance by reducing the ion diffusion length.[88] In 2018, Chen *et al*. utilized the cationic polyionic liquid (PIL) as the interfacial linker between the surfaces of MXene and polyoxometalate (POM)[89] to tackle the irreversible self-restacking of MXene and its low charge storage capacity limitations. Accordingly, the MXene-PIL-POM nanohybrid with the uniform distribution of POM nanoparticles on the MXene surfaces was obtained, which showed a better performance in the electrochemical process in comparison with the virgin MXene electrode. Yan *et al.*[90] synthesized a new conductive and flexible textile electrode *via* the deposition of polypyrrole (PPy) on the surfaces of MXene.

Typically, the synthesis of MXene-polymer nanocomposites involves two main methods: in-situ polymerization and ex-situ solution mixing. Several conducting polymers, including poly(3,4-ethylene dioxythiophene) (PEDOT), polyaniline (PANI), and polypyrrole (PPy), have been seamlessly integrated with MXene through in-situ polymerization.[80, 88] In this context, in-situ polymerizations are achieved through techniques such as electrochemical deposition, mild physical agitation, or photopolymerization. For instance, Qin *et al.*[91] devised various MXene-polymer nanocomposites using PPy and EDOT monomers in conjunction with Ti_3C_2 MXenes via electrochemical deposition**.** The electrochemical polymerization process involves the formation of cationic radicals from the monomers, which subsequently interact to create polymer chains. Concurrently, the negatively charged MXene migrates toward the working electrode, blending with the polymer chains to yield complex MXene-polymer composite films. These electrodeposited PEDOT with Mo1.33C and PPy with Mo1.33C present nanosphere-shaped architectures and form 3D porous structures, resulting in enhanced conductivity and superior electrochemical properties.

In addition to electrochemical polymerization, in-situ polymerization can be accomplished through mild physical agitation.[92] A case in point is the preparation of MXene/PANI nanocomposites by mixing an aniline/HCl solution into a MXene dispersion in water and subsequent precipitation, culminating in the fabrication of a freestanding MXene/PANI hybrid film.[93] Recently, Carey *et al.*[94] incorporated Ti_3C_2Tx MXene into the nylon-6 structure and obtained a melt-processable nanocomposite with a water permeation factor five times lower than that of the best-performing nylon/clay composite. In this study, the multilayered MXene was intercalated through *in situ* ring-opening polymerization of caprolactam monomers embedded between MXene nanosheets. As a result, the obtained film showed excellent barrier properties.

Conversely, ex-situ preparation methods involve the creation of MXene-polymer nanocomposites through solution mixing and filtration.[95] Two separate solutions of MXene and polymer are typically prepared and then mixed and stirred, followed by a filtration process to obtain a freestanding flexible MXene-polymer film. In this venue, in 2018, Feng *et al.*[96] prepared the gradient sandwich-like structure of MXene–Polyvinylidene Fluoride (PVDF) nanocomposite. Such a sandwich-like nanocomposite showed excellent integrated electrical properties accompanied by the homogeneous mono-layered distribution of MXene nanosheets. On the other hand, the ultrathin $Ti_3C_2T_x$/PEDOT: PSS [poly(3,4-ethylene dioxythiophene)/poly(styrene sulfonate)] nanocomposite flexible film through a drop-casting process leading to an improvement in specific surface area and enhanced electrochemical conductivity for the electromagnetic interference (EMI) shielding application[97].[98] Integrating 2D materials into 3D structures further enhances the ionic and electron transport in electrode materials, thereby enhancing electrochemical performance. For another example, Gund *et al.*[99] investigated the high-frequency performance of MXene and polymer nanocomposite electrodes (Ti_3C_2/PEDOT: PSS) for flexible AC-filtering electrochemical capacitors. They achieved remarkable high-frequency and high volumetric capacitance with exceptional working ability and a service life range. Xu *et al.* prepared light MXene-polyvinyl alcohol (PVA) nanocomposite foams with exceptional mechanical properties for the electromagnetic wave shielding application.[100]

Lastly, however, an innovative study reported a unique instance of an MXene-containing polymer electrolyte (MCPE) designed for all-solid-state lithium metal batteries (LMBs) by Pan *et al*. in 2019.[101] This MCPE, consisting of $Ti_3C_2T_x$ MXene flakes uniformly dispersed in a poly(ethylene oxide) / lithium bis(trifluoromethanesulfonyl)imide (PEO20-LiTFSI) complex, Figure 2.4, was prepared via a straightforward aqueous blending method.[101] The outcome was a versatile MXene-polymer membrane exhibiting increased ionic conductivity and improved lithium metal battery performance, primarily due to the interplay between the MXene flakes and the PEO. The MXene flakes affected PEO crystallization by promoting nucleation and restraining crystal growth, leading to an overall positive effect on the electrochemical attributes.

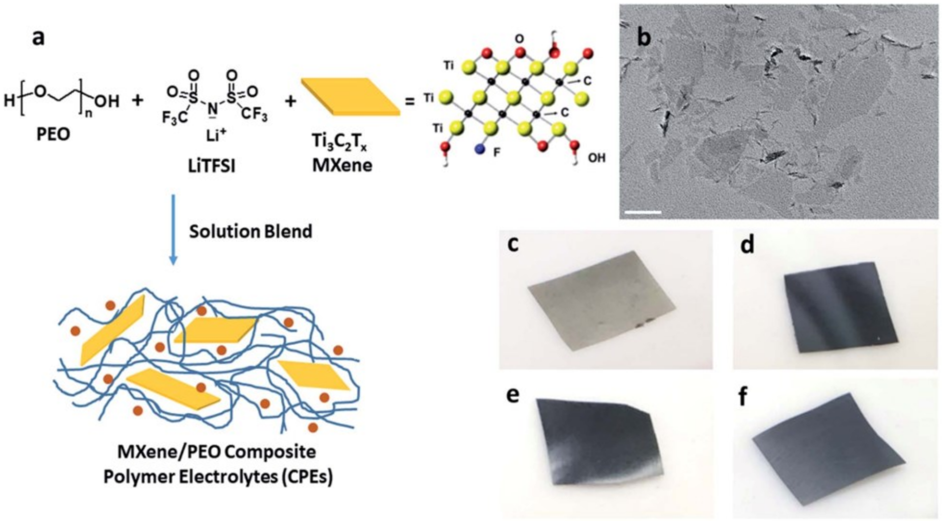

Figure 2.4 (a) The process of fabricating the PEO20-LiTFSI nanocomposite; (b) a transmission electron microscopy (TEM) image of the few-layer MXene, with a scale bar of 100 nm; (c–f) images displaying the nanocomposite membranes with various MXene concentrations.[101]

To summarize, the synergistic combination of conjugated and hydrophilic polymers, particularly PPy, PANI, PFDs, and PEDOT, as electrochemically active materials with 2D MXenes, presents a promising avenue for enhancing the physicochemical and electrochemical properties required for energy storage applications. These composites harness the strengths of both materials, resulting in improved interlayer separation of MXene sheets, enhanced mechanical strength, and structural integrity. This enhancement extends their utility across various applications. The electrochemical performance of MXene-based electrode materials is often hindered by the undesired restacking of MXene sheets during the fabrication of freestanding films. Surface modification of MXene nanosheets with conducting polymers, achieved through in-situ polymerization, addresses this issue by creating highly accessible structures with specific surface areas. The use of conducting polymers in MXene-polymer nanocomposites offers several advantages, including cost-effectiveness, structural flexibility, non-toxicity, and the presence of pseudocapacitive properties. The controlled synthesis of polymers with specific end functionalities holds promise for creating MXene-polymer nanocomposites with enhanced physicochemical and electrochemical attributes. Furthermore, these composites contribute to the enlargement of interfacial areas between the electrode and the electrolyte, leading to improved electrochemical performance by reducing ion diffusion length.

In the quest for sustainable energy solutions, these advances in MXene-polymer composites represent a significant step forward, underscoring their role in shaping the future of energy storage technologies.

2.5 Challenges in MXene Synthesis

MXenes, a class of 2D materials with great potential in a wide range of applications, are not without their challenges.

a) Long-term stability is a paramount concern during the synthesis and development of applications. MXenes are prone to oxidation when produced in aqueous media, a vulnerability that poses a significant threat to their long-term stability. This issue is particularly pronounced in the case of HF-etched MXenes, which exhibit reduced stability under ambient conditions. Several factors can exacerbate the kinetics of MXene oxidation, including elevated temperature, exposure to dissolved oxygen, and the presence of aqueous media, rendering long-term stability a critical concern.[102] Although some strategies like edge capping with polyanionic salts, such as polyphosphate, were applied to enhance the stability of MXenes,[103] further investigations are needed to thoroughly assess the impact of introducing ionic salts on the conductivity of MXenes.

More effective improvements are needed to stabilize MXenes. Additionally, defects in Ti_3C_2 MXene sheets have been identified as a factor that can instigate oxidation.[103] Further insights from molecular dynamics simulations based on reactive force fields reveal that MXene oxidation rates are influenced by storage conditions, temperature, and the concentration of oxidants.[38] These simulations show a positive correlation between temperature and MXene oxidation, as higher temperatures increase the rate of oxidation. Under high-temperature conditions, carbon and titanium dioxide (TiO_2) are formed at the edges, transforming Ti_3C_2 monolayer MXene flakes into TiO_2/carbon hybrid materials. The size of MXene flakes exhibits a negative correlation with the rate of oxidation, where smaller flakes display higher oxidation kinetics.[70, 104]

b) Poor dispersion and agglomeration: One of the primary challenges in polymer/MXene nanocomposites is achieving uniform dispersion of MXene within the polymer matrix. MXenes have a tendency to agglomerate due to their high surface energy. Agglomeration not only hinders the efficient transfer of stress and charge but also deteriorates the mechanical and electrical properties of the nanocomposites. Methods to improve the dispersion of MXenes, such as using functionalized MXenes or employing appropriate mixing techniques, should be explored to address this challenge.

c) Interface compatibility and bonding: Another challenge is obtaining strong interfacial interactions between MXenes and polymer matrices. The interface between MXenes and polymers plays a crucial role in determining the overall properties of the nanocomposites. However, due to the nature of MXenes and polymers, achieving strong interfacial bonding is not always straightforward. Surface functionalization of MXenes and selecting proper polymers with compatible functional groups can enhance interfacial interactions and improve the nanocomposites' overall mechanical, electrical, and thermal properties for developed applications.

The challenges associated with MXenes also extend to their synthesis protocols, which can impact their stability, increasing *d*-spacing, delamination and functionality. Surface terminations, such as –F terminations, can lead to the release of hydrofluoric acid (HF) during electrochemical reactions, potentially causing harm.[70] To address this concern, the development of fluoride-free/low-fluoride synthesis routes is required.

While the challenges in MXene synthesis are significant, ongoing research efforts aim to overcome these obstacles and unlock the full potential of MXenes in all applications, especially in energy storage devices.

2.5.1 Intercalation Pseudocapacitance in Electrochemical Energy Storage

An immediate worldwide demand arises for electrochemical energy storage materials capable of simultaneously delivering both high power and high energy density. Electrochemical energy storage (EES) can store electricity, which can subsequently be utilized in mobile transportation or to balance out peak power on the electrical system. Regenerative fuel cells, rechargeable batteries such as lithium-ion batteries [LIBs], non-lithium-ion batteries[NLIBs] like sodium-ion batteries and magnesium-ion batteries, metal-air batteries, lithium-sulfur batteries, as well as supercapacitors are among the numerous varieties of EES technologies. Multiple mechanisms contribute to the occurrence of EES at solid-state electrodes: (i) via the formation of an electrical double-layer (EDL), (ii) through surface redox reactions, (iii) via insertion of ions as in electrochemical intercalation, and (iv) with alloying, decomposition, or conversion reactions.[105] The last three processes are Faradaic in nature, as they represent charge transfer reactions across the electrochemical interface. Surface redox reactions and certain ion insertion reactions have been identified as pseudocapacitive. [105] Exploring pseudocapacitive electrode materials is driven by technological considerations such as surpassing the energy densities of electrical double-layer capacitors (EDLCs) while overcoming the kinetic limitations plaguing LIBs. Based on different Faradaic mechanisms, there are mainly three types of pseudocapacitance: (i) underpotential deposition, (ii) Faradaic redox pseudocapacitance, and (iii) intercalation pseudocapacitance. The last one takes place through a rapid Faradaic charge transfer and the intercalation of ions into the layers of a redox-active material while the crystallographic phase remains unchanged. As a result, its structure remains extremely stable during electrochemical reactions.[106] Ions can occupy vacant positions or spaces within the bulk of materials through intercalation. Intercalation pseudocapacitance has gained significant importance in recent years. Intercalation pseudocapacitors have the potential to integrate the advantages of batteries, such as high energy density, with those of supercapacitors, such as high power density. Reducing cation diffusion barriers can improve the rate performance of cation-intercalation pseudocapacitive electrode materials.

A limited number of materials exhibit intercalation pseudocapacitance behaviour; therefore, it is crucial to do further research to provide alternative electrode materials to provide exceptional intercalation pseudocapacitance performance.

The distinctive structural characteristics of MXenes that are essential for electrochemical energy storage (EES) comprise (i) an abundance of interlayer ion diffusion pathways, (ii) interlayer ion storage sites, and (iii) carbide/nitride conductivity. As a result, MXenes are potential materials for inherently pseudocapacitive energy storage.[105] Cyclic voltammetry, galvanostatic charge/discharge tests, or electrochemical impedance spectroscopy (EIS) are applied to examine the electrochemical features of pseudocapacitive materials.

Limited research has been dedicated to evaluating the intercalation pseudocapacitance induced by ion intercalation in NLIB batteries and supercapacitors. Developing new synthesis strategies, tuning MXene surface terminations, interactions between solvated or partially solvated cations and the MXene host, and the prediction of promising cation and solvent combinations for maximizing the pseudocapacitive would enhance the charge storage.

2.6 Ionomers

The introduction of polar functional groups into nonpolar polymers (*e.g.,* polyolefins) can improve their essential characteristics, such as toughness, adhesion, barrier, and surface properties.[20, 107] As a result, polyolefins can find their way to entirely new areas of applications in which their intrinsic properties are combined with the new ones imposed by the incorporation of polar functionalized monomers. [20] Ionomers are nanostructured materials, similar to nanocomposites,[108] consisting of a crystalline phase and an amorphous phase[22] and nanoscale ionic aggregates dispersed within the nonpolar polymer matrix. The critical feature of ionomers is a relatively modest concentration of ionic functional groups (typically less than 10 mol%) covalently bonded to the polymer backbone, providing substantial changes in the physical, mechanical, optical and dielectric properties of the polymer. They are used in ion transport membranes, fuel cells, thermoplastic elastomers, adhesives, *etc*. Through direct ethylene copolymerization with unprotected tetralkylammonium-containing acrylate-type ionic liquid comonomers, different hyperbranched polyethylene ionomers containing tetralkylammonium ions coupled with different counteranions [tetrafluoroborate (BF_4^-), hexafluorophosphate (PF_6^-), bis(trifluoromethane)-sulfonimide (Tf_2N^-), or hexafluoroantimonate (SbF_6^-), with a Pd−diimine catalyst, were synthesized by our group.[109] The hyperbranched topology comes from chain walking mechanism of the catalyst. By changing the feed concentration of the ionic liquid comonomers, the content of the ionic groups in the ionomers can be tuned in the copolymerization. It is demonstrated that structural, thermal, and rheological properties of the ionomers are developed through the incorporation of the ionic groups into polymer chains.

On the other hand, direct copolymerization of olefins with polar vinyl monomers has been successfully performed by late transition metal (LTM) catalysts. The α-diimine Ni^{II} and Pd^{II} complexes have created a vast revolution in the field of LTM catalysis for olefin (co)polymerization.[110-112] LTM catalysts can produce polyolefins with various types of branches through chain walking and tolerate the specific situations caused by the polar functional groups. Pd^{II} catalysts bearing α-diimine ligands are preferred due to their potential of enduring extensive chain walking, leading to the precise hyperbranched topology of ionomer. Moreover, Pd–diimine catalysts are able to copolymerize ethylene with polar-functionalized comonomers, rendering the hyperbranched product with the majority of polar groups located at the end of branches. Furthermore, the low oxophilicity and insensitivity of the catalyst toward the tetraalkylammonium ions guarantee the efficient incorporation of ionic liquid comonomers without severe catalyst poisoning.

Chapter 3 Stable Dispersions in Nonpolar/Low-Polarity Organic Solvents, Oxidation Protection and Potential Application in Polymer-Nanocomposites

This chapter is adapted from a paper published in *Journal of Materials Chemistry A*: **Bahareh Raisi**, Lingqi Huang, and Zhibin Ye, Modification of $Ti_3C_2T_x$ MXene with Hyperbranched Polyethylene Ionomers: Stable Dispersions in Nonpolar/Low-Polarity Organic Solvents, Oxidation Protection and Potential Application in Supercapacitors, *J. Mater. Chem. A*, **2023**, *11*, 17167.

Abstract

MXenes have attracted enormous research interest due to their 2D structure and advantageous properties. However, they show low/poor dispersibility in a wide variety of organic solvents, particularly nonpolar or low-polarity solvents, and tend to get oxidized in the presence of oxygen and water during storage, handling, delamination, and applications under ambient conditions. In the present study, we report a simple yet convenient noncovalent modification strategy with the use of hyperbranched polyethylene ionomers containing quaternary ammonium ions to prepare stable, highly concentrated $Ti_3C_2T_x$ MXene dispersions in various nonpolar and low-polarity organic solvents. Constructed with nonpolar hydrophobic hyperbranched polyethylene backbones, the ionomers contain covalently tethered quaternary ammonium cations, which can bind tightly onto negatively charged $Ti_3C_2T_x$ MXene surface by ionic interactions. Simple mixing renders the ionomer-modified MXenes (I-MXenes), with the hyperbranched polyethylene ionomers efficiently intercalated within the MXene sheets. Accordingly, the interlayer spacing of $Ti_3C_2T_x$ MXene expanded to more than 5 nm with at least a 400% increase compared with the original spacing of 1 nm and delaminated to a few or single nano-flakes. The surface modification effectively adjusts the surface property of MXene sheets and facilitates their compatibility with various nonpolar or low-polarity organic media. The resulting modified MXenes are readily stably dispersible in a broad range of nonpolar or low-polarity organic solvents, including tetrahydrofuran (THF), chloroform, xylene, and toluene, at high concentrations (as high as 30 mg mL^{-1} in THF) after simple sonication. Meanwhile, the modification also markedly improves the oxidation stability of MXene sheets due to the presence of the tightly surface-bound hydrophobic hyperbranched polyethylene protecting layer. In contrast to the easy oxidation of unmodified

MXenes, the ionomer-modified MXenes are stable in air-saturated water even for weeks with no/minimum oxidation.

3.1 Introduction

As a class of two-dimensional (2D) materials first discovered by Gogotsi *et al.* in 2011,[113] MXenes are a range of transitional metal carbide/nitride nanosheets with the general formula $M_{n+1}X_nT_x$ where M stands for transition metal (such as Ti, Sc, Zr, Hf, V, Nb, Ta, Cr, Mo, *etc*.), X is carbon and/or nitrogen, and T corresponds to the surface termination moiety (*e.g*., OH, O or F, *etc*.).[114] MXenes are fabricated through a selective etching process by the elimination of ″A″ interlayer element (*i.e*., the element in groups 13 and 14 of the periodic table such as Al) from the MAX phase (ternary transition metal carbides and/or nitrides with a general formula $M_{n+1}AX_n$ (M = an early transition metal; X = C/N; and n = 1, 2, or 3), in the form of stacks of sheets (or multi-layer sheets) and scrolls.[7,6] Though more than 30 MXene compositions have been explored, more than 70% of all MXene research has been focused on the first discovered MXene, $Ti_3C_2T_x$.[5] Featured with the unique combination of properties, including high electrical conductivity, mechanical properties, hydrophilic functionalized surfaces, and high negative zeta-potential, MXenes have found a large number of applications in such fields as electrochemical energy storages,[8,3] composites,[115] membranes,[116] catalysis,[117] electromagnetic,[118] and biomedical areas.[119]

To best benefit from their 2D nanosheet structures, intercalation and delamination of MXenes are often required to render few-layer or even single-layer MXene sheets with maximally exposed surface areas. In this regard, a variety of intercalation compounds,[4] has been employed for their liquid-phase exfoliation often performed under sonication, including hydrazine, urea, dimethyl sulphoxide (DMSO), *N*, *N*-dimethylformamide (DMF),[120,2] organic bases such as tetrabutylammonium hydroxide (TBAOH),[115,121] aqueous phase surfactant,[122] and aryl diazonium salts,[123] as the small molecule intercalants. Alternatively, the inclusion of functional polymers into MXene layers has also been employed to further develop MXene-based functional hybrid materials with distinct chemical, physical, mechanical, and electrochemical properties.[80] In this venue, different polymers, mainly those with polar functional groups in their structures, reactive surface chemistry, and hydrophilic nature, have been applied, including polyfluorene derivatives,[80] poly(vinyl alcohol),[81] polypyrrole,[82] polyacrylamide,[84] as well as other polymers.[86, 87, 89, 90, 97, 100, 124]

MXene dispersions are often employed for handling, synthesis of materials, and fabrication of devices in applications. To date, dispersions of exfoliated/delaminated MXenes have been limited to primarily aqueous phases, as well as a few polar organic solvents, such as *N*, *N*-dimethylformamide, *N*-methyl-2-pyrrolidone, dimethyl sulfoxide, propylene carbonate, *N*, *N*-dimethylacetamide, acetonitrile and ethanol.[121,125] In these polar solvents, MXene flakes display colloidal stability. Conversely, they are unstable in nonpolar or low-polar solvents. MXene dispersions in nonpolar or low-polarity solvents have been very rarely reported,[126] while critically important to significantly expand the spectrum of applications for MXenes. For example, it will facilitate the preparation of tailor-made MXene nanocomposites with a variety of nonpolar hydrophobic polymer matrices.

On the other hand, MXenes are prone to oxidation, particularly in aqueous suspensions,[127,16] limiting their performance and ability to be stored for any meaningful amount of time. They lose their intrinsic physicochemical properties within two weeks of storage in water with the formation of TiO_2–C hybrid structures.[17, 128, 129] Storage of MXenes in a nonpolar or low-polarity organic solvent can be the most promising solution as it prevents contact with water, and the low concentration of dissolved oxygen in the media also dramatically delays the surface oxidation of MXene.[130]

However, achieving stable MXene dispersions in nonpolar/low-polarity solvents is challenging, particularly for high-concentration dispersions with long-term stability, which requires proper modification of the surface of exfoliated/delaminated MXene sheets.[126,130] The modifying agents or intercalants are expected to bind strongly onto the surface of MXene sheets and meanwhile offer a good affinity with the solvent media. To date, there have been only two reports demonstrating the preparation of MXene dispersions in nonpolar solvents by modifying the MXene surface with di(hydrogenated tallow)benzyl methyl ammonium chloride and alkylphosphonic acid ligands.[126,130] Therein, though the dispersions were stable in nonpolar solvents for 10─30 days, longer-term stabilities of the dispersions were not demonstrated, and the antioxidation stability of the modified MXenes was not reported. Meanwhile, the highest concentration of the dispersed MXenes was limited to around 18 mg mL^{-1} in *p*-xylene.

In this work, we demonstrate the intercalation of MXene nanosheets with a range of hyperbranched polyethylene ionomers designed with covalently tethered quaternary ammonium ions at different contents as the polymeric intercalants to render ionomer-modified MXene multi- or few-layer sheets. The objective is to achieve highly stable high-concentration MXene dispersions in various nonpolar and low-polar solvents. Systematical characterizations of the resulting ionomer-modified MXenes (I-MXenes) have been undertaken. The effects of the quaternary ammonium ion content and dosage of the ionomers on the efficiency of intercalation have been studied. The oxidative stability of I-MXenes and their long-term dispersibility in a variety of organic solvents (nonpolar and low-polarity solvents, as well as some polar solvents) have been investigated. Our work helps expand the scope of MXene applications by endowing them with high dispersity in nonpolar or low-polarity low-boiling-point organic solvents, ionic liquids, gel polymers and their hybrid electrolytes for electrochemical energy storage devices.

3.2 Experimental

3.2.1 Materials

All manipulations involving air- and/or moisture-sensitive materials were conducted in a nitrogen (N_2)-filled glovebox or by using Schlenk techniques. The ternary titanium carbide (Ti_3AlC_2) powders with a size ≤ 40 μm as the MAX phase sample were obtained from Y-Carbon Ltd. (Ukraine). The Pd─diimine catalyst, $[\mathrm{ArN = C(Me) - (Me)C = NAr]Pd(CH_3)(N \equiv C(Me)]^+SbF_6^-(Ar = 2{,}6 - (iPr)_2C_6H_3)}$, was synthesized by following a literature procedure.[131] The acrylate-type ionic liquid comonomer, [2-(acryloxy)ethyl]trimethylammonium tetrafluoroborate ($AETMA^+BF_4^-$), was synthesized by following the procedure reported in our earlier paper.[39] Polymer-grade ethylene was obtained from Air Liquide and was purified by passing through a 3 Å molecular sieve column and an Oxiclear column. Acetone (Certified ACS grade, Fisher Scientific) was dehydrated with 3 Å molecular sieves before use. Deionized (DI) water was obtained using a Milli-Q water purification system. All other solvents or reagents were obtained from either Aldrich or Fisher Scientific and were directly used as received. The ethylene-olefin copolymer (EOC) elastomer used herein as the polymer matrix for the compounding of polymer nanocomposites is Engage 8130 obtained from Dow Chemical, which is an ethylene-octene copolymer with the octene comonomer content of 42 wt%. It has a density of 0.864 g·cm^{-3} and a melt flow index of 13 g·min^{-1} (at 190 ºC).

3.2.2 Synthesis of Quaternary Ammonium-Containing Hyperbranched Polyethylene Ionomers

The hyperbranched polyethylene ionomers of different ionic contents (I1─I5 samples) were synthesized by catalytic chain walking copolymerization of ethylene and an ionic liquid comonomer AETMA$^+$BF$_4^-$ according to our earlier paper.[109] The polymerization was performed in a 50 mL Schlenk flask equipped with a magnetic stirrer. The sealed flask was vacuumed and then purged with ethylene five times, and then filled with ethylene to 1 atm (*i.e.,* 1 atm absolute pressure). A solution of the ionic liquid comonomer (0.245−2.45 g in 5 mL of anhydrous acetone) was injected into the reactor under stirring. Subsequently, the polymerization was started upon the injection of the Pd─diimine catalyst solution (0.08 g, 0.1 mmol in 5 mL of anhydrous acetone). During the polymerization, ethylene pressure was maintained constant by continuous feeding, and the polymerization temperature was set at room temperature. After 24 h, the polymerization was stopped by shutting down the ethylene supply and venting the reactor. The black product containing Pd(0) particles, resulting from the decomposition of the Pd─diimine catalyst, was precipitated out with a large amount of methanol. The precipitate was purified to remove Pd black according to a procedure in our earlier paper,[109] and then dried under vacuum at room temperature, rendering the corresponding ionomer. As per ^{1}H NMR spectroscopy, the ionomers (I1─I5) with various quaternary ammonium ion contents from 0.31 to 2.87 mol% were obtained. One hyperbranched polyethylene homopolymer (HBPE) was also synthesized under the same conditions and procedures as above, except without any comonomer.

3.2.3 Synthesis of Multi-Layered $Ti_3C_2T_x$ MXene

Herein, we used directly regular commercial MAX (Ti_3AlC_2) powders as received, which were not sieved and contained some impurities (5-10 wt% of TiC and 1-5 wt% Al_2O_3 according to the supplier), for the synthesis multi-layered $Ti_3C_2T_x$ MXene. The multi-layered MXene was synthesized from the MAX (Ti_3AlC_2) powder by using the minimally intensive layer delamination (MILD) method with the use of a mild mixed etchant solution of lithium fluoride (LiF; 12 M) and hydrochloric acid (HCl; 9 M).[132] The etchant was prepared by slowly adding 1.6 g of LiF to 20 mL of 9 M HCl in a 125 mL Teflon beaker with a cap in a fume hood. After the complete dissolution of LiF in HCl solution, Ti_3AlC_2 (MAX) powders were carefully added to the etchant solution over the course of 10 min to avoid the initial overheating of the solution as a result of the exothermic nature of the etching reaction. The reaction mixture was kept stirred for 48 h at 38 °C. Afterward, the product was thoroughly washed with distilled water *via* centrifugation (Thermo Fisher Scientific, Sorvall Legend XT) at 3500 rpm for multiple cycles. After each cycle, the acidic supernatant was decanted, and fresh DI water was added. The washing cycle was repeated until the supernatant reached a pH of approximately 5-6. The final product was dried overnight in a vacuum oven at 100 °C. The resulting fine powders are multi-layered MXene sheets and are hereafter referred to as MXene.

3.2.4 Synthesis of Ionomer-Modified MXenes (I-MXenes)

Typically, the hyperbranched polyethylene ionomer (10−60 mg) was dissolved in 40 mL of THF. Afterward, the dispersion of MXene in DMF (10 mg in 0.5 mL) was added dropwise into the ionomer solution under sonication. The resulting dispersion was further sonicated for *ca.* 10 min and was then centrifugated at 10,000 rpm for 15 min. The precipitate was redispersed in 40 mL of fresh THF, followed by centrifugation. Three cycles of redispersion and centrifugation cycles were performed to remove non-intercalated ionomers. Finally, the precipitate was dried overnight under vacuum at *ca.*100 °C to render the ionomer-modified MXene, termed as I-MXene-x-y, with x noting for the ionomer (I1─I5) used and y indicative of the ionomer/MXene mass ratio.

3.2.5 Dispersibility of MXene and I-MXene-4-2 in Various Solvents

Dried unmodified MXene and I-MXene-4-2 (with a medium ionomer content) were respectively dispersed in 10 mL of various solvents, including DI water, methanol, ethanol, acetonitrile (ACN), dimethyl sulfoxide (DMSO), dimethylformamide (DMF), acetone, pyridine, chloroform, ethyl acetate (EAC), tetrahydrofuran (THF), benzene, toluene, xylene, n-hexane, and cyclohexane, at a concentration of 2 mg mL^{-1}. The dispersions were rendered by simple hand-shaking for 10 s, followed by sonication for 30 min. Subsequently, the various dispersions were left undisturbed, and their stabilities were monitored over a period of 3 months with photographs taken regularly. After 3 months, samples of I-MXene-4-2 dispersions were characterized with UV-Vis spectrophotometry. UV-Vis absorbance spectra were obtained in the range of 400−1000 nm (1 cm optical path length cell), with three scans performed on each dispersion.

3.2.6 Determination of Extinct Coefficient of I-MXene-4-2 for Dispersions in Various Solvents

To determine the concentration of MXene in the dispersions of I-MXene-4-2, extinction coefficients (ε) of MXene in various solvents were determined. For this purpose, a dispersion of I-MXene-4-2 (generally, 2 mg mL^{-1}) in each solvent was sonicated at room temperature for 30 min. The resulting dispersion was subsequently centrifuged at 3500 rpm for 1 min for the determination of the extinction coefficient of the exfoliated MXenes or at 3500 rpm for 30 min for the extinction coefficient of delaminated MXene and was then left undisturbed overnight. The supernatant dispersion was then collected and used for concentration quantification. The mass concentration of MXene (C_M) in the dispersion was quantified with the use of thermogravimetric analysis by evaporation of the solvent and the combustion of the ionomer with a heat ramp to 700°C, which was repeated three times on each dispersion to obtain an average C_M value. Subsequently, the dispersion with known C_M was diluted to at least 5 known concentrations, which were measured for the peak UV-Vis absorbance (at around 800 nm) to determine the extinction coefficients.

3.2.7 Simultaneous Interfacial Modification and Phase Transfer of MXene Flakes

Two aqueous MXene dispersions (each 2 mg mL^{-1} in 10 mL of water) were prepared. Two organic solutions of I4 (4 mg mL^{-1} in 10 mL of chloroform and toluene, respectively) were also prepared. Each organic solution was mixed with an aqueous MXene dispersion in a vial, which was hand-shaken and sonicated for 10 min. The immiscible mixtures were then left undisturbed for 24 h to observe the phase transfer of MXene from the aqueous phase to the organic phase.

3.2.8 Preparation of EOC Composites

The EOC composites were prepared using a solution-compounding method. A prescribed quantity of original unmodified and modified MXenes (equivalent to 0.1−5 wt % of neat MXene in composites) was dispersed at 10 mg mL^{-1} in THF. The dispersion was added dropwise into a toluene solution of EOC (50 mg mL^{-1}) within 1 h under magnetic stirring. The mixture was continuously stirred for 3 h before precipitation in a large amount of methanol. The precipitate was dried at 120 °C in a vacuum oven for 24 h.

3.2.9 Characterizations and Measurements

^1H NMR spectra were all collected on a Bruker 300 spectrometer (300 MHz) with $CDCl_3$ as the solvent. Thermogravimetric analysis (TGA) was performed on a TA Instruments Q50 thermogravimetric analyzer. Measurements were performed under a N_2 atmosphere at a continuous flow of 60 mL min^{-1} through the sample furnace and a flow of 40 mL min^{-1} through the balance compartment. In a typical measurement, the sample (*ca*. 5 to 10 mg) was heated from room temperature to 700 °C at 10 °C min^{-1}. Dynamic light scattering (DLS) measurements of the dilute dispersions (*ca.* 0.1 mg mL^{-1}) of the various MXene samples for their hydrodynamic particle size and ζ potential were performed on a Brookhaven NanoBrook Omni Instrument at 25 °C. Each sample was measured three times, and the average values were used. Wide-angle X-ray diffraction patterns of the unmodified MXene and modified MXenes samples were collected on a Bruker D8 Advance diffractometer with Cu Kα radiation at room temperature. UV-Vis spectroscopy was performed on a Thermo Scientific Genesys 10S UV-Vis spectrophotometer. The contact angles of unmodified MXene and modified MXene films were measured by utilizing a contact angle meter (VCA, AST Products, Inc., USA). Scanning electron microscopy (SEM) was carried out on an FEI Quanta 450 Environmental Scanning Electron Microscope (FE-ESEM). A thin platinum layer was coated on the samples prior to the imaging. The transmission electron microscopy (TEM) images were captured with a JEOL 2010F field emission electron microscope operated at 200 keV. Specimens for TEM observation were prepared by dispersing powders of the corresponding materials (MXene or I-MXenes) in THF by bath sonication, followed by the deposition of a few drops of the dispersion on a carbon-coated copper mesh grid. The grid was dried in the air prior to the TEM characterization.

3.3 Results and Discussion

A range of hyperbranched polyethylene ionomers (I1─I5) containing covalently tethered quaternary ammonium ions at different contents (0.31 to 2.87 mol%) has been synthesized in this work for the surface modification of $Ti_3C_2T_x$ MXene nanosheets. Their synthesis involves the well-established Pd─diimine-catalyzed direct copolymerization of ethylene with the ionic liquid acrylate comonomer ($AETMA^+BF_4^-$) (see Scheme 3.1a) developed by our group.[109] Through the chain walking mechanism of the Pd─diimine catalyst,[133,134] the resulting ionomers are featured with a hydrophobic hyperbranched polyethylene skeleton randomly tethered with quaternary ammonium cations, each balanced with a BF_4^- counter anion.

In view of the highly negatively charged surface of $Ti_3C_2T_x$ MXene nanosheets,[5,121,132] we reason that the ionomers should strongly bind onto the surface of MXene sheets through the strong ionic interactions between the quaternary ammonium cations and the negatively charged surface.[135,136]This is expected to facilitate the intercalation of the ionomers between the MXene sheets and the subsequent delamination of the MXene sheets by overcoming their interlayer interactions, rendering exfoliated ionomer-modified MXene (I-MXene) multi-/few-layer sheets (see Scheme 3.1b). With the surface-bound nonpolar hydrophobic hyperbranched polyethylene chain segments, I-MXenes are expected to have good dispersibility in nonpolar/low-polarity solvents that hyperbranched polyethylenes are known to have good affinity to.

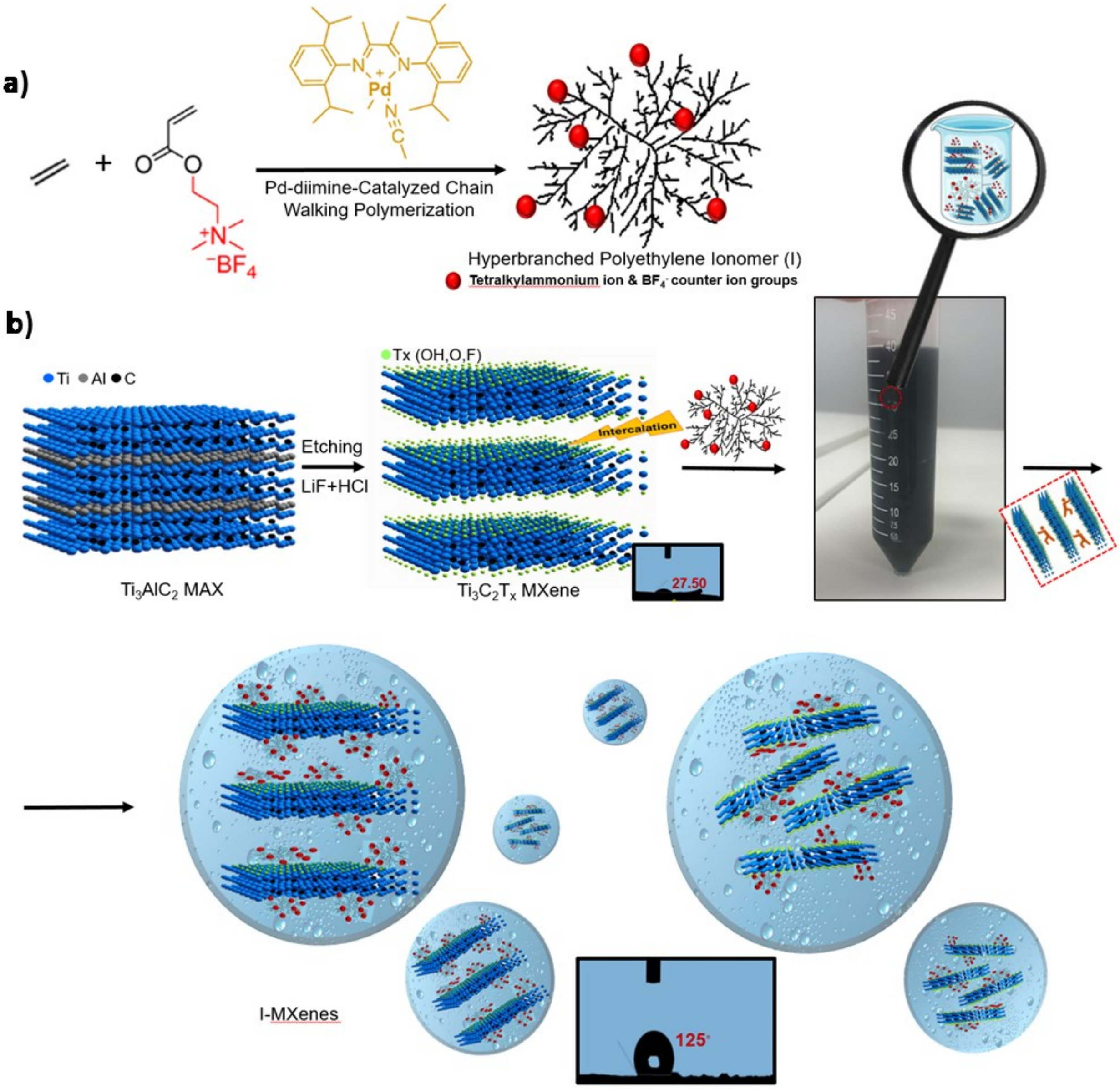

Scheme 3.1 (a) Synthesis of hyperbranched polyethylene ionomers and (b) their intercalation between hydrophilic MXene nanosheets to form modified MXenes (I-MXenes).

Table 3.1 summarizes the copolymerization conditions and detailed characterization results (including comonomer content and branching structure) of the ionomers. Figure S3.1 shows their ^{1}H NMR spectra, which confirm their possession of the covalently tethered quaternary ammonium ions (0.31, 0.73, 1.03, 2.05, and 2.87 mol % in terms of comonomer content for I1─I5, respectively) and the highly branched polyethylene skeleton (branching density of *ca.* 88 branches per 1000 C). When dispersed in solvents, the ionomers form three-dimensional physical cross-linking networks due to the aggregation of the quaternary ammonium ions.[109,133,134] DLS characterization of I4 as a representative ionomer in THF shows a large z-average hydrodynamic size of *ca.* 206 nm and a ζ potential of *ca.* +12 mV. With the increase of the content of the quaternary ammonium ions, ζ potential of the ionomers shows a trend of increase. In addition, one hyperbranched polyethylene homopolymer (HBPE) was synthesized for comparison purposes. It does not contain any specific functionality, though having a hyperbranched structure with a high branching density of 88 branches per 1000 carbon atoms from ^{1}H NMR spectroscopy. Detailed properties and specifications of these polymers have been reported in our previous papers.[137-139]

Table 3.1 Synthesis and characterization of quaternary ammonium-containing hyperbranched polyethylene ionomers (I1–I5)[a]

Ionomer	Catalyst (mmol)	Comonomer[b] (mol/L)	Yield (g)	C_2H_4 TOF[c] (1/h)	Comonomer Content[d] (mol%)	Branch Density[e] (1/1000C)
HBPE[f]	0.1	0	3.34	49.7	na	88
I1	0.1	0.1	1.6	23.8	0.31	89
I2	0.1	0.2	1.12	16.7	0.73	90
I3	0.2	0.3	2.78	20.7	1.03	89
I4	0.2	0.5	2.73	20.3	2.05	97
I5	0.2	1	2	14.9	2.87	88

[a] Polymerizations were all conducted under 1 atm ethylene pressure in 10 mL of acetone as solvent at room temperature for 24 h. [b] Feed concentration of ionic liquid comonomer, $AETMA^+BF4^-$. [c] Ethylene turnover frequency (TOF) calculated as $\frac{\frac{m_{yield}(g)}{24(h)\times 28(\frac{g}{mol})}}{n_{catalyst}\,(mol)}$. [d] Content of quaternary ammonium ions in the ionomers, determined with ^{1}H NMR spectroscopy as $100\% \times 4A_1/9A_2$, where A_1 represents the integration area for methyl protons on the ammonium ion (ca. 3.25 ppm), and A_2 represents peak integration area for protons on ethylene sequences (0.7–1.5 ppm). [e] Branch density determined with ^{1}H NMR as $1000\times 2A_3/3A_2$, where A_3 represents the integration area for methyl protons in ethylene sequences (0.7–1.0 ppm). [f] Hyperbranched polyethylene homopolymer.

3.3.1 Synthesis of Ionomer-Modified MXenes (I-MXenes)

Multi-layer $Ti_3C_2T_x$ MXene sheets used herein are produced from Ti_3AlC_2 MAX powders through the MILD method with the use of a mixture of lithium fluoride and hydrochloric acid (LiF/HCl) as the etching agent.[132] The synthesis of I-MXenes is achieved herein conveniently by the simple dropwise addition of MXene dispersion in DMF (20 mg mL^{-1}) into a dilute solution of the ionomer (I1─I5) in THF at desired concentrations with bath-sonication. During the dropwise addition of the MXene solution, the mixture remains a homogenous dispersion, though the colour changes from light grey/green to dark black. The phenomenon is drastically different from the control experiment with the use of the HBPE homopolymer without containing the quaternary ammonium ions, where visible large aggregates immediately form. This difference clearly indicates the critical role of the ionic groups in the modification of the ionomers. In each case, the resulting mixture is subsequently centrifugated, and the precipitate is washed with THF, rendering I-MXene as solid black powders after drying.

To illustrate the efficiency of the modification, Figure 3.1 shows the XRD pattern of a representative modified MXene sample, I-MXene-1-2, obtained with the use of I1 having the lowest ammonium ion content at the ionomer/MXene feed ratio [$(m_{ionomer}/m_{MXene})_0$] of 2, along with those of MAX powders and the unmodified MXene. The MAX powders show diffraction peaks at 2θ values of 9.57°, 19.2°, 34.05°, 36.79°, 39.05°, 41.86°, 44.99°, 48.55°, 54.34°, 56.57°, 60.45°, and 65.64°, assigned to (002), (004), (101), (103), (104), (105), (106), (107), (108), (109), (110) and (1011) planes of pure Ti_3AlC_2, respectively, according to JCPDS No. 52-0875[113, 128, 140]. Diffraction peaks arising from impurities, including TiC and Al_2O_3 (alpha and gamma phases), are also detected in the MAX phase.[141] The peaks of the impurities and/or trace unetched MAX phase (reflected from the peak at 39.05°) are also observed in the XRD patterns of both unmodified MXene and I-MXene-1-2. The XRD pattern of unmodified MXene confirms its distinctly different crystal structure compared to that of Ti_3AlC_2 after the etching treatment. The characteristic (002) and (004) peaks in MXene are broadened and shift to much lower values (2θ =8.15° and 16.86°, respectively). The (002) peak is a characteristic peak of MXene, demonstrating the ordered stacking of $Ti_3C_2T_x$ MXene multi-layer sheets.[121,142] This phenomenon results from the structural expansion upon the insertion of Li^+ ions between the sheets and then the formation of ─F and ─OH, ─O terminating groups on the sheet surface following the etching process.[141] The expansion of the interlayer spacing achieved after the removal of Al by etching is limited to about 11 Å and is not suitable for applications where better access to the surface area of MXene sheets is required.[1] Due to the presence of —OH, —O, —F groups on the surface, unmodified MXene shows a ζ potential of -38 mV in water.

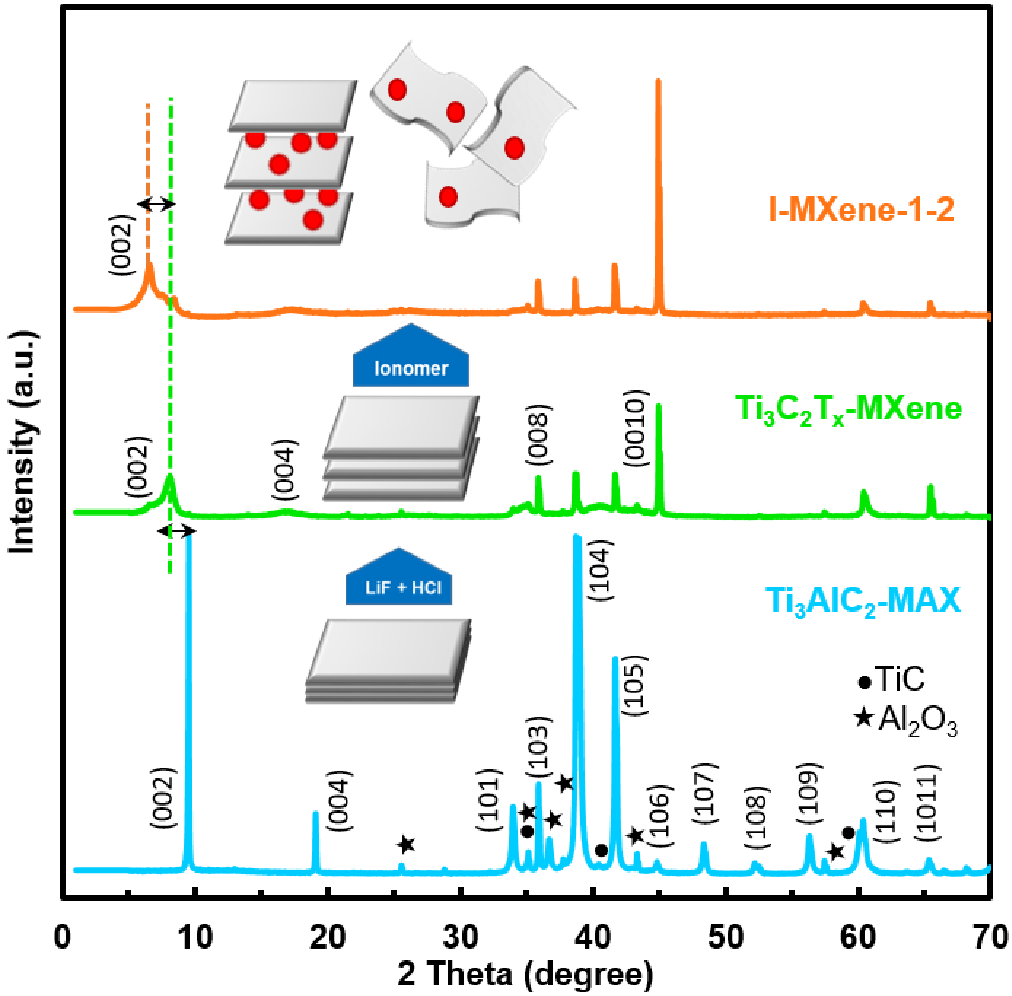

Figure 3.1 XRD patterns of Ti_3AlC_2-MAX powder, LiF/HCl etched unmodified $Ti_3C_2T_x$ MXene, and one representative modified MXene (I-MXene-1-2).

In the XRD pattern of I-MXene-1-2, the (002) peak is significantly broadened and shifted to a much lower 2θ value of 6.5°. The peak shift corresponds to the increase of *d*-spacing from 10.8 Å for unmodified MXene to 13.6 Å for I-MXene-1-2. This confirms the successful intercalation of I1 within the MXene sheets despite its the lowest quaternary ammonium ion content among the set of the ionomers.

Following the success with I1, we have subsequently investigated the effects of ionomer dosage and the different ionomers with varying ammonium ion contents on the intercalation. With I3 as the representative ionomer, the effects of the ionomer dosage [$(m_{ionomer}/m_{MXene})_0$ in the broad range of 1 to 6] have been studied by adjusting the concentration of the ionomer solution while at a fixed weight of MXene. With the other ionomers, the $(m_{ionomer}/m_{MXene})_0$ ratio is set at 2 to investigate the effects of the ionic content of the ionomers on the modification. Table 3.2 summarizes these resulting I-MXenes and some of their properties.

Table 3.2 I-MXenes prepared with different ionomers at varying ionomer/MXene feed ratios.

Modified MXenes (I-MXene)	**Ionomer**	**$(m_{Ionomer}/m_{MXene})_0$[a]**	**Ionomer Content[b] (wt%)**	**DLS[c]**			**XRD**	
				d_p (nm)	**PDI**	**ζ potential (mV)**	**2Θ(°) (002)**	**d(A°)**
MXene	na	0	0	288	0.2	-38	8.15	10.8
I-MXene-1-2	I1	2	1.8				6.5	13.6
I-MXene-2-2	I2	2	10	1800	0.3	30	6.5	13.6
I-MXene-3-1	I3	1	8.7	1071	0.3	30	5.8	15
I-MXene-3-2	I3	2	12.9	1100	0.2	34	6.4	13.8
I-MXene-3-3	I3	3	13.7	701	0.3	35	5.7	15.1
I-MXene-3-4	I3	4	20.8	718	0.3	39	6.4	13.8
I-MXene-3-6	I3	6	28.7	720	0.3	43	6.4 1.7	13.8 >50
I-MXene-4-2	I4	2	18.1	680	0.3	41	6.4 1.6	13.8 >50
I-MXene-5-2	I5	2	29	829	0.3	48	4.7 1.7	18.8 >50

[a] Feed mass ratio of ionomer to MXene employed in the synthesis of I-MXenes.

[b] Determined from percentage weight loss within the temperature range of 280−480 °C from TGA characterization.

[c] Z-average hydrodynamic particle size (d_p), polydispersity index (PDI) for size distribution, and ζ potential determined by DLS from dilute dispersions in water (for unmodified MXene) or THF (for I-MXenes).

TGA characterization was performed on the various I-MXenes in a N_2 atmosphere to confirm the ionomer incorporation and quantify their contents. Figure 3.2(a) shows the TGA curves of the I3-modified MXenes obtained at various $(m_{ionomer}/m_{MXene})_0$ ratios (I-MXene-3-1 to I-MXene-3-6), along with those of I3 as a representative ionomer and the unmodified MXene for comparison. I3 starts to decompose at 280 °C with the nearly complete weight loss at 480 °C. The other ionomers show nearly identical TGA curves and are thus not included in the figure. The unmodified MXene is stable with no considerable weight loss within the investigated temperature range up to 700 °C. All the I3-modified MXenes exhibit a one-step weight loss within 280-480 °C, attributable solely to the decomposition of the ionomer. Ionomer mass contents in the I-MXenes have thus been quantified from the TGA weight loss and are summarized in Table 3.2. The inset in Figure 3.2(a) plots the dependence of the mass content of I3 in the I-MXenes on the $(m_{ionomer}/m_{MXene})_0$ ratio. One can find a nearly linear increase of the mass content of I3 from 8.7 to 28.7 wt% with the increase of $(m_{ionomer}/m_{MXene})_0$ ratio from 1 to 6. This indicates the amount of the bound ionomer increases with the feed ratio. On the contrary, in the control experiment with the HBPE homopolymer at the $(m_{ionomer}/m_{MXene})_0$ ratio of 3, no weight loss is observed up to 700 °C in TGA (see Figure S3.2 in Supporting Information), indicating that the homopolymer cannot get intercalated within MXene sheets due to the absence of the quaternary ammonium ions. This highlights the critical role of the quaternary ammonium ions in the intercalation of the ionomers through their binding onto the negatively charged surface of MXene sheets.

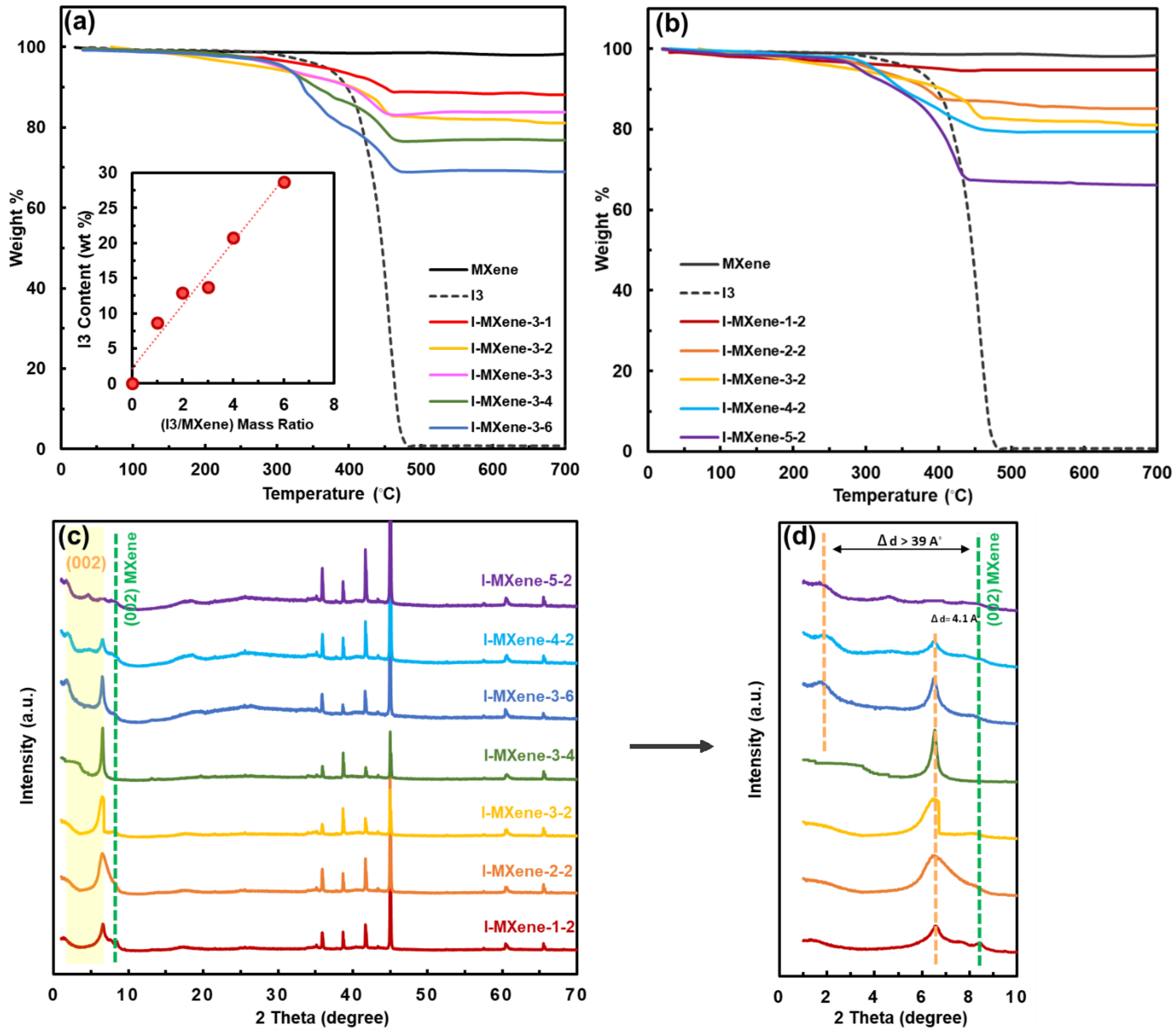

Figure 3.2 (a) TGA curves of unmodified MXene, I3, and I-MXenes modified with I3 at different I3/MXene mass ratios (I-MXene-3-1 to I-MXene-3-6), with the inset showing the effect of I3/MXene mass ratio on the content of I3 in the I-MXenes; (b) TGA curves of various I-MXenes prepared with different ionomers at the ionomer/MXene mass ratio of 2, along with those of unmodified MXene and I3 for comparison; (c) XRD patterns of unmodified MXene and I-MXenes; (d) magnified image of the selected region in (c).

Figure 3.2(b) shows TGA curves of I-MXenes obtained with the use of other ionomers at the $(m_{\text{ionomer}}/m_{\text{MXene}})_0$ ratio of 2. Similar TGA curves with a single-step weight loss within 280-480°C are found but with distinctively different ionomer contents. The ionomer content determined from the weight loss shows a clear trend of increase from 1.8 to 29 wt% with the increase of the ionic content in the ionomers from 0.31 (in I1) to 2.87 mol% (in I5). This indicates that increasing the ionic content in the ionomer leads to the enhanced ionomer intercalation due to the increased binding sites for ionic complexation with MXene.

Figure 3.2(c) compares XRD patterns of the various I-MXenes prepared with different ionomers, along with that of unmodified MXene. Diffraction peaks characteristic of the MXene structure are all well retained in I-MXenes.[132] However, relative to that of virgin unmodified MXene, (002) peak of I-MXenes is significantly broadened and weakened, along with lower-shifted 2Θ values (ranging from as low as 1.6° to ca. 6.5° relative to 8.15° in unmodified MXene; see Table 3.2). The trend is increasingly pronounced with the increase in ionomer content. In the I-MXene-3 set of samples, the (002) peak gets gradually broadened with the increase of $m_{ionomer}/m_{MXene}$ ratio, with increasing intensities in the low 2Θ range of 1.6-4° (see Figure 3.2(d)). Due to diffusion reasons, the intercalation is reasoned to start from the edge of the 2D nanosheets and then to the deep central locations. The broadening of the (002) peak signifies the enhanced intercalation with the increase of the ionomer dosage.

Those with high ionomer contents (I-MXene-3-6, I-MXene-4-2, and I-MXene-5-2) show two (002) peaks, with an additional lower-shifted peak at 2Θ of around 1.7° (corresponding to the enhanced interplanar *d*-spacing of 52 Å) beside the regular one (2Θ = 6.5°) seen with other I-MXenes. In particular, though weak, the (002) peak at 1.7° is the dominant one, with I-MXene-5-2 having the highest ionomer content. These indicate that, at high ionomer contents, the MXene sheets are effectively exfoliated and delaminated. Clearly, there is a loss of diffraction signal in the out-of-plane direction generated by exfoliation, and the nonplanar form of the nanosheets results in the broadening and weakening of the (002) peaks corresponding to in-plane diffraction.[117] Among various intercalated/delaminated MXenes reported to date, the 2Θ value of 1.7° for the (002) peak is the lowest. Prior to this work, the lowest 2Θ value reported for the (002) peak was about 2.3° for an alkylated MXene intercalated with di(hydrogenated tallow)benzyl methyl ammonium chloride.[126] These XRD results solidly confirm the successful intercalation of the ionomers within MXene sheets. Meanwhile, it can be concluded that increasing either the ionomer feed ratio or the ionic content of the ionomer is beneficial to the intercalation, and a nearly complete delamination of MXene sheets can be achieved with I-MXene-5-2 having the highest ionomer content.

Figure 3.3 shows and compares the SEM images of the Ti_3AlC_2 MAX phase, virgin unmodified MXene, and I-MXene-4-2 as a representative I-MXene sample. Etching converts solidly packed MAX phase (Figure 3.3(a)) to unmodified MXene with sheets loosely stacked on top of each other (Figure 3.3(b)). Intercalation of the ionomer between MXene sheets leads to more extensive exfoliation/delamination and creates higher *d*-spacings between layers in I-MXene-4-2. The well-exfoliated accordion-like morphology of I-MXene-4-2 can be seen in Figure 3.3(c). In Figure 3.3(d-f), some delaminated few-layer sheets are clearly observed.

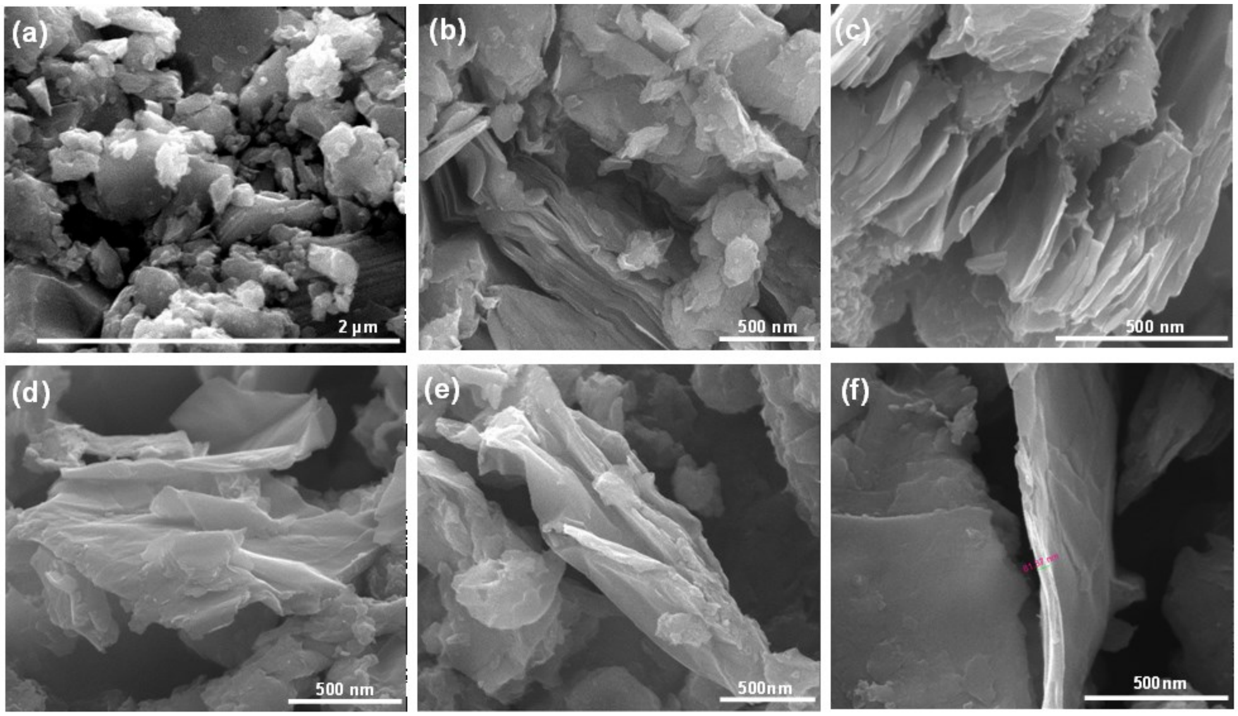

Figure 3.3 SEM images of (a) Ti_3AlC_2 MAX phase as received, (b) unmodified MXene after etching, (c-f) ionomer-modified MXene (I-MXene-4-2).

Figure 3.4 shows the transmission electron microscopy (TEM) images of virgin unmodified MXene and I-MXene-4-2. The particles of unmodified MXene are dense and not transparent under TEM. Layered 2D-sheet structures with an interplanar d-spacing of ca. 1 nm are observed in the unmodified MXene, which is in good agreement with the XRD results. The selected area electron diffraction (SAED) (Figure 3.4(c)) shows that the basal planes' atomic arrangement is identical to that in the parent MAX phase.[14] On the contrary, transparent 2D sheets are observed in I-MXene-4-2 under the electron beam (Figure 3.4(d, g)), confirming the successful delamination of MXene into few-layer nanosheets upon the intercalation with the ionomer at a high content. The flakes have a uniform surface without visible holes, particles, or defects. In agreement with the XRD result, large interplanar d-spacings in the range of 3.76 to 9.33 nm (see Figure 3.4(e,f)) are observed between the nanosheets, further confirming the efficient intercalation of the ionomer at a high volume between MXene sheets. In particular, the SAED pattern of an I-MXene-4-2 flake (Figure 3.4(i)) suggests that the basal planes' hexagonal structure is well retained after the ionomer intercalation. It shows interplanar spacings of 0.263 nm (0-110) and 0.153 nm (1-210), rendering lattice parameter a of 0.307 nm that is very close to that of Ti_3AlC_2 reported before.[113,120]

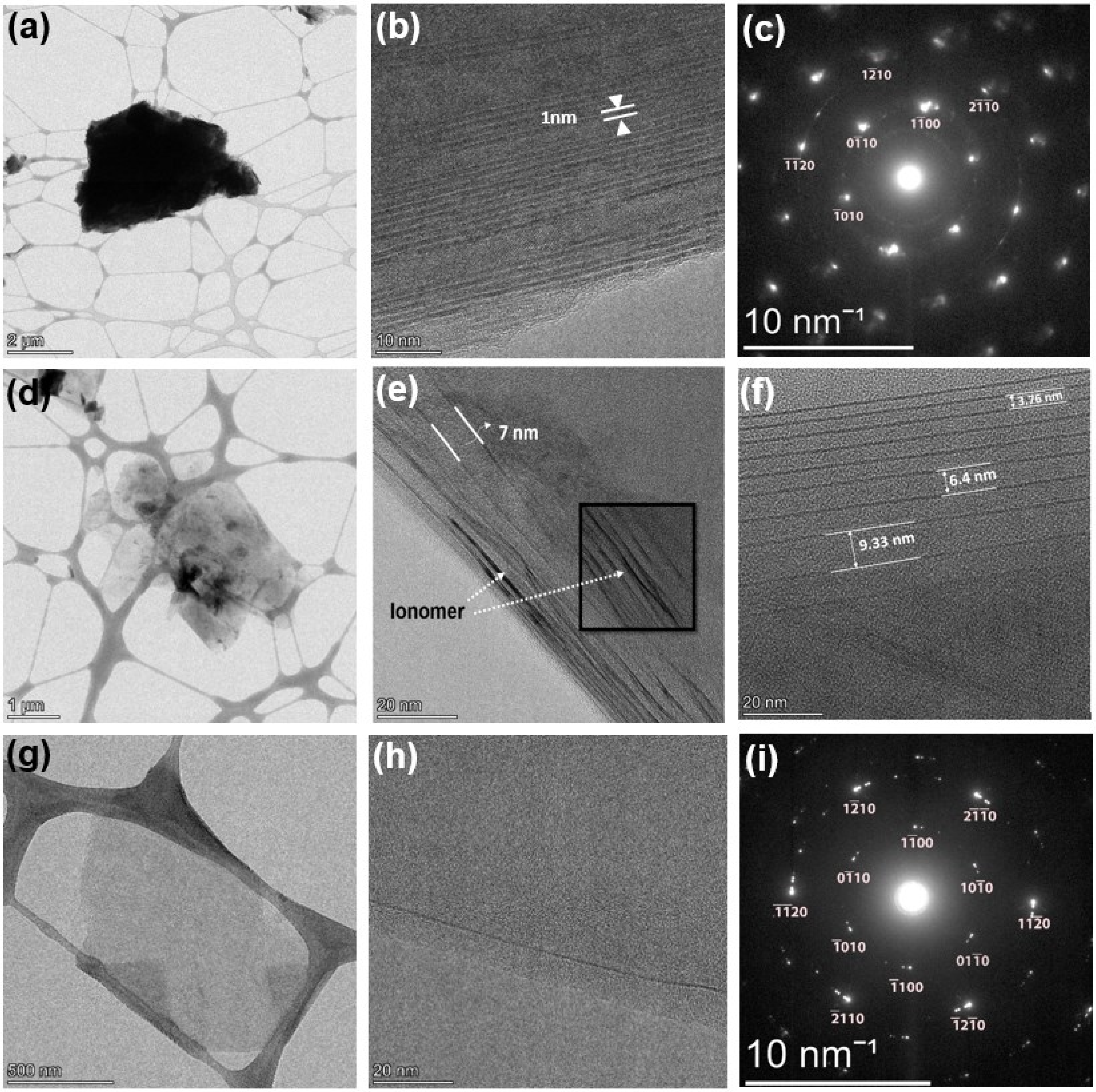

Figure 3.4 TEM images of virgin unmodified $Ti_3C_2T_x$ MXene (a-b) and ionomer-modified MXene, I-MXene-4-2 (d-h). The SAED patterns of unmodified MXene and I-MXene-4-2 are shown in (c) and (i), respectively.

DLS measurements have been performed on the dilute dispersions of I-MXenes in THF to determine their Z-average hydrodynamic size (d_p), polydispersity index (PDI) of size distribution, and ζ potential. The results are also summarized in Table 3.2. Relative to those of the unmodified MXene in water ($d_p = 288$ nm; PDI = 0.2), all the I-MXenes show much greater d_p values (generally within 680—1800 nm) and broader distribution (PDI= 0.3). The larger particle sizes and broader distributions suggest the presence of MXene aggregates as a result of the cross-linking effect of the multidentate ionomers. The ionomer modification also dramatically changes the ζ potential of the particles. Relative to the negative ζ potential of −38 mV of unmodified MXenes, the set of I-MXenes obtained with different ionomers at the same $(m_{ionomer}/m_{MXnen})_0$ ratio shows the increasing ζ potential from 30 to 48 mV, with the gradual increase of ionic content in the ionomers. These ζ potential data confirm the expected ionic binding of the cationic ionomers onto the negatively charged MXenes, which effectively changes the surface charge of the particles.

Films of I-MXene-4-2 as a representative I-MXene and unmodified MXene have been prepared by filtering their respective dispersions in THF, followed by drying. Water contact angle measurements were performed on the films (see Figure S3.3 in Supporting Information). The unmodified MXene film shows a water contact angle of 27.5°, which suggests its high hydrophilicity. On the contrary, due to the strong ionic bonding of the ionomer with a hydrophobic hyperbranched polyethylene shell, I-MXene-4-2 exhibits a high water contact angle of 125°, indicative of its strong hydrophobicity. This also confirms that the intercalation of the ionomer leads to the successful surface modification of the MXene sheets with the hydrophobic hyperbranched polyethylene segments. The dispersibility of $Ti_3C_2T_x$ MXene in various organic solvents has been evaluated in the literature and has been found to be closely related to the surface chemistry and the solvent polarity.[14] The presence of the hyperbranched polyethylene segments on the surface is expected to significantly improve the dispersibility of I-MXenes in nonpolar/low-polarity solvents relative to the unmodified MXene.

3.3.2 Dispersibility of I-MXenes in Various Organic Solvents

We have first studied qualitatively the dispersibility of I-MXene-4-2 as a representative ionomer-modified MXene of high ionomer content in 16 solvents, including nonpolar (hexane, cyclohexane, toluene, xylene, benzene), low-polarity (THF, chloroform, ethyl acetate), and polar solvents (water, ethanol, methanol, acetonitrile, DMSO, DMF, acetone, pyridine). A parallel comparison has also been made with unmodified MXene. For this purpose, dispersions of I-MXene-4-2 and MXene (2 mg mL^{-1}) have been prepared in the respective solvents, and their stabilities have been monitored over an extended period of 100 days in sealed vials. Figure 3.5

shows the photos of the dispersions taken after standing for different periods of time (up to 100 days), where the dispersions are arranged in the order of the decreasing solvent polarity from water to cyclohexane. Table S3.1 summarizes the physical-chemical properties of the solvents.

Uniform dispersions are achieved with both the unmodified MXene and I-MXene-4-2 in all the solvents right after sonication. The quick settling of the unmodified MXene can be seen shortly after 24 h of standing from its dispersions in the nonpolar solvents (benzene, toluene, xylene, hexane, and cyclohexane), as well as in DMSO and pyridine as two polar solvents, where the dispersions become transparent with the presence of the dark precipitate at the bottom. After 72 h, the MXene dispersion in chloroform also becomes transparent. After 10 days and 1 month, only MXene dispersions in six polar solvents (water, methanol, ethanol, acetonitrile, DMF, acetone) and one low-polarity solvent (ethyl acetate) are still stable, while nearly complete settling of MXene has occurred in all the other solvents. These are not surprising given the compatibility of unmodified MXene primarily to only selected highly polar solvents. After 100 days, stable dispersions of MXene are only seen in ethanol, acetonitrile, acetone, and ethyl acetate. The complete settling of MXene has occurred even in polar solvents, including water, methanol, and DMSO, with a change in the colour of the supernatant to light yellow because of the oxidation of MXene after long-standing.

On the contrary, I-MXene-4-2 shows stable dispersions in all the nonpolar and low-polarity solvents, as well as even in four polar solvents (acetonitrile, DMSO, DMF, acetone) after 72 h of standing. Though with the slight lightening in colour with those in acetone, benzene, and hexane, the dispersions are still stable even after 100 days. This is significant given the substantially extended period of time of standing. In the literature, the stability of dispersions of various modified MXenes has been commonly reported for a maximum of 30 days.[126,130] Though hyperbranched polyethylene homopolymer is soluble only in nonpolar or low-polarity solvents, the ionomers are dispersible to some extent in some polar solvents such as DMF and acetonitrile due to their possession of the polar ionic groups. This imparts desirably the dispersibility of I-MXene-4-2 in the four polar solvents herein, in addition to the nonpolar and low-polarity solvents.

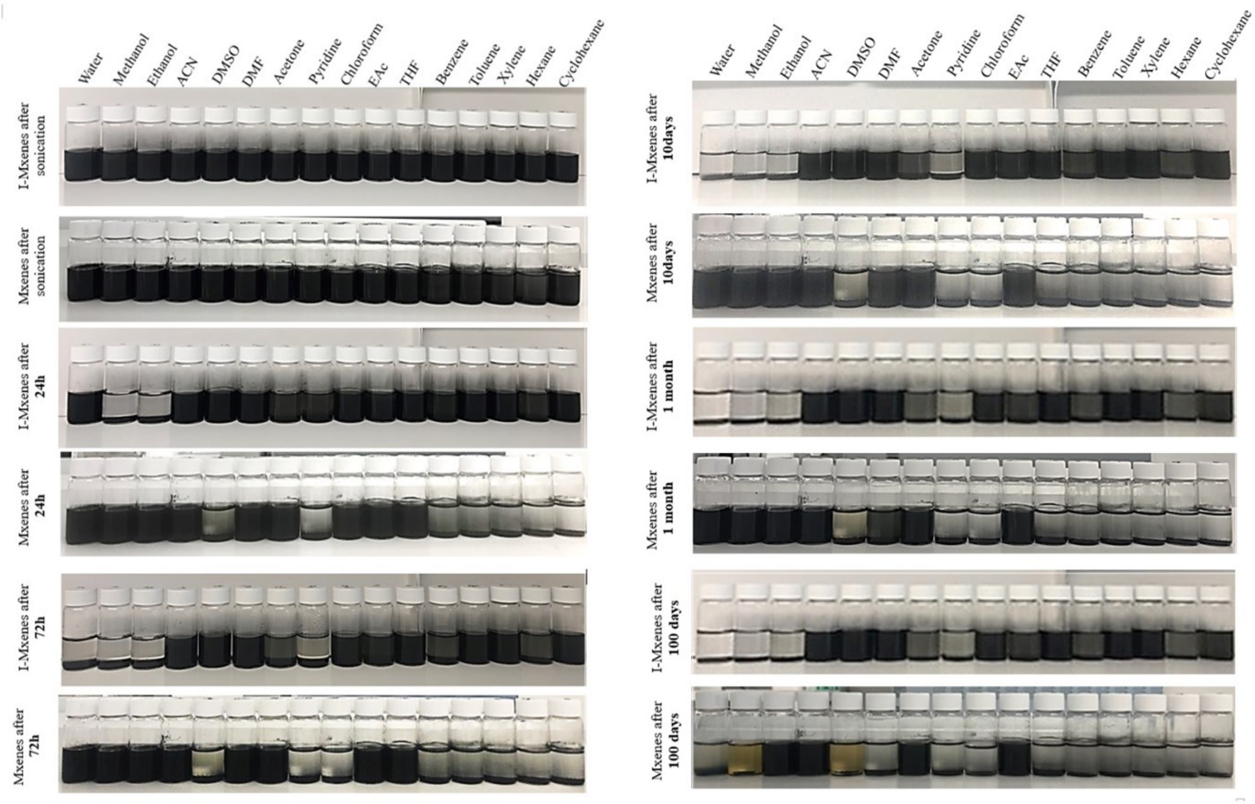

Figure 3.5 Photographs of dispersions of I-MXene-4-2 and unmodified MXene in various solvents after standing for different periods of time (right after sonication, 24 h, 72 h, 10 days, 1 month, and 100 days). Dispersions are arranged in the order of decreasing solvent polarity from left to right.

The stability of colloids, indicating the ability to withstand aggregation or sedimentation, can be evaluated with ζ potential.[143,144] The magnitude of the ζ potential indicates the degree of repulsion (electrostatic) between adjacent particles in the dispersion. It is well known that the solution has the highest stability when the ζ potential crosses a magnitude of 30 mV (+30 mV for positively charged particles and -30 mV for negatively charged particles).[145] Herein, the majority of the stable dispersions of I-MXene-4-2 obtained after 100 days of standing (except those in acetonitrile, benzene, and hexane) show high ζ potentials greater than +30 mV (see Figure S3.4 in Supporting Information), confirming their strong ability in resisting aggregation.

The highly stable dispersions of I-MXene-4-2 in low-boiling-point solvents like cyclohexane, THF, and chloroform, even after over 100 days, are desirable in many processing and application techniques. The use of such low-boiling-point solvents facilitates rapid solvent evaporation and thus expedites materials synthesis or device fabrication. On the other hand, the excellent stability in high-viscosity solvents like DMSO makes I-MXenes appropriate for some potential applications, such as spray coating and ink printing. It is worth emphasizing that unmodified MXene precipitates out quickly in DMSO only after 24 h, with the colour of the dispersion gradually changing to yellow due to oxidation, which was similarly observed by others.[126] This differs from some of the earlier reports where DMSO has been used as an intercalating agent for $Ti_3C_2T_x$ MXene.[120,2]

We now discuss the effect of the various solvents on the dispersibility of I-MXene-4-2. It has been well demonstrated that $Ti_3C_2T_x$ MXene has stable dispersion in polar solvents with high surface tension, high boiling point, and a high dielectric constant yield.[121,125] Surface energy is an essential factor that can influence the solubility/dispersibility of a 2D nanomaterial; a suitable solvent should possess a surface energy value close to that of the nanomaterial.[146,147] The Hildebrand solubility parameter, defined as the square root of the cohesive energy density and Hansen Solubility Parameters (HSP), has proven to be a powerfully practical way to quantitatively understand the solubility or dispersion of polymers, nanoparticles, and nanosheets. In the latest method, "*Like Dissolves Like*" can be well characterized with just three parameters, δ_D for dispersion (van der Waals), δ_P for polarity (related to dipole moment), and δ_H for hydrogen bonding. A combination of Hilderbrand and Hansen solubility parameters has been applied to predict particle stability in various colloidal environments.[148-151]

The Hildebrand solubility parameter is defined as the square root of the cohesive energy density (δ_T) (Eq 1):

$$\delta_T = \sqrt{\frac{\Delta H_v - RT}{V_m}} \qquad \textbf{(1)}$$

where ΔH_v, R, T, and V_m represent the heat of vaporization, gas constant, temperature, and molar volume of the condensed phase, respectively. A quantitative measurement of the cohesive properties of a polymer is the cohesive energy. The cohesive energy per unit volume is called cohesive energy density, which is frequently used in the coating industry to aid in the selection of solvents and to predict the compatibility of polymers. The sum of squares of three Hansen parameters should be equal to a square of the Hildebrand solubility parameter, which represents the total cohesive energy density (Eq 2).[121, 125]

$$\delta_T{}^2 = \delta_D{}^2 + \delta_P{}^2 + \delta_H{}^2 \qquad \textbf{(2)}$$

The Hildebrand and Hansen parameters of the solvents used in this study are presented in Table S3.2. It is worth mentioning that polypropylene and polyethylene have δ_D=18, δ_P=0, δ_H=1, and δ_D=16.9, δ_P=0.8, δ_H=2.8, respectively (Table S3.2).

Herein, UV-Vis absorbance measurements were taken on the I-MXene-4-2 dispersions in various solvents after 100 days to quantify their long-term dispersion stability with the use of absorbance per cell length (A/l) instead of concentration according to earlier studies on dispersions of 2D transition metal dichalcogenides,[150] and virgin MXene etched with HF and LiF/HCl.[125] From each UV-Vis spectrum (see Figure 3.6(a)), A/l at the position of the first visible peak at 775 ± 15 nm, depending on the solvent, is used for comparison. Plotting A/l versus the Hildebrand parameter (Figure 3.6(b)) suggests I-MXene-4-2 shows good dispersion in solvents with a Hildebrand solubility parameter of 14.9 to 24.8 MPa$^{1/2}$ with the peak at ~18 MPa$^{1/2}$ (for THF). It signifies that I-MXene-4-2 disperses best in solvents with a cohesive energy close to this value, as opposed to the optimal value of ~27 MPa$^{1/2}$ found for untreated MXene in polar solvents.[81, 82] Our results are in good agreement with the previously reported Hildebrand parameter for modified-MXene,[121,126,149] with the advantage of I-MXene-4-2 covering a wider range of nonpolar solvents (Figure 3.6(g)).

The correlations of A/l with Hansen solubility parameters δ_D, δ_P, and δ_H of the solvents used in this study are individually represented in Figure 3.6(c-e), respectively, along with a radar plot shown in Figure 3.6(f). For good solvents for I-MXene-4-2, δ_D is within a narrow range of 15.3─18.4 MPa$^{1/2}$, δ_P varies in a broad range from low to high (0─18 MPa$^{1/2}$), while δ_H is within a broad range from 0 to 11.3 MPa$^{1/2}$. Thus, a good solvent for I-MXenes covers from zero polarity (nonpolar) to moderately polar one (THF) and polar aprotic solvents. It is worth mentioning that THF can dissolve a wide range of nonpolar and polar chemical compounds and is miscible in water. Nonpolar aromatic solvents (like toluene) providing high-strength of dispersion interactions also work well in this system for dispersing I-MXenes. In particular, the inset in Figure 3.6(a) shows the Tyndall effect of the I-MXene-4-2 in THF, demonstrating its good dispersibility. Figure 3.6(f) compares the ranges of Hildebrand and Hansen parameters of the solvents where I-MXene-

4-2 well disperses with those previously reported in the literature for tetrabutylammonium hydroxide-modified MXene,[94] di(hydrogenated tallow)benzyl methyl ammonium chloride-modified MXene,[126] and unmodified MXene.[125] This comparison shows the broader range of nonpolar/low-polarity organic solvents where I-MXene-4-2 can well disperse relative to the two modified-MXenes reported in the literature.

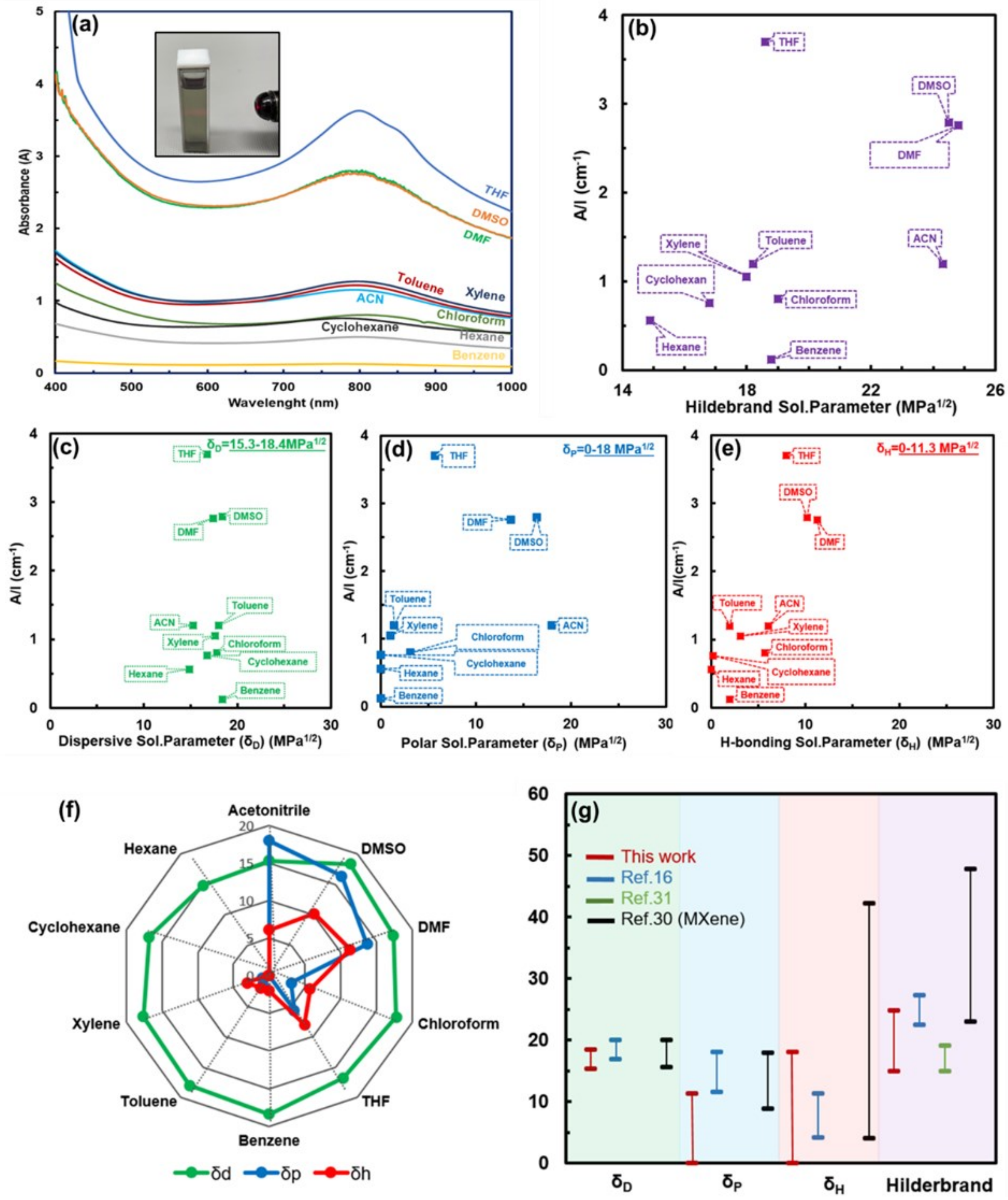

Figure 3.6 (a) UV-Vis absorbance spectra of I-MXene-4-2 in different organic solvents after 100 days, with the inset showing the Tyndall effect for I-MXene-4-2 dispersion in THF; (b) A/l (at 775 ± 15 nm) of the dispersions of I-MXene-4-2 vs. Hildebrand solubility parameters of the corresponding solvents; (c-e) relationships of A/l (at 775 ± 15 nm) of the dispersions with the Hansen solubility parameters of the solvents, dispersive, polar, and hydrogen bonding, respectively; (f) Hansen solubility parameters (δD, δP, and δH values; see Table S3.2) for each solvent; (g) comparison of Hildebrand and Hansen solubility parameters of the good solvents for I-MXene-4-2 with those reported for unmodified and modified MXenes in previous literature.[94,107,108]

We have further quantified the solubility of I-MXene-4-2 as a representative ionomer-modified MXene in four nonpolar/low-polarity solvents (chloroform, toluene, xylene, and THF) with the best dispersion stability. For this purpose, the UV-Vis extinction coefficients of I-MXene-4-2 in the four solvents have been measured. In the procedure, dispersions of I-MXene-4-2 in the four solvents (at 2 mg mL^{-1}) were prepared, following a quick centrifugation at 3500 rpm for 1 min to remove possible large particles. They were quantified for MXene concentration with TGA (0.95, 0.86, 0.92, and 1.05 mg mL^{-1} in chloroform, toluene, xylene, and THF, respectively). Different dilutions were prepared from the mother dispersions and were characterized with UV-Vis spectroscopy. The insets in Figure 3.7(a-d) show their UV-Vis spectra, with the absorbance peak maxima of the visible range at 792 nm, 773 nm, 761 nm, and 780 nm for chloroform, xylene, toluene, and THF, respectively. As per our earlier studies,[139,152], the ionomer should not have absorbance in the entire UV-Vis wavelength range at the concentrations used herein. Calibration curves have thus been constructed in Figure 3.7(a-d) by plotting the absorbance at the peak maxima in the visible region vs. MXene concentration (C_M), rendering the extinction coefficients 12.91, 16.05, 16.72, and 16.93 mL mg^{-1} cm^{-1} in chloroform, xylene, toluene, and THF, respectively. These correspond to the values for the dispersion comprised of a mixture of the multi-layered and delaminated single-/few-layered I-MXene-4-2 sheets.

With the dispersion of I-MXene-4-2 in THF, we have further obtained the dispersion fraction containing only the delaminated single-/few-layered flakes (MXene concentration, $C_M = 0.156$ mg mL^{-1} as per TGA) by removing the multi-layered sheets through centrifugation at 3500 rpm for 30 min (see Figure 3.7(f)). Figure 3.7(e) shows its UV-Vis calibration curve, along with the digital photo of the dispersion and the UV-Vis spectra of the various diluted dispersions. An extinction coefficient of 30.43 mL $mg^{-1}cm^{-1}$ is found for the delaminated I-MXene-4-2, which is significantly higher than that (16.93 mL $mg^{-1}cm^{-1}$) found above for the mixture of multi-layered and delaminated I-MXene-4-2 in THF. This is the first demonstration of the effect of layers on the extinction efficiency of the MXene structures. Meanwhile, according to DLS measurements, the delaminated I-MXene-4-2 shows a much smaller z-average particle size and a narrower particle size distribution compared to the mixture of multi-/few-layered I-MXene-4-2 in THF (see Figure 3.7(g)), confirming he significantly reduced number of 2D layers in the former.

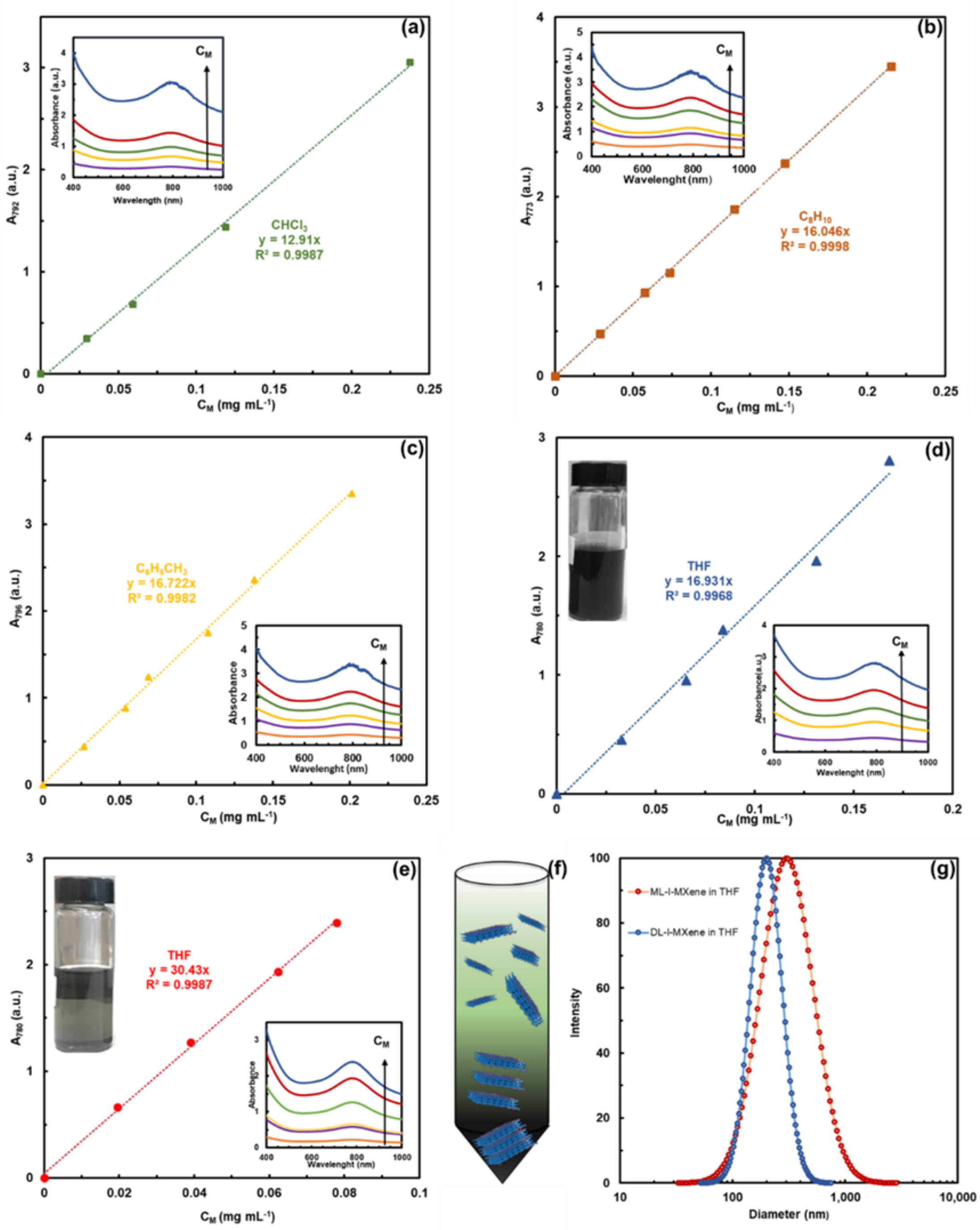

Figure 3.7 (a-d) UV−Vis calibration curves for I-MXene-4-2 in chloroform, xylene, toluene, and THF, respectively (sonicated for 30 min; centrifuged at 3500 rpm for 1 min), with the inset in each figure showing the absorption spectra of I-MXene-4-2 dispersions at different CM's and the photo for the dispersion in THF in (d); (e) UV-Vis calibration curve for delaminated single-to-few layered I-MXene-4-2 flakes in THF (sonicated for 30 min; centrifuged at 3500 rpm for 30 min),

with the inset showing the absorption spectra at different CM's and a digital photo of a dispersion; (f) a schematic of the separation of the delaminated single to few-layered I-MXenes from the multi-layered I-MXenes; (g) DLS particle size distributions of the multi-layered and delaminated I-MXene-4-2 in THF.

The extinction coefficients determined herein in the organic solvents are close to the value of 29.1 mL $mg^{-1}cm^{-1}$ reported for aluminum-oxoanion-functionalized MXene in water at 808 nm,[153] and 32.4 mL $mg^{-1}cm^{-1}$ for $Ti_3C_2T_x$ MXene in water.[154] The values are quite comparable to those required for state-of-the-art NIR photothermal materials with substantial optoelectronic properties. Furthermore, Li *et a*l. [155] demonstrated outstanding internal light-to-heat conversion efficiency (~100%) of multi-layered MXene, the extinction coefficient between 14.4 to 16.9 mL $mg^{-1}cm^{-1}$ at 785 nm. Changes in MXene synthesis methods,[140,141] different sizes, surface functional groups,[155] and MXene flakes can cause differences in the extinction coefficient.

With the corresponding extinction coefficients determined herein, the stable I-MXene-4-2 dispersions obtained after standing for 100 days in Figure 3.5 have been calculated to have the MXene concentrations (excluding the ionomer) of 0.06, 0.08, 0.07, and 0.21 mg mL^{-1} in chloroform, xylene, toluene, and THF, respectively.

To study the maximum concentration of MXene that can be stably dispersed in good solvents, we have further investigated the effects of the feed mass ratio of ionomer to MXene $[(m_{ionomer}/m_{MXene})_0$ on the final MXene concentration (C_M) in the dispersed colloids, by changing the concentration of the ionomer solution while at a fixed weight of MXenes. For this purpose, I3 has been used as the ionomer for the dispersion of MXene in THF and xylene, respectively, at a MXene feed concentration ($C_{M, F}$) of 3 mg mL^{-1}. Figure 3.8(a) shows the dependence of C_M on the I3/MXene mass ratio, which varies from 0 to 10. In both solvents, an increase in C_M is noted with the increase of the mass ratio from 0 to 0.5 and to 2, which should be attributed to the increased coverage of ionomer binding on the MXene surface and, thus, the higher exfoliation efficiency. At the mass ratio of 2, the highest C_M values of 2.04 and 0.87 mg mL^{-1} are achieved in THF and xylene, respectively, corresponding to 76% and 32%, respectively, of the feed MXene. The further increase of the mass ratio from 2 to 10, however, leads to a level off or even a slight decrease in $C_{M,}$ possibly resulting from the aggregation and precipitation of particles by cross-linking through the multidentate ionomers at the excess concentrations.

Figures 3.8(b, c) show the effect of $C_{M,F}$ on the C_M value of the resulting dispersions in THF and xylene, respectively, at the I3/MXene mass ratio of 2. Increasing $C_{M,F}$ from 1 to 50 mg mL^{-1} leads to increased C_M from 0.56 to 31.1 mg mL^{-1} in THF and from 0.2 to 14.6 mg mL^{-1} in xylene. In particular, about 60% of the feed MXene gets stably dispersed in THF following a simple, convenient modification with the ionomer. These results further confirm the high efficiency of the ionomers in rendering high-concentration MXene dispersions in the nonpolar or low-polarity solvents.

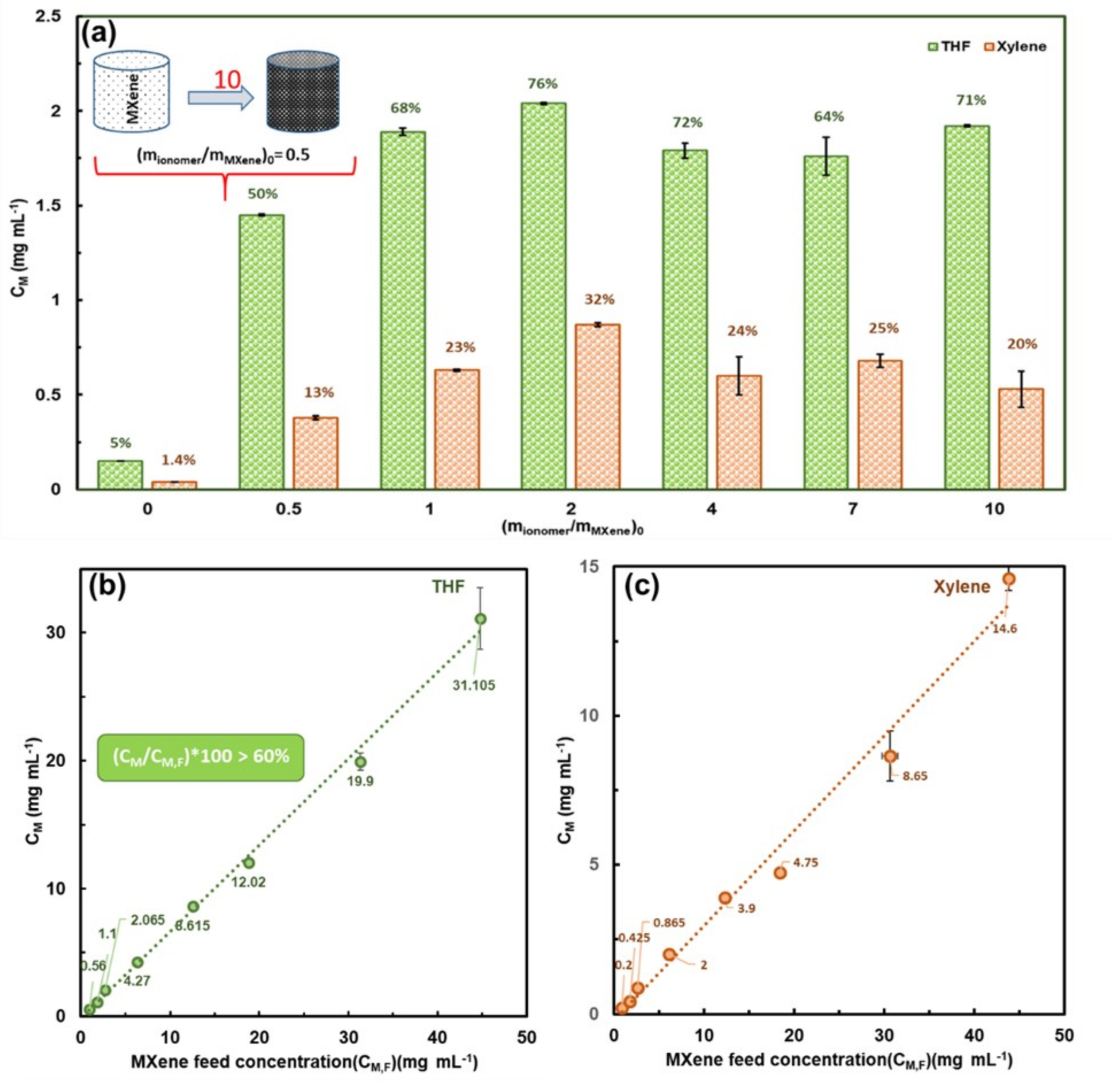

Figure 3.8 (a) The concentration of dispersed MXene (CM) as a function of I3/MXene feed mass ratio in THF and xylene, respectively, at MXene feed concentration (CM, F) of 3 mg mL-1, with the numbers on bars showing CM/CM, F (C M, F = MXene amount in each I-MXene-3 based on

TGA results); (b,c) MXene concentration (CM) as a function of different MXene feed concentrations (CM, F) in THF and Xylene, respectively.

3.3.3 Simultaneous Interfacial Modification and Phase Transfer of MXene Flakes

In addition to our above procedure for the synthesis of ionomer-modified MXenes, we have also conducted an alternative interfacial modification/phase transfer strategy that will further expand the toolbox of ionomer-functionalized MXenes. Convenient phase transfer of MXene from the aqueous phase to various water-immiscible nonpolar or low-polarity organic phases can be achieved with the use of an ionomer. To enable the phase transfer, the dark-coloured aqueous phase of MXene (20 mg in 10 mL) is placed in contact with a colourless organic phase (chloroform and toluene used herein for demonstration) containing dissolved I4 (40 mg in 10 mL) (see Figure 3.9(a) for the biphase mixtures prior to phase transfer). During the thorough mixing, the positively charged ionomer in the organic phase binds to the negatively charged surface of MXene at the liquid-liquid interface. Vigorous hand-shaking and sonication of the mixture increase the liquid-liquid interfacial area and promote the intercalation of the ionomers between MXene sheets, rendering the ionomer-modified MXene. Subsequent settling of the mixtures re-establishes the phase separation, along with the relocation of MXene to the organic phase under gentle stirring. As shown in Figure 3.9(b), the organic phases turn dark with no precipitates, while the aqueous phases become almost colourless following the phase transfer, indicating the complete transfer of MXene from the aqueous phase to the organic phase following the interfacial modification. Meanwhile, a volume expansion of the organic phases is seen, suggesting the swelling of MXene upon the successful ionomer intercalation. Moreover, the two-phase systems have been found stable over one year after the phase transfer.

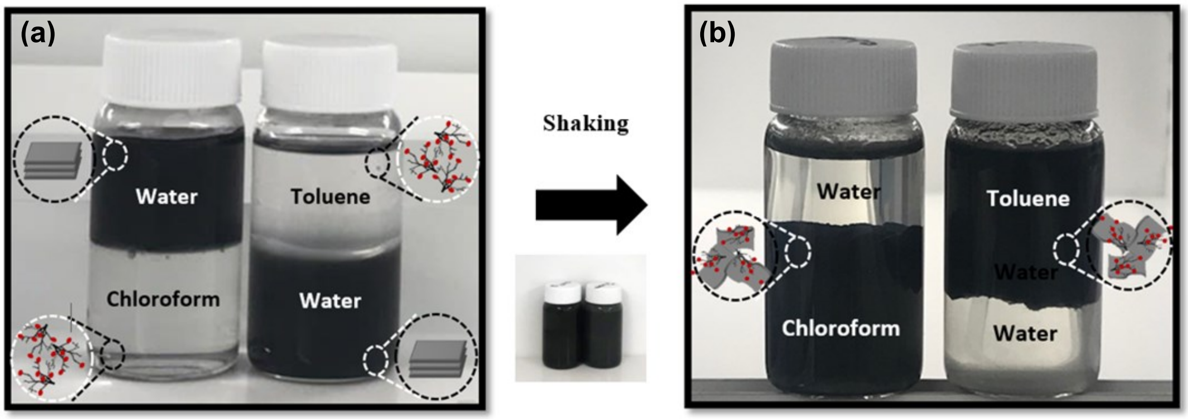

Figure 3.9 Phase transfer of $Ti_3C_2T_x$ MXene from the aqueous phase to the nonpolar or low-polarity organic phase (chloroform and toluene, respectively) containing I4.

3.3.4 Oxidation Stability of I-MXenes

When exposed to air and/or water, $Ti_3C_2T_x$ MXene oxidizes and degrades rapidly over days, resulting in the decomposition of the layered, 2D structure and the generation of titanium dioxide (TiO_2) and carbon (C).[156,157] This degradation by oxidation can be revealed with TEM and even direct observation of the colour change of the MXene dispersions from a black/dark green to a hazy white/brownish colour.[158,159] The oxidation of $Ti_3C_2T_x$ has been observed in all the media, but it is fastest in the liquid media and slowest in the solid media (including polymer matrice).[160] Various strategies have been explored to improve the oxidative stability of MXene. Compared to water, some organic solvents can prevent or slow down MXene oxidation due to the reduced oxygen concentration in the latter, but often with unstable MXene dispersibility. Storage of degassed $Ti_3C_2T_x$ MXene aqueous dispersions in closed argon-filled containers at 5 °C has been proposed,[143] although oxidation still occurs at a reduced rate. The carbon nano-plating technique has been used to modify the surface of $Ti_3C_2T_x$ MXene to stabilize it against oxidation for energy storage and conversion applications.[161] Other strategies include the addition of an antioxidant to aqueous MXene dispersions and the edge capping of 2D MXene sheets with polyanionic salts.[17] Despite these attempts, efficient strategies for preventing or restricting MXene oxidation remain lacking while critical for their processing, handling, and storage.

In addition to rendering their stable dispersion in various organic solvents, ionomer modification has been found to markedly improve the oxidative stability of MXene. To demonstrate this, aqueous dispersions have been prepared with the unmodified MXene and I-MXene-4-2, respectively, each at the MXene concentration of 3 mg mL^{-1}. After brief stirring, two dispersions (MXene and I-MXene-4-2) were stored in open-cap vials, and two others were kept in closed-cap vials, all at room temperature. The water volume of the open-cap vials was monitored and was replenished with fresh water over time to maintain the constant volume. In closed-cap vials, no degassing was conducted before or during the storage so that the MXene and I-MXene-4-2 dispersions were in contact with the headspace air in the vials. Vials were kept undisturbed for 100 days. Subsequently, the MXene samples were recovered from the dispersions and were dried in a vacuum oven for analysis with SEM and XRD.

The rapid oxidation of the unmodified MXene in the open-cap vial was clearly seen after 15 days, with the formation of white TiO_2 precipitate in the vial and a change of the colour of the dispersion from black/dark green to cloudy white (see Figure 3.10(b)). Meanwhile, for the unmodified MXene in the closed-cap vial for 100 days, SEM pictures (Figure 3.10(a)) demonstrate the occurrence of oxidation at the edge of MXene sheets with the formation of large quantities of small particles (size of around 80 nm), which is in agreement with previous works.[2, 156] It is generally considered that multi-layered MXenes are less prone to oxidation than single-layered nanosheets because of the decreased surface-to-volume ratio of the stacked structure.[159] But the observed fast oxidation of multi-layer sheets in the open-cap vial over the course of several days indicates its poor oxidative stability. It is worth mentioning that the oxygen solubility should be very low (around 8 mg L^{-1} at 25 °C) in the open-cap dispersion. In addition to the dissolved oxygen, water itself may likely play a significant role in oxidation.[146] The SEM images in Figure 3.10(b) reveal that the morphology of the I-MXene-4-2 flakes after 100 days in the open-cap vial is still intactly retained as the fresh sample seen in Figure 3.3 with smooth, clean surfaces. These images confirm the absence of TiO_2 particles and the inhibited oxidization. Clearly, the presence of the tightly surface-bound hydrophobic hyperbranched polyethylene efficiently protects MXene from contact with dissolved O_2 and water, which markedly decreases the propensity of MXene toward oxidation. Figure 3.10(c) compares the XRD patterns of the four samples. The patterns of I-MXene-4-2 samples in both open-cap and closed-cap vials are nearly identical to that of the fresh sample shown in Figure 3.2(c), with no TiO_2 peaks observed. On the contrary, both unmodified MXene samples following the oxidation study show distinct TiO_2 diffraction peaks, with the complete loss of the characteristic MXene peaks. While the oxidized MXene sample in the open-cap vial appears to be primarily rutile TiO_2 phase, that in the closed-cap vial shows a mixed phase of both rutile and anatase TiO_2.

Delaminated few-/single-layer MXene sheets generally show deteriorated oxidative stability compared to multi-layered MXenes, though with improved electrical performance, colloidal stability, and processability.[156] The delaminated I-MXene-4-2 has also been investigated herein for its stability when dispersed in THF. In an open-cap vial with regularly replenished THF, the dispersion remains stable under air for at least 30 days (see Figure S3.5 in Supporting Information). Our results solidly confirm the distinctly enhanced oxidative stability of MXene following the modification of the ionomers.

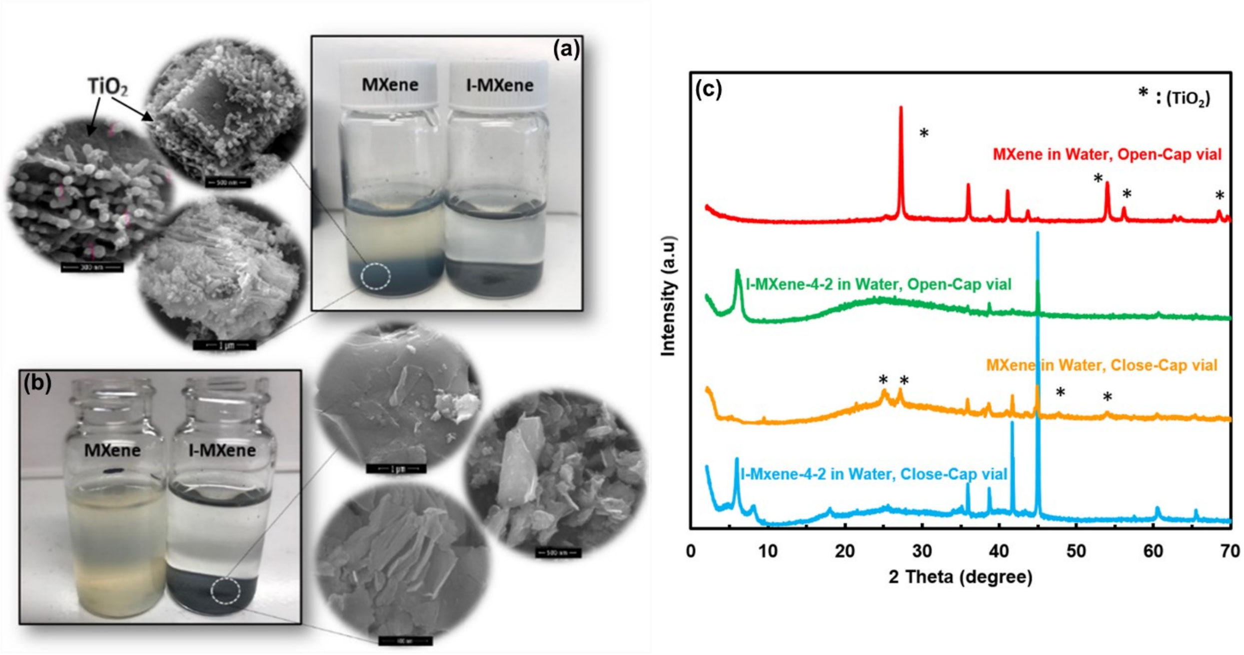

Figure 3.10 Oxidative stability of unmodified MXene and I-MXene-4-2: (a) photos of their aqueous dispersions (3 mg mL^{-1}) stored after 100 days in a closed-cap vial and SEM images of the recovered MXene sample; (b) photos of the aqueous dispersions (3 mg mL^{-1}) stored after 100 days in an open-cap vial and SEM images of the recovered I-MXene-4-2; (c) XRD patterns of the MXene and I-MXene-4-2 samples recovered from the four dispersions stored for 100 days (peaks

marked with an asterisk correspond to TiO_2 anatase (JCPDS card no. 21-1272), TiO_2 rutile (JCPDS card no. 21-1276), and TiO_2 brookite (JCPDS card no. 29-1360)).

3.4 The Ethylene-Olefin Copolymer (EOC) Nano-Composites with I-MXene-4-2 as Reinforcing Filler

The range of I-MXenes and virgin MXenes was further investigated for their dispersion quality and reinforcing performance as fillers in a commercial EOC elastomer by means of the polymer matrix. Given their structural similarity and high branching density, the EOC is chosen here because it should have good compatibility with the highly branched polyethylene skeleton in the ionomers (estimated at ca. 56 branches per 1000 carbons for EOC). Furthermore, it has low crystallinity, thus avoiding complications arising from changes in the crystalline structure upon the addition of nanofillers. Using the solution compounding method, all composites were formulated using the targeted dry MXene loading of 0.1 to 5 wt%. Composites were prepared with ionomer-modified MXene (I-MXene 4-2) and dried unmodified MXene at the same dry MXene loading for comparison. TGA characterization of the composites was conducted. Figure S3.6 shows their TGA curves. All the composites show that one-step weight loss occurs between 350 and 500 °C, which is attributed to the decomposition of EOC. In good agreement with the targeted value, the mass content of dry MXenes in all composites was quantified from the TGA remaining weight after 500 ˚C according to the stability of MXene in this range (Figure 3.2). The tensile mechanical properties of the various composites were characterized. The results are summarized in Table 3.3. Figure 3.11 compares Young's modulus, elongation at break, and Maximum tensile strength data of the various composites and neat EOC. It is known that the insertion of fillers in a polymer matrix has a reinforcing and stiffening effect, which is usually responded to by a significant loss in ductility.[135] While increases in the moduli of polymer matrices are generally expected upon the addition of reinforcing fillers, this reinforcement effect in polymer composites is typically accompanied by a significant reduction in elongation at the break because of the presence of large aggregates that create weak spots. Herein, upon adding only 0.1 wt% of I-MXene-4-2 filler, the modulus increases 16% (from 1.43 MPa to 1.66 MPa). The increasing trend in all the composites confirms the significant reinforcing effects of all the MXene-based fillers on the EOC. However, there is a clear difference trend between the composite compound with the modified and unmodified MXene with the same amount of composition. While the addition of 1%

pure MXene increases the modules by 14%, adding 1% I-MXene-4-2 has a double effect and causes the modulus to a 30% increase. The worst dissension is realized for mixing 5% virgin MXene with 5% I-MXene-4-2 (9% modulus increases against 44% increase, respectively). This is while a dramatic decrease (16%) in maximum tensile strength in 5% virgin MXene occurred versus a 22% increase in I-MXene-4-2. It is contributed to the better and more uniform dispersion of I-MXene in the EOC polymeric matrix. The TGA results also approve the more efficient dispersion of I-MXene versus virgin MXene(Figure S3.6 and Table 3.3).

The different extent of reductions in the elongation at break is recognized. The reduction is most severe in EOC composites with 1% MXene, and 5% MXene, by their values (1399 and 1807%, respectively) reduced nearly by half relative to that of neat EOC (2574%). On the other hand, composites prepared with the I-MXene-4-2 have maintained elongation at break (within the range of 1600 to 2512%). Relative to pure MXene, their higher elongation at break also confirms the improved dispersion of the modified MXenes in the matrix, along with the improved interfacial adhesion between the modified MXenes and the matrix following ionomer modification. These tensile data thus confirm the advantages of the ionomer modification in improving the reinforcing performance of MXenes relative to unmodified ones.

The ionomer modification makes the nano-fillers more compatible with the EOC matrix, thus minimizing filler aggregation and increasing the filler-matrix interface, presenting a more synergic effect. The significant improvement caused by ionomer modification upon the dispersibility of the modified MXenes in EOC relative to the unmodified MXenes is expandable for other polymers, especially polyolefine matrixes.

Table 3.3 Thermal and Mechanical Properties of EOC and Its Composites with virgin MXene and I-MXene-4-2

Composite	**Dry MXene Content(wt%)**[a]	**σ_{max}**[b] **(MPa)**	**ε_{max}**[b] **(%)**	**Moduluse** [b] **(MPa)**
Neat EOC	0	2.5	2574	1.43
EOC+1% MXene	1	2.26	1399	1.63
EOC+5% MXene	3.5	2.09	1807	1.56
EOC+0.1% I-MXene-4-2	0.1	2.28	2337	1.66
EOC +0.2% I-MXene-4-2	0.2	2.44	1846	1.75
EOC+0.5% I-MXene-4-2	0.5	2.37	1600	1.86
EOC +1% I-MXene-4-2	1	2.58	1874	1.86
EOC +2% I-MXene-4-2	2	2.5	1961	1.94
EOC +5% I-MXene-4-2	4.8	3.04	2512	2.06

[a] Based on TGA results- The weight percentage of dry MXene in the composites after 500°C

[b] Maximum tensile strength (σ_{max}), elongation at break (ε_{max}), and Young's modulus determined during tensile tests at 500 mm min^{-1}.

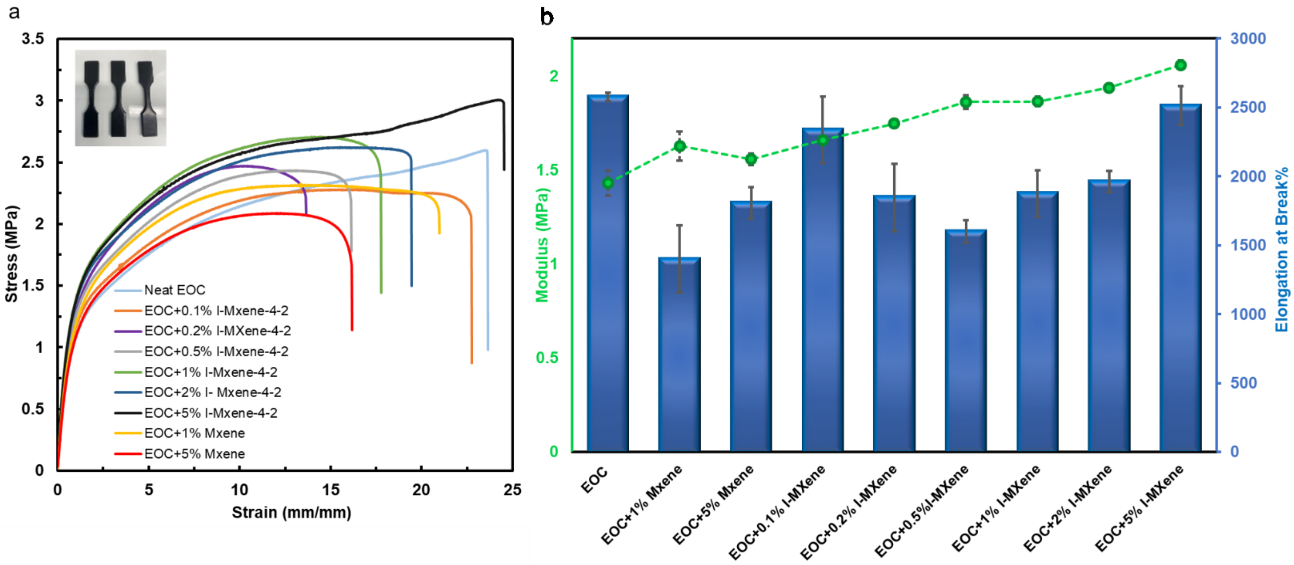

Figure 3.11 (a)Tensile strength vs. strain curves of neat EOC and various composites with MXene and I-MXene-4-2; (b) comparison of Young's modulus and elongation at break of neat EOC and various composites with MXene and I-MXene-4-2 (It comes as I-MXene in graph).

3.5 Conclusion

In summary, we have demonstrated the efficient synthesis of a range of ionomer-modified MXenes, I-MXenes, with the use of hyperbranched polyethylene ionomers designed with quaternary ammonium ions as the intercalants. The ionic interactions between the positively charged quaternary ammoniums and the negatively charged MXene surface facilitate the highly efficient intercalation of the ionomers within the MXene sheets. I-MXenes show significantly enhanced interlayer spacings (as high as 70─90 Å) relative to the unmodified MXene (about 11 Å). Increasing the ionic content in the ionomers, or the ionomer/MXene feed mass ratio $(m_{ionomer}/m_{MXnen})_0$ ratio, leads to the increased ionomer content in I-MXenes and increased interlayer spacing. The surface-binding of ionomers renders I-MXenes with hydrophobic surface properties and stable dispersibility in a range of nonpolar/low-polarity solvents (benzene, toluene, xylene, hexane, cyclohexane, THF, chloroform, ethyl acetate), as well as some polar solvents (acetonitrile, DMSO, DMF, acetone). In these solvents, the dispersions of I-MXene-4-2 with moderate ionic content are stable for 100 days. With THF as the solvent, the dispersions of I-MXene-4-2 at a concentration as high as 31.1 mg mL^{-1} can be achieved. Meanwhile, I-MXene-4-2, as a representative I-MXene, shows outstanding oxidative stability due to the presence of the tightly bound hyperbranched polyethylene protecting layer, with minimum oxidation observed for its dispersion in water under open air for 100 days. This modification strategy thus facilitates the processing and handling of MXene in nonpolar/low-polarity solvents and significantly expands their applications.

Chapter 4 Pillar-Structured $Ti_3C_2T_x$ MXene with Engineered Interlayer Spacing for High-Performance Magnesium-Ion Batteries

The chapter is adapted from a manuscript accepted in *Small Methods:* Pillar-Structured $Ti_3C_2T_x$ MXene with Engineered Interlayer Spacing for High-Performance Magnesium-Ion Batteries by **Raisi, B**.; Liu, X.; Rahmatinejad, J.; Ye, Z., *Small Methods,* **2024**, 2400004.

Abstract

Two-dimensional (2D) $Ti_3C_2T_x$ MXene has attracted significant attention in non-lithium-ion batteries due to its excellent electrical conductivity, high volumetric capacity, and ability to accommodate intercalants. Rechargeable magnesium-ion batteries (MIBs) with Mg metal anodes are noted for their high theoretical energy density, potential safety, earth abundance, dendrite-free Mg^{2+} plating/stripping mechanism on the anode side, and low cost. Nevertheless, owing to the large polarity of divalent Mg^{2+} ions, the insertion of Mg^{2+} into the MXene layers suffers from sluggish kinetics, which limits the performance for storage of Mg^{2+} ions. Herein, we demonstrate a simple self-assembly strategy to achieve high magnesium ion storage capability with pillar-structured $Ti_3C_2T_x$ MXene by intercalating a hyperbranched polyethylene ionomer containing quaternary ammonium ions within MXene nanosheets. The ionomer intercalation/modification leads to the expansion of interlayer spacing of $Ti_3C_2T_x$ MXene to more than 5 nm with a 400% increase relative to the unmodified MXene and, meanwhile, improves its affinity to low-polarity THF-based electrolyte due to the hydrophobic hyperbranched polyethylene-skeleton of the ionomer. In consequence, the delaminated ionomer-modified MXene shows significantly improved electrochemical performance as a cathode material for Mg batteries, with the reversible intercalation charge-storage mechanism demonstrated. It shows a promising cycling stability with a capacity retention of 86% after 400 cycles at 200 mA g^{-1}, as well as the outstanding high-rate performance with a capacity of 110 mAh g^{-1} retained at 1,000 mA g^{-1} (52% of retention) relative to 213 mAh g^{-1} at 20 mA g^{-1}. This work offers a unique strategy on the engineering of 2D MXene materials for applications in electrochemical energy storage.

4.1 Introduction

Rechargeable lithium-ion batteries (LIBs) have dominated today's electrochemical energy storage market owing to their comprehensive performance.[162] However, the broad use of LIBs for electrical energy storage is restricted by the uncertainty of limited lithium supply, high production costs, and safety issues. Therefore, developing new alternative battery technologies is crucial for sustainable energy storage.[162] Alternatively, post-lithium ion batteries (NLIBs) based on other alkali metal ions (Na^+, K^+) and multivalent metal ions (Zn^{2+}, Mg^{2+}, Al^{3+}) have attracted tremendous attention.[163] Among these, rechargeable magnesium batteries (RMBs) are regarded as one of the promising batteries attributable to the high volumetric theoretical capacity of 3833 mAh cm^{-3} and theoretical specific capacity of 2205 mAh g^{-1} of magnesium metal anodes. In addition, magnesium is abundant in the earth's crust; its lower price versus higher oxidative stability than lithium[164] and dendrite-free nucleation/growth during cycling make it safer with reversible deposition in several electrolytes.[165] Since the pioneering work conducted by Aurbach *et al.*[166] in 2000, RMBs are expected to be a potential candidate for large-scale energy storage systems. [162, 167-173] Nevertheless, many challenges exist with RMBs, such as the complex sluggish diffusion of Mg^{2+} in solid-state electrode materials due to its unique divalent nature[174] and effective ion radius[175], and the compatibility of the electrolyte with Mg metal anodes.[173] The developments of novel cathode materials facilitating faster Mg^{2+} insertion and electrolytes favouring rapid Mg^{2+} solvation are the main strategies addressing the challenges.[169, 176] Currently, few cathode materials are capable of rapid Mg-ion insertion and extraction at room temperature.[174]

Among pioneering works that have been devoted to developing RMBs cathode materials, materials of layered structures have recently gained much interest[164] for the construction of elaborate cutting-edge cathodic electrode materials. However, the layered structure is often subject to structural degradation and collapse during cycling, severely restricting their applications. [164, 167] MXenes, as a new class of 2D layered transition metal carbides and nitrides, are attracting particular interest in this field due to their excellent conductivity, large surface area, and high volumetric capacity.[163] MXenes are generally produced by selectively removing the "A" layer from their parent MAX phases expressed as $M_{n+1}AX_n$ (n = 1, 2, 3, or 4), where "M" represents the early transition metal (e.g., Ti, V, Nb, Mo), "A" is mostly 13 and 14 group element (e.g., Al, Si, Ga), and "X" is carbon and/or nitrogen, respectively.[113] The general formula of MXene is denoted as $M_{n+1}X_nT_x$, where T_x represents the functional groups such as —OH, —O, and —F generated during the etching process. Despite its layered structure, MXene, however, still suffers from the sluggish kinetics of divalent or multivalent metal ions (such as Mg^{2+}) during intercalation/deintercalation processes.[177] The other main challenge with MXene is restacking, which causes hindered ion accessibility and profound volumetric change during the cycling process.[50]

The first report on MXenes as cathode materials dated back to 2016 by Byeon *et al.*[178] Therein, negligible capacities[179] (~105 mAh g^{-1} at 0.01A g^{-1}) were reported for the freestanding film of a delaminated $Ti_3C_2T_x$/carbon nanotube composite cathode for magnesium-ion batteries (MgIBs) in conventional APC (all-phenyl-complex)-THF electrolyte. Zhao *et al.* demonstrated that the as-prepared Mg2+ pre-intercalated porous MXene films delivered a capacity of 140 mAh g^{-1} at 0.1 A g^{-1} in APC electrolyte, which sharply decreased to 50 mAh g^{-1} at the 20th cycle.[180] They showed that the intercalation with Mg^{2+} increases the interlayer spacing from 13.6 to 15.5Å. Xu et al., by pre-intercalating cetyltrimethylammonium bromide (CTAB) between MXene sheets, reduced the migration energy barrier of Mg atoms and achieved a reversible capacity of 100 mAh g^{-1} at 0.05 A g^{-1}.[181] Subsequently, sandwich-structured MXene/carbon nanosphere hybrid samples via electrostatic self-assembly technology[182] and MoS_2/MXene petal-like hybrid nanosheets as MXene/2D hybrid models[183] have also been applied for MgIBs. Indeed, for the last one, the presence of MXene significantly improved the electrical conductivity of MoS_2 for high-capacity utilization. [183] Recently, by introducing 40% of polyaniline into the MXene matrix (PANI/Ti_3C_2 composite) to open the ion transport channel for Mg-ion, a specific capacity of 132.2 mAh g^{-1} at 0.05 A g^{-1} is achieved with 70.3% retention after 20 cycles.[184] Nevertheless, within the aforementioned works, the capacities and capacity retentions achieved in the literature works with the intercalated MXenes are still far from being satisfactory, with significant room for improvement. The main challenge remains to achieve reversible insertion and extraction of magnesium ions between MXene sheets at high capacity with the maintained stability of MXene cathode materials over extended charge/discharge cycles. Particularly, magnesium-ion insertion and extraction can result in structural changes in the MXene materials, which over time can contribute to an eventual reduction in battery capacity, cycling stability, or rate performance.

Herein, we demonstrate for the first time the use of ionomer-modified MXene composites by a self-assembly method as the cathode materials for MgIBs. In this strategy, the specially designed hyperbranched polyethylene ionomers bearing positively charged quaternary ammonium groups on a hydrophobic polyethylene backbone are employed for the modification of $Ti_3C_2T_x$ MXene, where the ionomers tightly bind onto the negatively charged surface of MXene nanosheets. Such a modification has been shown in our earlier study to markedly expand the interlayer spacing of MXene sheets and adjust their surface properties, rendering their stable, highly concentrated dispersions in nonpolar or low-polarity organic solvents along with significantly enhanced oxidation stability.[185] We reason the significantly expanded interlayer space between MXene sheets following ionomer intercalation will promote ion transport and increase insertion sites for Mg-ions, thus leading to improved electrochemical performance as cathode materials. Herein, a systematic study has been undertaken on the structure and electrochemical performance of the ionomer-modified MXenes as cathode materials for MgIBs.

4.2 Experimental

4.2.1 Chemicals and Materials

All manipulations involving air- and/or moisture-sensitive materials were conducted in an argon-filled glovebox or by using Schlenk techniques. The ternary titanium carbide (Ti_3AlC_2) powders with a size ≤40 µm as the MAX phase were provided by Y-Carbon Ltd. (Ukraine) and were used as received. According to the supplier, they contained some impurities, including 5-10 wt% of TiC and 1-5 wt% of Al_2O_3. The hyperbranched polyethylene ionomers containing quaternary ammonium ions were synthesized in our earlier paper.[185] Cetyltrimethylammonium bromide (CTAB, ≥98%) was obtained from Sigma-Aldrich.[135] Deionized (DI) water was obtained using a Milli-Q water purification system. All other solvents or reagents were obtained from either Sigma-Aldrich or Fisher Scientific and were directly used as received.

4.2.2 Synthesis of the Multi-layered $Ti_3C_2T_x$ MXene (ML-MXene)

In a fume hood, the etchant was prepared by gradually adding 1.6 g of LiF to 20 mL of 9 M HCl in a 125 mL Teflon beaker with a lid.[8, 132] Following the complete dissolution of LiF, 1 g of Ti_3AlC_2 (MAX) powder was slowly added over the course of 10 min to the etchant solution. The reaction mixture was stirred at 40 °C for 24 h. After that, the acidic mixture was centrifuged at 3500 rpm, and the supernatant was removed, followed by the addition of fresh distilled water to wash the sediment. The washing-precipitation cycles were repeated until the pH of the supernatant was between 5 and 6. The product was collected, dried overnight at 70 °C in a vacuum oven, and grounded for further use. The resulting fine powders are multi-layered MXene, termed as ML-MXene.

4.2.3 Synthesis of the Delaminated $Ti_3C_2T_x$ MXene (DL-MXene)

The clay-like ML-MXene was dispersed in a large amount of distilled water and sonicated in an ice bath for 10 min. The suspension was centrifuged at 3500 rpm for an hour to separate the delaminated few- and single-layer MXene sheets from multi-layer MXene or possible un-etched MAX phase. The homogeneous dark-green supernatant containing delaminated MXene was collected, dried overnight in a vacuum oven at 70 °C, and grounded. The resulting fine powders are delaminated MXene, termed as DL-MXene.

4.2.4 Preparation of the Ionomer-Modified DL-MXene (I@DL-MXene)

Typically, a hyperbranched polyethylene ionomer at the prescribed amount was dissolved in 40 mL of THF. Afterward, the dispersion of MXene in DMF (10 mg in 0.5 mL) was added dropwise into the ionomer solution under bath sonication. The ionomer to MXene feed mass ratio was controlled at 2:1 or 3:1. The resulting dispersion was further hand-shaken. Subsequently, the dispersion was centrifuged at 10,000 rpm for 20 min, and the sediment was thoroughly dispersed in 40 mL of fresh THF and then centrifuged. The redispersion-centrifugation cycle was repeated 3 times to remove the excess non-intercalated ionomer. Finally, the sediment was dried overnight at *ca.* 70°C under vacuum to render the ionomer-modified MXene, termed as I@DL-MXene-x-y, with x noting for the ionomer (I3 or I5) used and y indicative of the ionomer/MXene mass ratio. For the purpose of comparison, the ionomer (I5)-modified multi-layered MXene sample at the ionomer/MXene ratio of 2, I@ML-MXene-5-2, was also prepared as described in our previous study. In addition, two cetyltrimethylammonium bromide (CTAB)-modified DL-MXenes, termed C@DL-MXene-0.2 and C@DL-MXene-2, were similarly prepared by replacing the ionomer with CTAB as a small molecular analogue at CTAB/MXene feed mass ratio of 0.2 and 2, respectively, in fresh DI water instead of THF.

4.2.5 Characterizations and Measurements

Thermogravimetric analysis (TGA) was carried out on a TA Instruments Q50 thermogravimetric analyzer. Measurements were performed under a N_2 atmosphere at a continuous flow of 60 mL min^{-1} through the sample furnace and a flow of 40 mL min^{-1} through the balance compartment. In a typical measurement, the sample (*ca*. 5 to 10 mg) was heated from room temperature to 700 °C at 10 °C min^{-1}. Dynamic light scattering (DLS) measurements of the dilute dispersions (*ca.* 0.1 mg mL^{-1}) of the various MXene samples for their hydrodynamic particle size and ζ potential were performed on a Brookhaven NanoBrook Omni Instrument at 25 °C. Each sample was measured three times, and the average values were used. Wide-angle X-ray diffraction patterns of the MXene and ionomer-modified MXenes samples were collected on a Rigaku SmartLab SE X-ray diffractometer with Cu Kα radiation at room temperature. Scanning electron microscopy (SEM) was carried out on an FEI Quanta 450 Environmental Scanning Electron Microscope (FE-ESEM). A thin platinum layer was coated on the samples prior to the imaging. The TEM images were captured with a Thermo Scientific Talos 200X transmission electron microscope operating at 200 kV. Specimens for TEM observation were prepared by dispersing powders of the corresponding materials (pristine MXene or ionomer-modified MXenes) in THF by bath sonication, followed by the deposition of a few drops of dispersion on a carbon-coated copper mesh grid. The grid was dried in the air prior to the TEM characterization.

4.2.6 Electrochemical Tests

To fabricate the working electrodes, slurries were prepared by mixing each MXene sample (including DL-MXene, I@DL-MXene, I@ML-MXene, C@DL-MXene), Super-P conducting carbon, and PVDF (polyvinylidene fluoride) as a binder at a mass ratio of 60: 30: 10 in N-methyl-2-pyrrolidinone (NMP). The homogeneous slurry was coated on carbon paper disks followed by drying at 65 ℃ for 5 h and then at 40 ℃ in a vacuum oven overnight. The mass loading of the active material (virgin MXene) on each electrode was about 1.0-2.0 mg cm^{-2}. Mg battery cells were assembled as coin cells (CR2032 type) in an argon-filled glove box, each with an Mg disc as the anode, a Whatman glass fibre membrane as the separator, and 0.4 M $(PhMgCl)_2$-$AlCl_3$/THF (APC) as the electrolyte. The APC electrolyte was formulated by mixing 0.4 M phenyl magnesium chloride (a Lewis base) in tetrahydrofuran (2 M PhMgCl in THF, Aldrich, 99%) solution with 0.2

M aluminum trichloride ($AlCl_3$, Aldrich 99.999%) in THF (Aldrich, inhibitor-free, anhydrous) in an argon-filled glovebox.[180] The obtained electrolyte solution was vigorously stirred overnight before use.

Galvanostatic charge/discharge (GCD) tests were performed on a commercial battery testing system (Land®, CT2001A, China) within the voltage window of 0.01/0.1 to 2.0 V (vs. Mg/Mg^{2+}). Current density and specific capacity were calculated based on the mass of virgin MXene in the cathodes. Cyclic voltammetry (CV) measurements were recorded on a Metrohm Autolab PGSTAT128N electrochemical workstation at a scan rate of 0.2 mV s^{-1}. Electrochemical impedance spectroscopy (EIS) measurements were performed over the frequency range of 100 kHz to 0.01 Hz with an AC amplitude of 50 mV.

4.3 Results and Discussion

In the present study, two hyperbranched polyethylene ionomers synthesized in our earlier paper, I3 and I5, containing quaternary ammonium ions at 1.03 and 2.87 mol%, respectively,[185] are employed for the modification of $Ti_3C_2T_x$ MXene. Both ionomers were synthesized by Pd—diimine-catalyzed direct copolymerization of ethylene with an ionic liquid comonomer, which was detailed in our earlier papers.[135]. Herein, both ML-MXene with a multi-layer sheet structure and DL-MXene containing few- or single-layer sheets are used as the MXene precursors, with the latter expected to have better ion transport properties due to the widened ion transport passage as a result of its few-layer structure. The schematic synthesis of ionomer@MXene nanocomposites by an electrostatic self-assembly approach is illustrated in Scheme 4.1. As elucidated in our earlier paper,[185] the surface of MXene nanosheets is negatively charged due to their surface terminations (–O, –OH, and –F). The ionomer containing multiple quaternary ammonium groups per chain binds to the surface of MXene nanosheets through strong electrostatic interactions. This self-assembly strategy is simple and convenient without the use of high temperature or high energy. To replicate and support our previous findings[185] regarding ionomer ions contents effect on DL-MXene exfoliation/delamination, the modification of DL-MXene has been performed with the two ionomers at different ionomer/MXene mass ratios (2 and 3), rendering two nanocomposites, I@DL-MXene-5-2 and I@DL-MXene-3-3, respectively, with the first number indicating the ionomer used and the second number indicating the ionomer/MXene feed mass ratio. For the purpose of comparison, I@ML-MXene-5-2 has also been synthesized with ML-MXene.[185] Additionally, the modification of DL-MXene has also been performed with CTAB, as a small-molecular analogue of the ionomers to render C@DL-MXene-0.2 and C@DL-MXene-2 (at CTAB/MXene feed mass ratio of 0.2 and 2, respectively). CTAB-intercalated DL-MXenes have been demonstrated to show improved electrochemical performance, compared to unmodified ML-MXene, as cathode materials for MgIBs.[181] They are included herein as the control samples to elucidate the effects of the intercalation of ionomers as the macromolecular intercalants on the electrochemical performance of the modified MXenes.

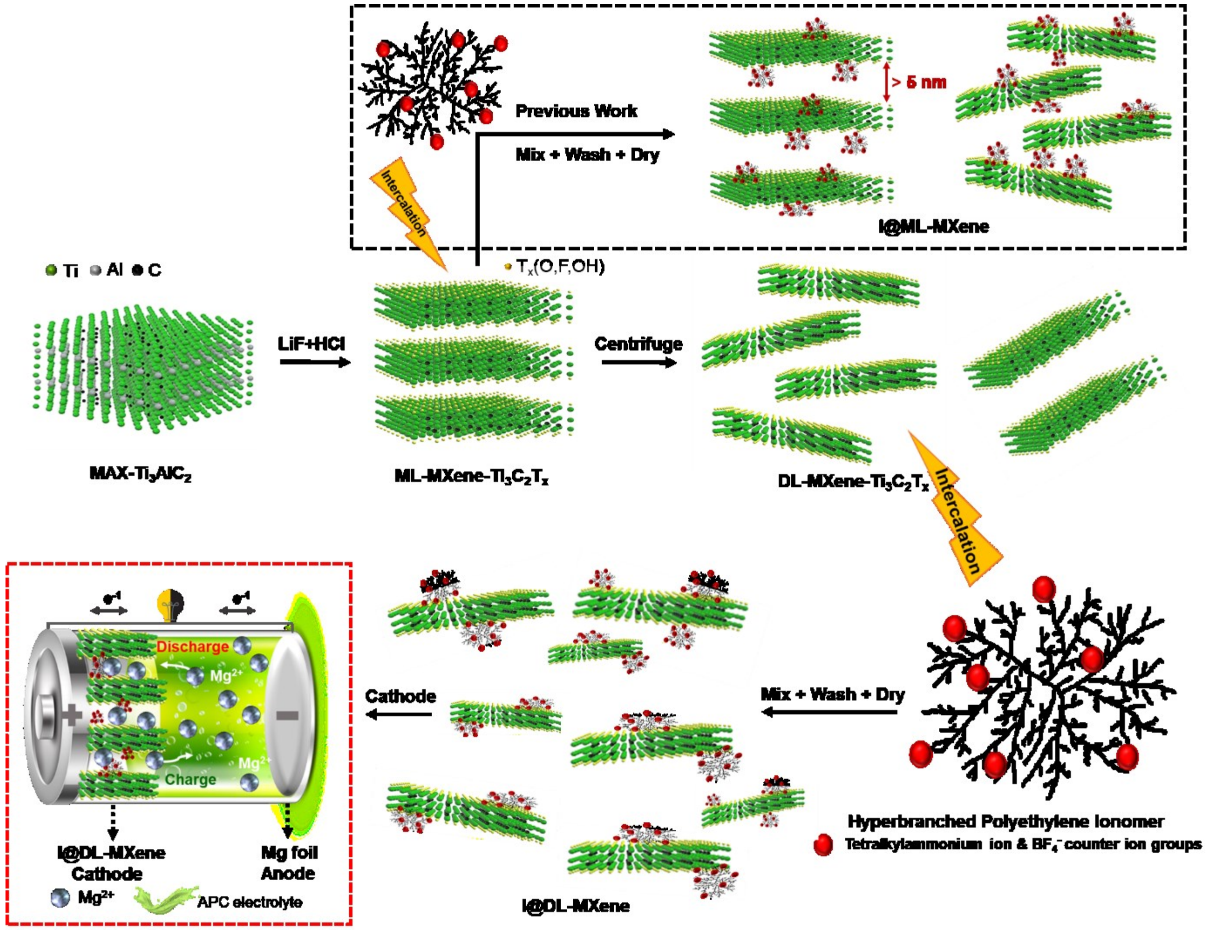

Scheme 4.1 Schematic illustration of the synthesis of I@DL-MXenes as cathode materials for the magnesium-ion battery.

The modified MXenes have been characterized with TGA to quantify the content of the corresponding modifying agent (ionomer or CTAB). Figure 1a shows the TGA curves of I@DL-MXene-3-3 and I@DL-MXene-5-2, along with those of ionomers (I3 and I5); unmodified virgin

DL-MXene, pure CTAB, and C@DL-MXene samples. Ionomers start to decompose at 280 °C with a nearly complete weight loss at 480 °C. Unmodified DL-MXene exhibits good stability with no considerable weight loss up to 600°C. Both I@DL-MXene samples exhibit a one-step weight loss within 280—480 °C, attributable solely to the decomposition of the corresponding ionomer. The mass contents of the ionomers/CTAB in the modified DL-MXenes have thus been quantified from the weight loss and are summarized in Table S4.1. The ionomer contents in I@DL-MXene-3-3 and I@DL-MXene-5-2 are 25 and 38 wt%, respectively. Consistent with our earlier study in multi-layers Mxene for I@ML-MXenes, increasing the quaternary ammonium content in the ionomers from I3 to I5 leads to the increased ionomer content in the I@DL-MXenes despite the lower dosage of the latter. The two CTAB-modified samples (C@DL-MXene-0.2 and C@DL-MXene-2) show the CTAB content of 9 and 15 wt%, respectively. The ionomer content of I@ML-MXene-5-2 is 29 wt%.

Figure 4.1b shows XRD patterns of the modified DL-MXene samples as well as the unmodified DL-MXene. Relative to that in unmodified DL-MXene (2θ = 6.6°; *d*-spacing = 1.3 nm), the characteristic (002) peak is broadened and obviously shifts to much lower diffraction angles centred at 2θ = 5.5° and 4.7° (corresponding *d*-spacings of 1.6 and 1.9 nm) in I@DL-MXene-3-3 to I@DL-MXene-5-2, respectively (Figure 4.1b), indicating the increase of interlayer distance upon ionomer intercalation. Meanwhile, one can also find that the increase in the ionomer content from I@DL-MXene-3-3 to I@DL-MXene-5-2 leads to an appreciable increase in *d*-spacing, indicative of enhanced intercalation. I@DL-MXene5-2, due to superior d-spacing, is selected for further study and performance tests in Mg batteries.

Meanwhile, relative to I@DL-MXenes, the d-spacing of C@DL-MXenes is appreciably lower at 1.45 nm (2θ =6.1°) for both C@DL-MXene-0.2 and C@DL-MXene-2, which is similar to the results reported earlier by Xu *et al.* [181, 186] It can be noted that the CTAB content has a negligible effect on the d-spacing of the two C@DL-MXenes. Clearly, relative to the small molecular analogue, the ionomers are much more efficient in expanding the interlayer spacing between the DL-MXene sheets, which may better facilitate the transport of Mg^{2+} ions in the channels.

The d-spacing of I@ML-MXene-5-2 from our previous work[185] is presented in Table S4.1 for reference.

DLS measurements have been performed on the dilute dispersions of the various modified MXene samples, including I@DL-MXenes and I@ML-MXene samples in THF and C@DL-MXene-2 in water, to determine their ζ potential and Z-average hydrodynamic size (dp) and distribution. The results are also summarized in Figure 1d, Figure S4.1, and Table S4.1. Relative to the unmodified DL-MXene in water (dp = 133 nm; PDI = 0.3), I@DL-MXenes show much bigger dp values (generally about 200 nm). The larger particle sizes suggest the presence of MXene aggregates as a result of the cross-linking effect of the multidentate ionomers. The ionomer modification also dramatically changes the ζ potential of the particles. Relative to the negative ζ potential of −38 mV and −53 mV of unmodified ML-MXene and DL-MXene, respectively, I@DL-MXenes show markedly increased ζ potentials of about 60 mV. These ζ potential data confirm the expected ionic binding of the cationic ionomers onto the negatively charged MXenes, which effectively changes the surface charge of the particles. C@DL-MXene-2 also shows the enhanced ζ potential of 57 mV.

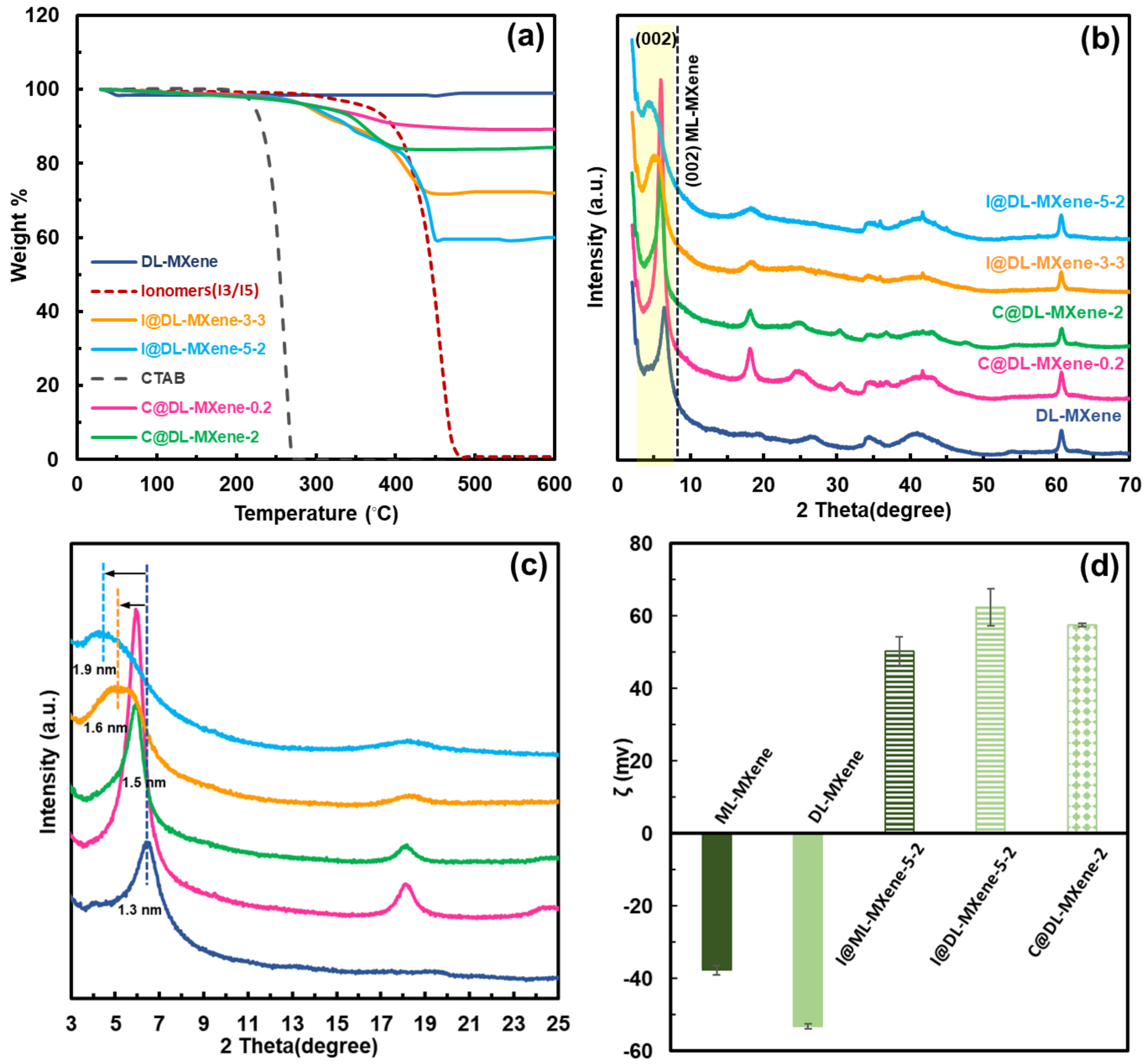

Figure 4.1 (a) TGA curves of unmodified DL-MXene, Ionomers, CTAB, and the various modified MXene samples; (b) XRD patterns of unmodified DL-MXene, I@DL-MXenes, and C@DL-MXenes; (c) magnified image of the selected region in (b); (d) ζ potential results of unmodified ML- and DL-MXene, and C@DL-MXene-2 in water, and I@MXene samples in THF.

Figure S4.2 in Supporting Information shows the N_2 adsorption−desorption isotherms for DL-MXene and I@DL-MXene-5-2, along with the surface area and pore volume data summarized in Table S4.2. While unmodified DL-MXene shows an appreciable surface area of 55.3 m2 g^{-1} and pore volume of 0.15 cm3 g^{-1}, I@DL-MXene-5-2 is nearly nonporous with negligible surface area or pore volume. This also suggests the successful intercalation of the ionomer, with the voids within DL-MXene almost fully filled with the soft ionomer.

Figure 4.2 shows TEM images of unmodified ML-MXene and DL-MXene, I@ML-MXene-5-2, and I@DL-MXene-5-2. Layered 2D-sheet structures with an interplanar spacing of ca. 1 nm are observed in the unmodified ML-MXene (Figure 4.2a). The selected area electron diffraction (SAED) (inset in Figure 4.2a) shows that the basal planes' atomic arrangement is identical to that in the parent MAX phase.[14] 2D sheets are observed in I@ML-MXene-5-2 (Figure 4.2b) but with a significantly enlarged interplanar spacing of 8.6 nm, confirming the successful exfoliation of the ML-MXene into large interplanar spacings upon the intercalation with the ionomer at a high content. Relative to ML-MXene, DL-MXene shows single- and few-layer structures with a decreased number of layers (Figure 4.2c,d). The TEM images of I@DL-MXene-5-2 show many few-layered structures, including mono- and bi-layers and aggregated flakes (Figures 4.2e,f,g) due to the cross-linking effect of the multidentate ionomer. From its SAED images (Figures 4.2h, i), the hexagonal atomic structure is well retained in I@DL-MXene-5-2. Consistent with the XRD results, the TEM images provide additional evidence supporting the effective intercalation of the ionomer into the nanosheets, which results in the entire exfoliation for some of them. The strong ionic interactions between the quaternary ammonium ions on the ionomer and the negatively charged MXene layer surface are reasoned to contribute to the high efficiency of intercalation and subsequent exfoliation of the nanosheets. Expanded interlayers can provide sufficient space and extra pathways for multivalent ions like Mg^{2+}.[182] In particular, I@DL-MXene-5-2 with few-layered structures and reduced layer numbers is expected to provide more accessible active sites and shortened pathways to accommodate Mg^{2+}.[187]

TEM elemental mapping of C, F, O, and Ti in Figure 4.2j shows qualitative changes in functional group distribution on DL-MXene before and after ionomer intercalation. Qualitatively, it displays an appreciably lowered intensity of F element relative to other elements (Ti, O) in I@DL-MXene-5-2 (Figure 4.2j (VII/VI)) compared to DL-MXene (Figure 4.2j (III/II)), indicating the removal of some F^{-} ions from the nanosheet surface upon ionomer binding.

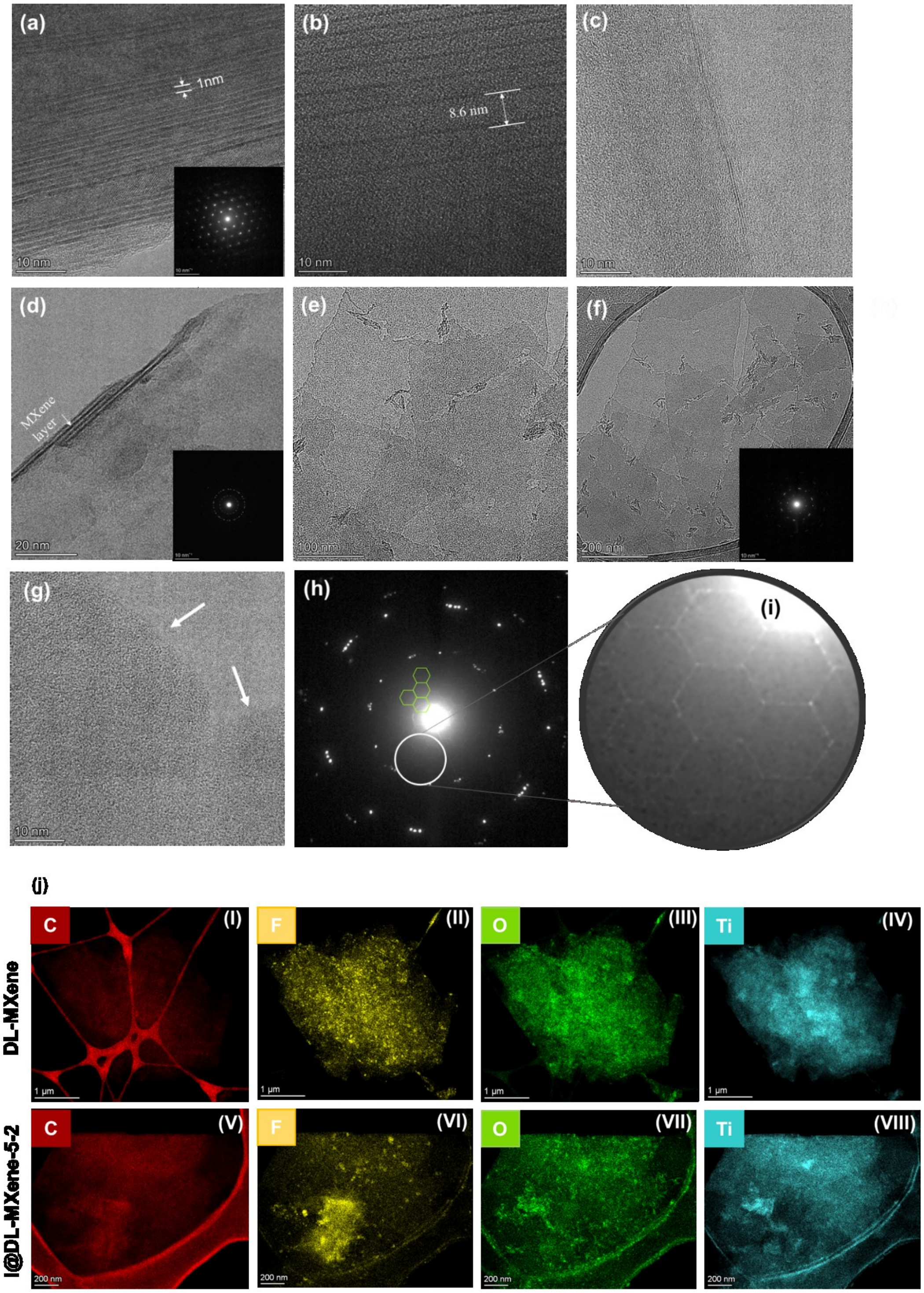

Figure 4.2 (a) TEM images of virgin unmodified $Ti_3C_2T_x$ ML-MXene; (b) I@ML-MXene-5-2; (c,d) DL-MXene; and (e, f, g) I@DL-MXene-5-2; the insets in (a),(d), and (f) are the SAED patterns in 10 nm-1; (h) the SAED pattern of (g); (i) magnification of (h) ; (j) EDS elemental mapping images of DL-MXene surface (I-IV) and I@DL-MXene-5-2 flake surface (V-VIII).

The electrochemical performance of I@DL-MXene-5-2 featured with the highest *d*-spacing has been systematically evaluated on cells constructed with an I@DL-MXene-5-2 cathode against a magnesium metal anode, with 0.4 M $(PhMgCl)_2$+$AlCl_3$/THF (APC) electrolyte. It should be noted that because of its nonpolar hyperbranched polyethylene skeleton, the ionomer has a high dispersibility in low polarity THF, thus facilitating the fast transport of the electrolyte within the ionomer. Comparisons are made with other unmodified/modified ML-/DL-MXene cathodes.

Figures 4.3a, b and S4.3a compare the first, second, 10th and 100th galvanostatic charge-discharge (GCD) curves of DL-/ML-MXene and I@DL-MXene-5-2 cathodes at a current density of 50 mA g^{-1} within the potential window of 0.05─2.0 V. The GCD curves affirm the dramatic difference between I@DL-MXene-5-2 and DL-/ML-MXene cathodes. Though all cathodes display sloping voltage curves, I@DL-MXene-5-2 cathode provides a high initial capacity of 235 mAh g^{-1} and a reversible discharge capacity of around 200 mAh g^{-1} in contrast to the significantly lower reversible capacity of 70 mAh g^{-1} for DL-MXene cathode and negligible capacity of only around 3 mAh g^{-1} for ML-MXene. Moreover, the discharge capacity of I@DL-MXene5-2 is maintained well at 190 mAh g^{-1} even after 100 cycles, representing a capacity retention of about 95% relative to the first stable cycle. Figure 4.3c compares the 2nd-cycle cyclic voltammetry (CV) curves of ML-MXene, DL-MXene, I@ML-MXene-5-2, C@DL-MXene-2 and I@DL-MXene-5-2 cathodes at a scan rate of 0.2 mV s^{-1} within the potential range of 0.05 to 2.0 V. One can notice the significant differences in the capacity among the five cathodes, with the enclosed CV area of I@DL-MXene-5-2 cathode significantly higher than those of others. In particular, ML-MXene and I@ML-MXene-5-2 cathodes exhibit extremely low current responses, confirming their negligible capacities due to the multi-layered nanosheet structures. From the EIS spectra recorded for the fresh cell of ML-MXene and I@ML-MXene-5-2 (Figure S4.3b), the Nyquist plots show high ion diffusion resistance, indicating difficult Mg^{2+} insertion/extraction through multi-layered MXenes even after the ionomer modification.

The CV curves show broader Mg^{2+} ion intercalation/extraction peaks for DL-MXene, C@DL-MXene-2, and I@DL-MXene-5-2 cathodes, respectively. The latter reveals a much-improved capacity compared to the former control samples. Improved responses for DL-MXene cathode should result from its delaminated few-layered structures. The CV results of DL-MXene and C@DL-MXene-2 cathodes are analogous to those reported in previous related papers.[178, 181] These capacity increases are attributable to the enhanced *d*-spacing of MXene layers. Expanding the interlayer space improves the Mg-ions storage performance. Actually, as the interlayer spacing increases, the interaction between intercalation guests and host lattices weakens, dramatically improving "cation" mobility in cathode materials. An increase in the number of accessible sites in cathode materials due to the enlarged lattice spaces also leads to improved reversible Mg-ions storage capacity.[168] According to the above results, the cationic ionomer plays a critical role in endowing the MXene electrode with distinctly enhanced Mg^{2+} storage capability.

To improve the charge-storage capabilities of 2D MXenes, most efforts have addressed increasing their interlayer spacing in order to enhance the accessible surface area and promote ion transport rates.[177] However, the electrolyte solvent selection significantly influences the ion intercalation process for $Ti_3C_2T_x$ MXene electrodes in organic electrolytes.[188]The wettability of electrodes by electrolytes is a critical factor affecting the access to electrolytes and the diffusion rate of the charge carriers in the electrodes.[18] The THF-based all phenyl complex (APC) electrolyte is one of the notable electrolytes for rechargeable magnesium batteries.[189] We previously demonstrated that the hydrophobic hyperbranched polyethylene segments in the adsorbed ionomer facilitate and improve the dispersion of the modified MXenes in both non- and low-polarity organic solvents.[185] To evaluate the effect of different organic solvents in the electrolyte system on the interlayer distance, XRD patterns of dry ML-MXene, dry I@ML-MXene-3-2, [185] and wet I@ML-MXene-3-2 saturated with different electrolyte organic solvents including THF, dioxolane (DOL), propylene carbonate (PC), dimethyl sulfoxide (DMSO) and dimethoxyethane (DME) are compared in Figure S4.3c. Dry I@ML-MXene-3-2 has a spacing of 13.6 A° relative to 10.8 A° for dry ML-MXene. The *d*-spacing of the wet I@ML-MXene-3-2 samples saturated with THF and DMSO shows distinct enhancements to 19.6 A° and 20.1 A°, respectively, while no noticeable changes are seen in the XRD patterns of the sample with other solvents; in agreement with our previous work where stable dispersions of I@ML-MXenes were achieved in THF and DMSO[185] . Thus, THF and DMSO molecules can effectively penetrate into the ionomer-modified MXene interlayer spaces, which correlates to the better ion transport ability in the electrolytes formulated with these two solvents. With the even enlarged *d*-spacing, the APC electrolyte in THF applied herein can penetrate freely between ionomer-modified DL-MXenes layers.

On the other hand, CTAB is a cationic surfactant with good solubility in water (36.4 g L^{-1} at 20 °C), methanol (>200 g L^{-1} at 20 °C) and alcohol, but insoluble in some nonpolar or low-polarity organic solvents like ether, benzene, and diethyl ether. In THF, it forms an opaque dispersion (see Figure S4.4) relative to the transparent solution in water, indicating it is only slightly soluble in the former. Meanwhile, C@DL-MXene-2 cathode composite is not dispersible in THF and tends to quickly aggregate and settle down even after vigorous shaking. In contrast, the as-synthesized ionomer featured extensive branch-on-branch structures; the hyperbranched polyethylene skeleton makes it completely amorphous and dispersible/soluble in many nonpolar, and low-polarity solvents at room temperature[136] and resulting in modified MXenes would thus inherit the dispersibility in these solvents[185]. Accordingly, the I@DL-MXene-5-2 cathode is completely dispersible in THF and remains stable for a long time Figure S4.4. Therefore, ionomers have not only been found to bind strongly onto the negatively charged MXene surfaces and effectively delaminate MXenes to few-/single-layers and nano-flakes to open the channel for Mg ion transportation, but also render the modified MXenes dispersible in an organic solvent, THF herein, compatible with fascinating APC electrolyte. Overall, we validated that, for Ti_3C_2 MXene electrodes in organic electrolytes, the selection of the electrolyte solvent does indeed have a considerable impact on the Mg-ion intercalation process, similar to Li-ions.[188] During cycling using an electrolyte APC in THF, the Mg ions present in the interlayer space of the ionomer-modified Ti_3C_2 MXene are found to be fully desolvated, leading to a charge-discharge mechanism dominated by a smooth deintercalation-intercalation process. Indeed, efficient penetration of THF molecules controls the accessibility and transport of magnesium ions inside the structure of the MXene cathodic electrode. Based on our knowledge, this is the first demonstration of solvent's influences on charge storage for Mg ions in titanium carbide MXenes.

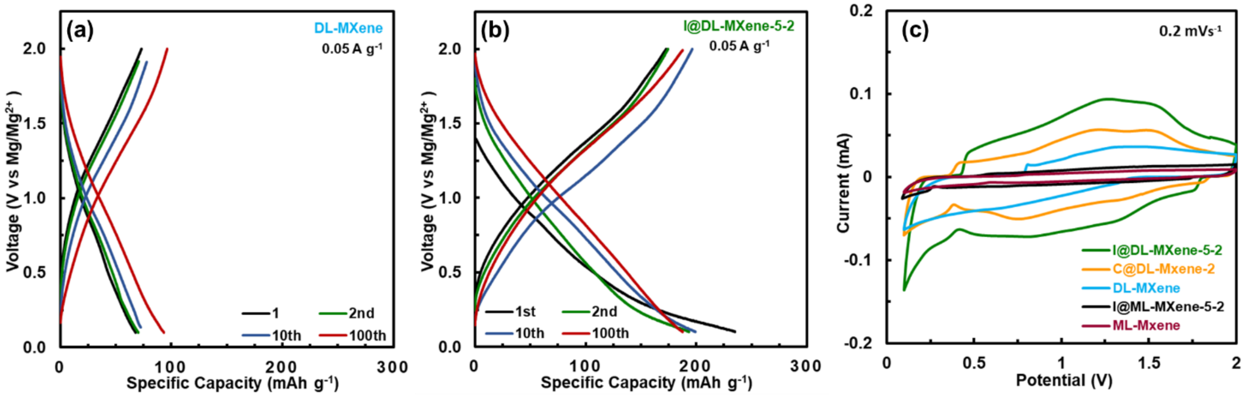

Figure 4.3 (a) GCD curves of DL-MXene electrode at 50 mA g^{-1}; (b) GCD curves of the ionomer modified MXene, I@ DL-MXene-5-2 electrode at 50 mA g^{-1}; (c) Cyclic voltammetric (CV) curves for all sample electrodes for comparing at 0.2 mV s^{-1}.

Nevertheless, in $Ti_3C_2T_x$ MXene, T_x represents three types of termination groups, *i.e.*, —OH, —F, and —O. It is demonstrated that termination groups' chemistry can be tuned to control the electrochemical performance of Mg ion batteries.[190-192] Furthermore, Y. Xie *et al.*[193] demonstrated both O-terminated and bare MXenes (the nonterminated MXenes) are promising electrode materials for Mg batteries and exhibit higher capacities and better rate capabilities. In fact, Mg^{2+} is not easily adsorbed on either — OH or —F terminated Ti_3C_2; conversely, Mg^{2+} exhibits a high affinity for adsorbing on the O-terminated Ti_3C_2 surface.[181] DFT simulations for multi- and single-layered $Ti_3C_2T_x$ Mxene showed fluorine and hydroxyl terminations contribute a negative average voltage for Mg^{2+} intercalation and are thus thermodynamically unfavourable, but it has spontaneous intercalation (negative intercalation energy) in the case of oxygen termination.[179] Regarding the higher ratio of O to F groups in I@DL-MXene-5-2 compared to DL-MXene based on qualitative results in TEM elemental mapping, Mg^{2+} can reach the O-terminated Ti_3C_2 surface with the enhancement diffusion kinetics of electrolyte in I@DL-MXene-5-2.

Finally, it has been demonstrated before that solvated or complex Mg cations exhibit significantly less charge polarization and migration barrier than naked Mg-ions because of their larger ionic radius and/or reduced charge numbers.[168] So, the electrochemical Mg-ions storage capabilities can improve by intercalating solvated or complex Mg-containing cations by weakened electrostatic intercalation between these cations and host lattices.[194] Herein, the ionomer not only expands the interlayer of the MXene cathode but also shields the interactions between Mg-ions and the MXene host. Compared with the bivalent Mg-ions, the attainable solvated Mg-ions as monovalent $MgBF_4$ -ions have a relatively weak charge polarization, which, therefore, displays the lower diffusion barriers in the MXene host lattice than that of naked Mg-ions.

The electrochemical performance of the I@DL-MXene-5-2 cathode has been further evaluated in detail. Figure 4.4a compares four cycles of CV curves of I@DL-MXene-5-2 at 0.2 mV s^{-1} within the potential range of 0.05 to 2.0 V. During the first discharge, a minor reduction peak appearing at 0.75 V is ascribed to the decomposition of the electrolyte to form a solid-electrolyte interface (SEI) film.[182] In the following cycles, the CV curves almost overlap, which signals the good reversibility of the cathode and also suggests easy and fast insertion/extraction of Mg^{2+} ions into/from MXene sheets. The step current drop at ~1.75 V in the reduction peak and the step current increasing in 0.5 V, as well as the oxidation peak situated located around 1.5 V, are related to the insertion and extraction of the Mg^{2+} within the MXene layers. [182]

To study the charge storage mechanism of I@DL-MXene-5-2, CV curves at different voltage scan rates were acquired (Figure 4.4b), and Equation (1) was applied to distinguish between the surface-controlled pseudocapacitive ($k_1\nu$) and diffusion-controlled battery ($k_2 v^{1/2}$) contributions to the current response.[195]

$$i = k_1 v + k_2 v^{1/2} \qquad \textbf{(1)}$$

where i is current at a scan rate of ν at each fixed potential. k_1 and k_2 can be determined as the slope and interception of a linear fit of $i/_{v^{1/2}}$ versus $v^{1/2}$.

Accordingly, the pseudocapacitive contribution in charge storage at different scan rates was calculated (e.g. Figure 4.4c provides an illustration of the pseudocapacitive contribution at 0.7 mV s^{-1}). As depicted in Figure 4.4d, the observed trend aligns with expectations: an increase in scan rate corresponds to a heightened pseudocapacitive contribution (71%, 81%, 86%, and 89% at 0.1, 0.5, 0.7, and 0.9 mV s^{-1}, respectively). Notably, even at the low scan rate of 0.1 mV s^{-1}, a substantial pseudocapacitive contribution to the current response (71%) is evident. This remarkable surge in pseudocapacitive behaviour can primarily be attributed to the distinctive pillared structure leveraging its extensive surface area that effectively reduces ion diffusion pathways and enhances the availability and accessibility of surface-active sites.[196]

Figure 4.4e shows the voltage profiles of the I@DL-MXene-5-2 cathode in the GCD tests at different current rates. All the voltage profiles show sloping curves with no obvious plateaus observed at any current, which can be ascribed to the 2D nature of the ionomer-modified MXene sheets.[178] The capacity retention plots of the battery at different currents illustrated in Figure 4.4f show the different rate performances of the cathode. Figure 4.4f plots the capacity retention curve of the cathode at different currents, with a retention of about 52% achieved at 1000 mA g^{-1} relative to 20 mA g^{-1}. Figure 4.4g shows the rate performance of the cathode, with the capacities plotted at different GCD currents ranging from 20 to 1000 mA g^{-1}. Stable reversible capacities are achieved at each current, with the values of 213, 200, 195, 194, 186, 169, 140 and 110 mAh g^{-1} at 20, 40, 50, 80, 100, 200, 500 and 1000 mA g^{-1}, respectively. Moreover, a remarkable reversible higher capacity of ~ 250 mA h g^{-1} is maintained when the current density is switched back to 20 mA g^{-1}. Relative to the initial value of 213 mA h g^{-1}, the appreciably higher capacity value is attributed to the activation effect following the rate performance test. Clearly, the significantly expanded interplanar spacing and THF-permeable ionomer matrix facilitate rapid ion diffusion, high Mg^{2+} storage capacity, and superior rate performance.

Figure S4.5 shows the rate performance of the C@DL-MXene-2 cathode. It shows capacities of 130, 132, 123, 134, 133, 123, 112 and 98 mAh g^{-1} at 0.0220, 0.0440, 0.0550, 0.0880, 0.1100, 0.2200, 0.5500 and a 1 1000 mA g^{-1}, respectively. Clearly, I@DL-MXene-5-2 shows a higher capacity than C@DL-MXene-2 at each current.

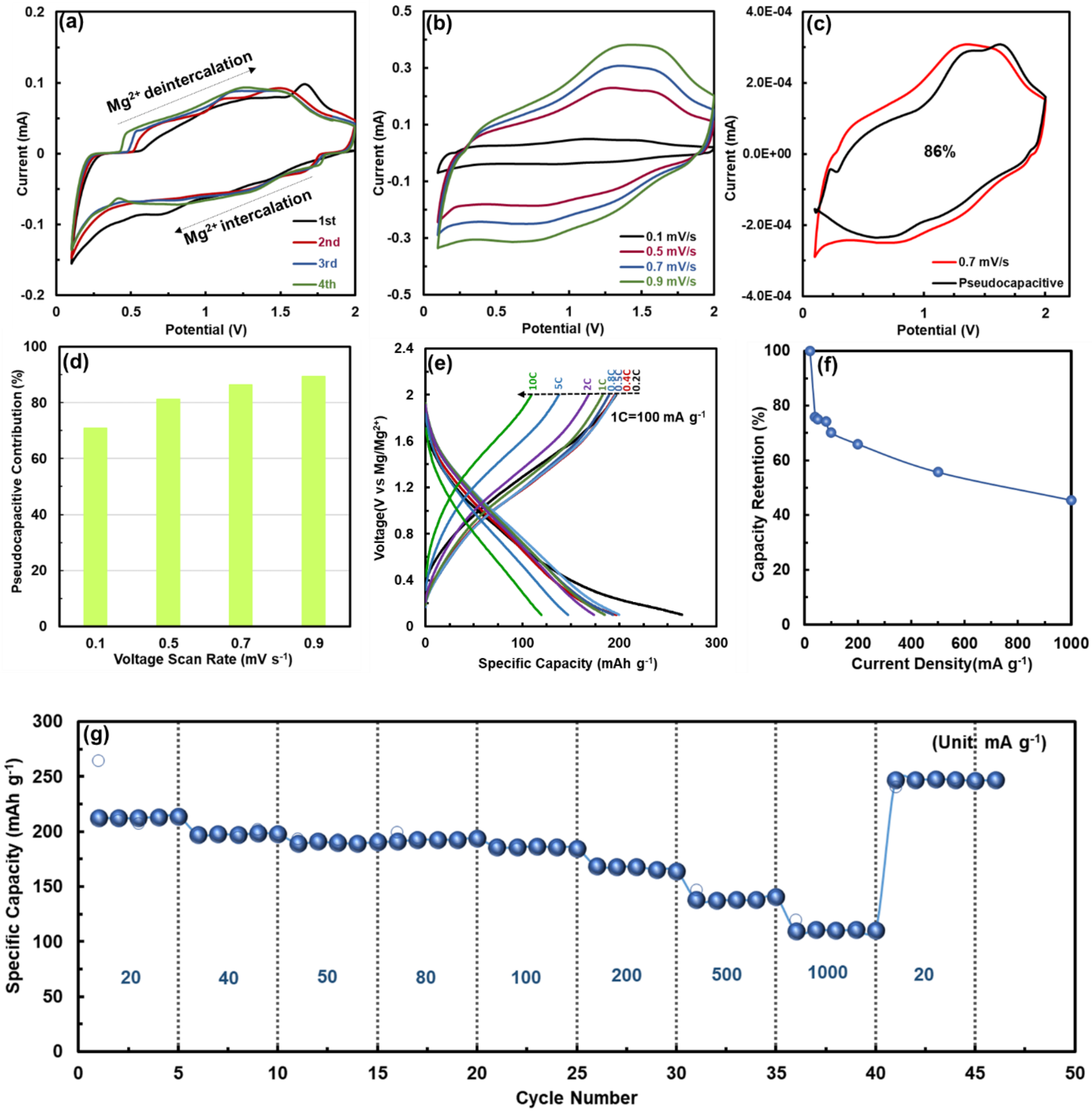

Figure 4.4 (a) CV curves of I@DL-MXene-5-2 cathode at a sweep rate of 0.2 m V s^{-1}; (b) CV curves of I@DL-MXene-5-2 cathode at different sweep rates from 0.1 to 0.9 mV s^{-1}; (c) the pseudocapacitive contribution to the current response for Mg-Battery with I@DL-MXene-5-2 cathode at a voltage scan rate of 0.7 mV s^{-1}; (d) comparison of pseudocapacitive contributions to the current at different scan rates; (e) Galvanostatic charge-discharge curves of I@DL-MXene-5-2 cathode at currents from 0.2C to 10C (1C = 100 mA g^{-1}) ; (f) Capacity retention of I@DL-

MXene-5-2 cathodes at different current densities; (g) gravimetric capacities of I@DL-MXene-5-2 cathode at different current densities.

The kinetic effects and mechanism of charge and discharge reactions have been further investigated on the three different cathodes, including I@DL-MXene-5-2, C@DL-MXene-2, and DL-MXene cathodes. Figures 4.5a and 4.5b show Nyquist plots of their fresh cells and cells after 100 GCD cycles at 50 mA g^{-1}, respectively. Fresh cells of I@DL-MXene-5-2 and C@DL-MXene-2 show nearly overlapping curves, with a much higher electrode resistance found for DL-MXene. For the cycled cells, the cell with I@DL-MXene-5-2 cathode shows the smallest semicircle[197] in the middle-high frequency region, correspondingly with the lowest charge transfer resistance (R_{ct}) of 36.9 Ω. The cell with DL-MXene cathode instead shows the highest R_{ct} of 116.1 Ω, followed by the value of 94.5 Ω for that with C@DL-MXene-2 cathode. The higher R_{ct} of the cell with C@DL-MXene-2 cathode indicates the relatively inferior interface charge transfer with C@DL-MXene-2, which stems from the low wettability of C@DL-MXene-2 by low polarity THF solvent as discussed earlier. Compared to the other two cathodes, the charge transfer resistance of the I@DL-MXene-5-2 cathode is reduced significantly upon ionomer intercalation within the 2D nanosheet structure.

Figure 4.5c shows the cycling performances of I@DL-MXene-5-2 cathodes at 50 and 200 mA g^{-1}, respectively, for 500 and 1000 cycles. Reversible capacities of 138 and 125 mAh g^{-1} are achieved at the two respective currents after 500 cycles, corresponding to the capacity retentions of 76% and 83%, respectively, in reference to the initial capacities of 181 and 150 mAh g^{-1}. The initial Coulombic efficiency for 50 and 200 mA g^{-1} is recorded at 111.7% and 95.3%, respectively. The Coulombic efficiency is maintained at nearly 100% during the entire test, indicating highly reversible insertion/extraction of Mg^{2+} over the long cycling. As shown in the inset in Figure 4.5c, the I@DL-MXene-5-2 cathode exhibits a gradual capacity increase from the first cycle to 210 mAh g^{-1} at the 60*th* cycle. This initial capacity increase, known as electro-activation, is a common phenomenon arising from continuous intercalation/deintercalation of the ions and, consequently, the increasing active surface area.[172]

After 1000 cycles at 200 mA g^{-1}, the capacity of the cathode is still maintained at 107 mAh g^{-1} with a retention of 71% compared to the initial capacity. Delaminated MXene flakes possess more active sites and larger surface areas but tend to restack or aggregate because of the van der Waals interaction and/or hydrogen bonding force.[172] It has been shown before that stacking can reduce diffusion by 8–20 orders of magnitude.[198, 199] In this respect, ionomer modification not only modifies the surface of the nanosheets but also effectively prevents DL-MXene from restacking and improves their electrochemical performance. The ionomer with hyperbranched polyethylene segments acts like a committed spring between MXene layers for a reversible charge-discharge process with long cycles.

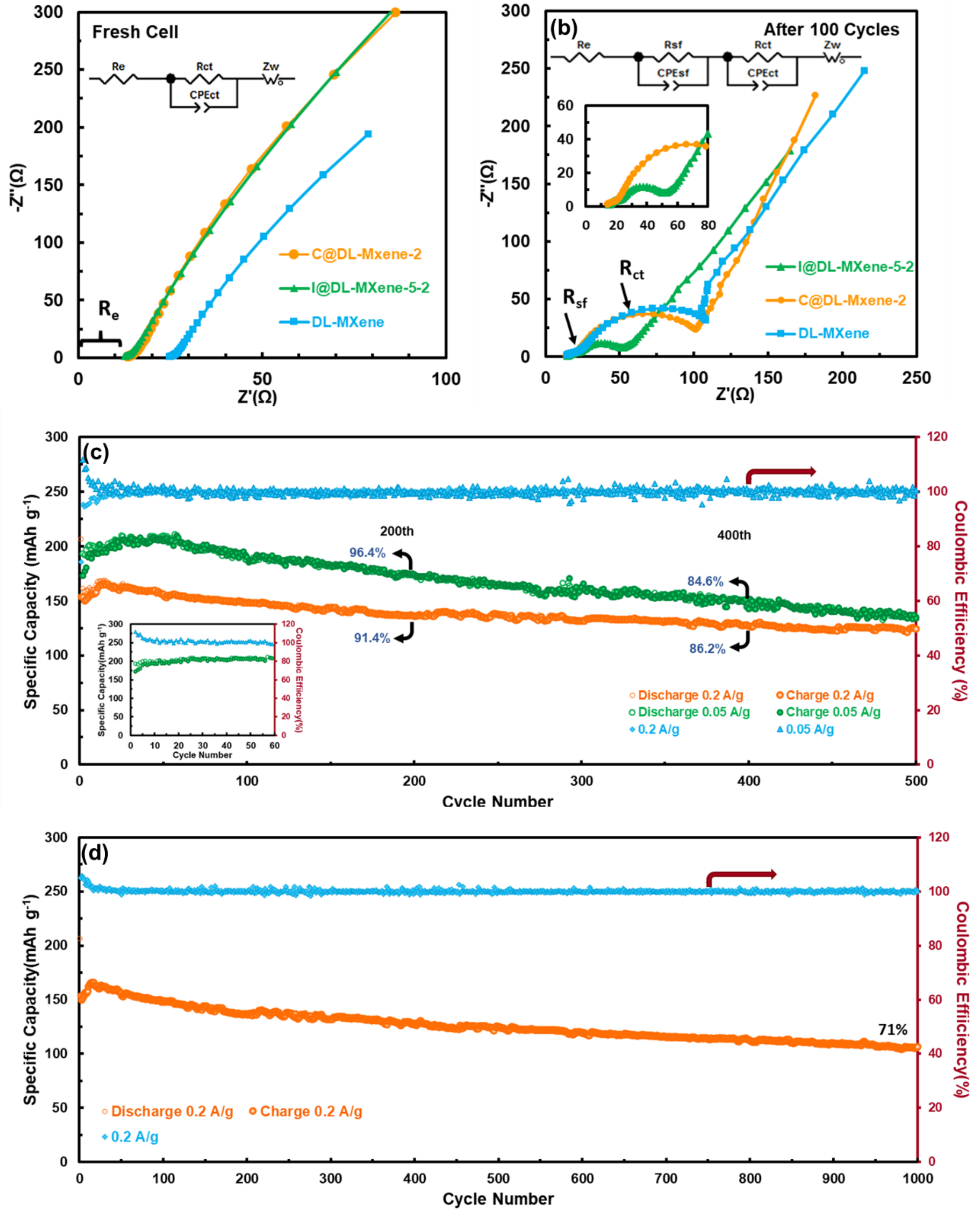

Figure 4.5 Nyquist plots of (a) fresh I@DL-MXene-5-2, C@DL-MXene-2 and DL-MXene cathodes tested at open circuit potential and (b) the cathodes after 100 cycles of GCD test at 50 mA g^{-1} with the inset showing their high-frequency regions and equivalent circuit; cycling tests of I@DL-MXene-5-2 cathode in mg battery (c) at 50 and 200 mA g^{-1} for 500 cycles and (d) at 200 mA g^{-1} for 1000 cycles.

Figure 4.6 compares all other reported MXene cathode materials for rechargeable Mg batteries; the high performance of I@DL-MXene is highlighted. In reference to the literature results, I@DL-MXene-5-2 shows the best overall performance among MXene-based cathodes reported for Mg batteries. Based on our knowledge, acquired performances are the highest among all the reported Mg batteries with MXene-based cathodes. Although 3D MXenes could deliver high capacities of 210 mAh g^{-1} at 50 mA g^{-1}, the conversion-type charge storage was irreversible due to a significant activation barrier to recharge Mg-containing compounds.[200] Consequently, the capacity of the 3D macroporous $Ti_3C_2T_x$ cathode was reduced from 170.5 mAh g^{-1} at the first cycle in 100 mA g^{-1} to 140 mAh g^{-1} during the following cycles and finally stabilized at 50 mAh g^{-1} before reaching 20 cycles. The rate performance of the electrode delivered a sharp decrease in capacity from 210 mA h g^{-1} at 50 mA g^{-1} to capacities of 140 and 70 mA h g^{-1} at 100 and 300 mA g^{-1}, respectively.[180]

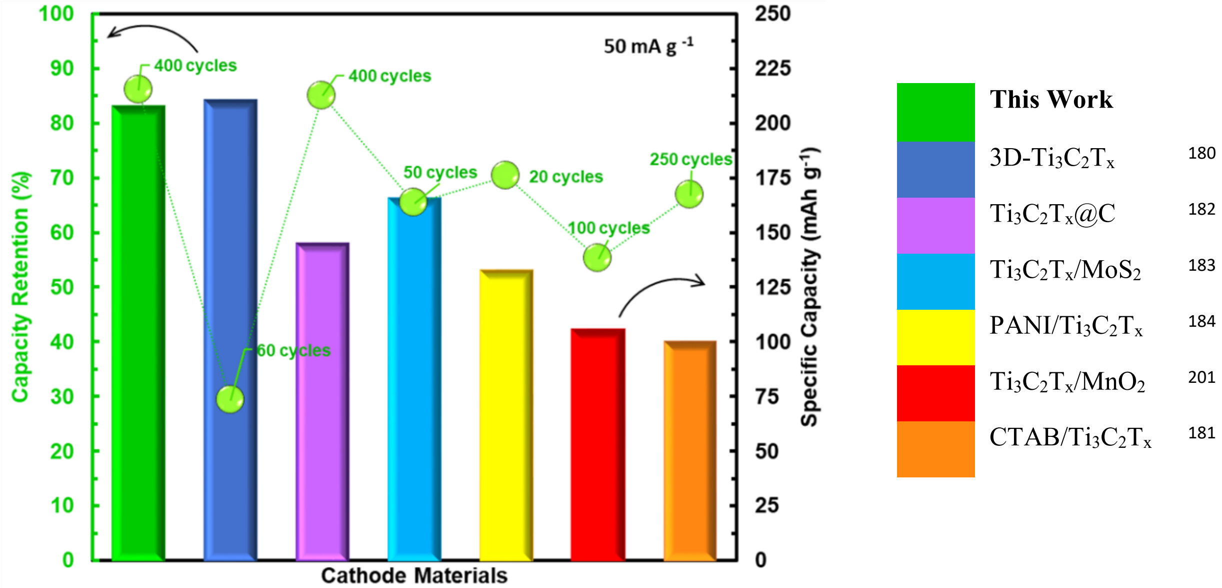

Figure 4.6 Comparison of I@DL-MXene-5-2 capacity retention, cycles and specific capacity with other MXene-based cathodes.

4.4 Conclusion

Ionomer-modified DL-MXene with enlarged inter-layer spaces, I@DL-MXenes, have been designed by intercalation/exfoliation of DL-MXene with hyperbranched polyethylene ionomers with quaternary ammonium ions. The quaternary ammonium cations allow the ionomer to strongly bind onto the negatively charged surface of DL-MXene nanosheets, thus stably exfoliating the nanosheets at enhanced inter-layer distance and preventing their restacking. The ionomer thus acts as the pillar in the pillared MXene, which renders the layers open and endows the pillared MXene with extra capacity for magnesium-ion storage. The ionomer also acts as a surfactant and modifies the surface of DL-MXene sheets by reducing fluorine to oxygen ratio and enhancing the wettability with THF-based APC electrolyte, which can effectively reduce the strong electrostatic interaction between Mg^{2+} and the surface terminals and thus improve the diffusion kinetics.

Our results have shown that I@DL-MXene-5-2 cathode demonstrates exceptionally enhanced magnesium-ion storage capacities (*e.g.*, 213 mAh g^{-1} *vs* about 3 mAh g^{-1} for ML-MXene and 80 mAh g^{-1} for DL-MXene at 0.02 A g^{-1}). I@DL-MXene-5-2 cathode is also distinctly featured with the improved electrode/electrolyte interface charge transfer, which effectively overcomes the sluggish solid-state kinetics of Mg^{2+} in MIBs. I@DL-MXene-5-2 outperforms the small molecule intercalant CTAB-modified DL-MXenes. Hence, the design of I@DL-MXene by rationally constructing DL-MXene material's structure and regulating the electrode/electrolyte system offers high-capacity, long-life, and high-safety Mg-ion batteries with potential for promising applications.

Chapter 5 Improving Supercapacitic Capabilities of $Ti_3C_2T_x$ MXene Electrodes in Ionic-Liquid Electrolyte by Enhancing Interlayer Spacing and Surface Modification

Abstract

MXenes are emerging as a very promising electrode material for high-performance supercapacitors. However, modified MXene-based supercapacitors with conductive polymers have been reported to exhibit low performance due to their narrow working voltage in aqueous systems. Herein, we report for the first time the use of hyperbranched polyethylene ionomer-modified MXene as high-capacitance electrode materials for symmetric supercapacitors in an ionic liquid electrolyte. Ionomer-modified MXene working at 3 V in 1-ethyl-3-methylimidazolium tetrafluoroborate ($EMIM^+BF_4^-$) exhibits a high capacitance of 220 F g^{-1} at 2 mV $s^{-1,}$ which is among the highest values reported for MXene based electrodes in ionic liquid electrolyte. This work explains a simple and fast approach for the fabrication of MXenes/non-conducting polymer hybrid electrodes with superior electrochemical performance.

5.1 Introduction

Supercapacitors have received significant interest in recent years due to their advantageous features, including fast charging and discharging capabilities, high power density, and exceptionally long cyclic stability compared to conventional batteries.[202-208] Therefore, the development of supercapacitors with high energy and high-rate capabilities is an ongoing area of interest within the field.[209] Supercapacitors have the capability to store energy through the electric double-layer capacitance (EDLC) mechanism. This process involves the accumulation of charges at the interfaces between the electrode and electrolyte, which leads to charge storage.[210] Another type of supercapacitor is known as a redox capacitor, often referred to as a pseudocapacitor.[211] This particular type of capacitor can store charges through rapid surface Faradaic reactions. Several factors, including the electrochemical characteristics of the electrode materials, the electrolyte selection, and the electrodes' potential window, determine the performance of supercapacitors.[212]

Given the high surface-area-to-volume ratios, two-dimensional (2D) materials are emerging as promising electrode materials for supercapacitors.[93] Transitional metal carbide or nitride, commonly referred to as MXene, is a fascinating member of the 2D material family due to its remarkable electrochemical energy storage capabilities.[213] The 2D MXenes are expressed as $M_{n+1}X_nT_x$, where M is an early transition metal such as Ti, V and Mo, Cr; X represents C and/or N, n = 1, 2, or 3, and T_x is a surface terminal functional group such as –O, –OH, or –F. Supercapacitor electrodes represent one of the most promising applications for MXenes.[214] As an electrode, MXene can function as either a capacitor or a pseudocapacitor.[106] MXenes usually reveal cation intercalation in aqueous electrolytes and have rectangular cyclic voltammetry (CV) curves. In contrast, MXenes exhibit pseudocapacitive characteristics with non-aqueous electrolytes characterized by significantly distorted rectangular CV curves.[215] The aggregation and self-restacking of flexible MXene flakes are commonly observed during the electrochemical process. This phenomenon can be attributed to the presence of strong van der Waals interaction and hydrogen bonding between nanosheets.[216] In order to mitigate the self-stacking tendency of MXene flakes, various intercalated agents such as cetrimonium bromide (CTAB) [186] and tris(2-aminoethyl) amine (TAEA)[217] as small molecules and conducting polymers including polypyrrole[82, 88, 218], polyaniline[93] and their derivatives[219] have been introduced to expand the interlayer space.

On the other hand, The vast majority of reported $Ti_3C_2T_X$ MXene electrode materials are typically produced in aqueous electrolytes. Consequently, the primary drawback of aqueous electrolytes is the small electrochemical potential window, which induces an energy density bottleneck.[220] Meanwhile, MXenes without sufficient modification have low oxidative stability in aqueous electrolytes. Using non-aqueous electrolytes, including ionic liquids, organic electrolytes, or their hybrids, can significantly increase the supercapacitors' voltage window and energy density[220, 221] as well as render enhanced MXene oxidative stability.

Herein, the colloidal supernatants of multi-layer MXene as delaminated MXene are modified with specially designed hyperbranched polyethylene ionomers bearing positively charged quaternary ammonium groups on a hydrophobic polyethylene backbone. The ionomers tightly bind onto the negatively charged surface of MXene nanosheets. Such a modification markedly expands the interlayer spacing of MXene sheets and adjusts their surface properties, rendering their stable, highly concentrated dispersions in non-polar or low-polarity organic solvents along with significantly enhanced oxidation stability. Ionomer-modified MXene is used as the electrode material to fabricate symmetrical two-electrode supercapacitors with $[EMIM]^+[BF4]^-$ as the electrolyte. Due to the ionomer intercalation with expanded interlayer spacing, the ionomer-modified MXene electrodes are expected to render improved ion transport with more accessible surface active sites for ion adsorption and, in turn, enhanced capacitance.

5.2 Experimental

5.2.1 Materials

All manipulations involving air- and/or moisture-sensitive materials were conducted in an Argon-filled glovebox or by using Schlenk techniques. The batch of Ternary Titanium Carbide (Ti_3AlC_2) powders as MAX phase samples with size ≤40µ provided by Carbon-Ukraine company (Y-Carbon Ltd. (Ukraine)). The Pd—diimine catalyst, $[\mathrm{ArN=C(Me)-(Me)C=NAr}]\mathrm{Pd(CH_3)(N\equiv C(Me)]^+SbF_6^-(Ar=2,6-(iPr)_2C_6H_3)}$, was synthesized by following a literature procedure.[135]

The acrylate-type ionic liquid co-monomer [(2─(acryloxy)ethyl]trimethylammonium tetrafluoroborate]($AETMA^+BF4^-$) was prepared by following the procedure reported in an earlier paper.[109] Polymer-grade ethylene was obtained from Air Liquide and was purified by passing through a 3 Å molecular sieve column and an Oxiclear column. All other solvents or reagents were obtained from either Sigma-Aldrich or Fisher Scientific and were directly used as received.

5.2.2 Synthesis of Quaternary Ammonium-Containing Hyperbranched Polyethylene Ionomers

The hyperbranched polyethylene ionomers (I) were synthesized by catalytic chain walking copolymerization of ethylene and ionic liquid co-monomer $AETMA^+BF_4^-$ in a 50 mL Schlenk flask equipped with the magnetic stirrer by following the procedure reported in an earlier paper.[109] The sealed and vacuumed flask was purged with ethylene five times and then filled with ethylene to 1 atm (*i.e.,* 1 atm absolute pressure). The ionic liquid co-monomer solution (2.45 g) in 5 mL of anhydrous acetone) was slowly introduced into the reactor under stirring. Subsequently, the polymerization was started through the injection of Pd—diimine catalyst solution (0.16 g, 0.2 mmol in 5 mL of anhydrous acetone). During the polymerization, ethylene pressure was maintained constant by continuous feeding, and the polymerization temperature was set at room temperature. After 24 h, the polymerization was stopped by shutting down the ethylene supply line and venting the reactor. The black product containing Pd (0) particles, resulting from the decomposition of the Pd—diimine catalyst, was precipitated out with a large amount of methanol. The precipitate was redissolved in a small amount of tetrahydrofuran (THF) for multiple washing with methanol. The polymer precipitate was purified to remove Pd black according to a procedure in our earlier paper[109] and then dried under vacuum at room temperature, rendering the corresponding ionomer.

5.2.3 Synthesis of the Multi-layered $Ti_3C_2T_x$ MXene (ML-MXene)

In a fume hood, the etchant was prepared by gradually adding 1.6 g LiF to 20 mL of 9 M HCl in a 125 mL Teflon beaker with a lid. [8, 132] LiF was thoroughly dissolved in HCl solution, then 1 g of Ti_3AlC_2 (MAX) powder was slowly added over the course of 10 minutes to the etchant solution. The reaction mixture was stirred and maintained at 40 °C for 24 hours. After that, the acidic mixture was repeatedly centrifuged (Thermo Fisher Scientific, Sorvall Legend XT) at 3500 rpm while being thoroughly washed with distilled water. The acidic solution was separated as waste following each cycle and replaced with fresh DI water. The washing cycles were repeated until the pH of the supernatant was between 5 and 6. The final product, which had some water and seemed to be clay-like, was collected, dried overnight at 70 °C in a vacuum oven, and grounded for further use. The resulting fine powders are multi-layered, ML-$Ti_3C_2T_x$/ML-MXene.

5.2.4 Synthesis of the Delaminated $Ti_3C_2T_x$ MXene (DL-MXene)

The clay-like ML-$Ti_3C_2T_x$ were dispersed in a large amount of distilled water and sonicated in an ice bath for 10 minutes. The suspension was centrifuged for an hour at 3500 rpm to separate the few- and single-layer MXene sheets from thick multi-layer MXene or the un-etched MAX phase. The homogeneous dark-green delaminated $Ti_3C_2T_x$ supernatant was collected, dried overnight in a vacuum oven at 70 °C, and grounded for further action. The resulting fine powders are delaminated, DL-$Ti_3C_2T_x$/DL-MXene.

5.2.5 Preparation of the Ionomer-Modified MXene (I@ML-/DL-MXene)

The hyperbranched polyethylene ionomer (20 mg) was typically dissolved in 40 ml THF. Afterward, the dispersion of MXene (ML- or DL-) in DMF (10 mg in 0.5 mL) was added drop wisely into the ionomer solution under bath sonication. The $Ti_3C_2T_x$ to Ionomer mass ratio was controlled at 1:2. The resulting dispersion was further bath sonicated for *ca.* 5 min. It is worth mentioning that 5-minute bath sonication was replaced with hand-shaking (which was demonstrated efficient for this procedure) to ensure reproducibility. At that point, with the assistance of a centrifuge, the supernatant was decanted, and the sediment was thoroughly dispersed in 40 ml fresh THF and washed 3 times to be sure all non-intercalated ionomers were removed. Finally, the sediment dried overnight under vacuum at *ca.*70 °C to render the ionomer-modified MXene, termed as I@ML-MXene or I@DL-MXene. In addition, a cetyltrimethylammonium bromide (CTAB)-modified DL-MXene, termed C@DL-MXene, was similarly prepared by replacing the ionomer with CTAB as a small molecular analogue in fresh DI water instead of THF.

5.2.6 Characterizations and Measurements

Thermogravimetric analysis (TGA) was carried out on a TA Instruments Q50 thermogravimetric analyzer. Measurements were performed under N_2 atmosphere with a continuous flow of 60 mL min^{-1} through the sample furnace and a flow of 40 mL min^{-1} through the balance compartment. In a typical measurement, the sample (*ca*. 5 to 10 mg) was heated from room temperature to 700°C at 10 °C min^{-1}. Dynamic light scattering (DLS) measurements of the dilute dispersions (*ca.* 0.1 mg mL^{-1}) of the various MXene samples for their hydrodynamic particle size and ζ potential were performed on a Brookhaven NanoBrook Omni Instrument at 25 °C. Each sample was measured three times, and the average values were used. Wide-angle X-ray diffraction patterns of the MXene and modified MXenes samples were collected on a Bruker D8 Advance diffractometer with Cu Kα radiation at room temperature. Scanning electron microscopy (SEM) was carried out on an FEI Quanta 450 Environmental Scanning Electron Microscope (FE-ESEM). A thin platinum layer was coated on the samples prior to the imaging. The TEM images were captured with a JEOL 2010F field emission electron microscope operated at 200 keV. Specimens for TEM observation were prepared by dispersing powders of the corresponding materials (pristine MXene or ionomer-modified MXenes) in THF by bath sonication, followed by the deposition of a few drops of dispersion on a carbon-coated copper mesh grid. The grid was dried in the air prior to the TEM characterization. High-resolution transmission electron microscopy (HRTEM) has been used to define the structures of the obtained materials in detail.

5.2.7 Electrochemical Measurements

All electrochemical measurements, including cyclic voltammetry (CV), galvanostatic charge/discharge (GCD), and electrochemical impedance spectroscopy (EIS), were conducted with a Metrohm Autolab PGSTAT 128N potentiostat/galvanostat on both 3-electrode and 2-electrode cells.

To fabricate the working electrodes in different electrolytes, a homogeneous slurry of the mixture of ML-MXene/DL-MXene/I@DL-MXene, Super-P conducting carbon, and PVDF (polyvinylidene fluoride) as a binder at a mass ratio of 60: 30: 10 in N-methyl pyrrolidinone (NMP) solvent was prepared. The formed slurry was then uniformly coated on the carbon paper collector at a virgin MXene mass loading of ca. 1.0-2.5 mg cm^{-2}, followed by drying at 40 °C under vacuum overnight.

Electrochemical measurements of all MXene-based samples were first conducted in a three-electrode system in 1 M H_2SO_4 aqueous electrolyte at room temperature. A coiled platinum wire and a saturated calomel electrode (SCE) were used as the counter and reference electrodes, respectively. The specific capacitance (C_{SP} in F g^{-1}) was calculated from the CV curves through the following equation:[222]

$$C_{\mathrm{sp}} = \frac{\frac{1}{2}\int idV}{mv\Delta V} \qquad \textbf{(1)}$$

where i and V are the current (A) and voltage (V), respectively, in the CV curves, $\int idV$ is the integration of the current loop over the whole voltage range, m is the mass of the active MXene, and v is the voltage sweep rate (V s^{-1}). GCD measurements were performed at different current densities. The specific capacitance was calculated from the discharge curve through the following equation:[222]

$$C_{\mathrm{sp}} = \frac{i}{mdV/dt} \qquad \textbf{(2)}$$

where i is the discharge current, m is MXene mass, and dV/dt is calculated as the slope of the discharge curve within the voltage range following the end of an ohmic drop to the end of the discharge curve.

Furthermore, symmetrical two electrode supercapacitors were assembled as CR2032-type stainless steel coin cells using the glass fiber membrane (Whatman GF/C) as the separator and LiTFSi or [EMIM][BF_4] ionic liquid as respective electrolytes in a glovebox filled with ultrahigh purity argon.

Specific capacitance C_{sp} in (F g^{-1}) was calculated from the CV curves according to the following equation:[223]

$$C_{\mathrm{sp}} = \frac{\int idV}{mv\Delta V} \qquad \textbf{(3)}$$

where V is the voltage (V), i is the current (A) in CV curves, v is the voltage sweep rate (V s^{-1}), and m is the active MXene mass in a single electrode (g). For GCD measurements, the C_{sp} in (F g^{-1}) was calculated from the discharge curves according to:[223]

$$C_{\mathrm{sp}} = \frac{2i}{mdV/dt} \qquad \textbf{(4)}$$

where m is the mass of the active material in a single electrode, i is the specified discharge current, and dV/dt corresponds to the slope of the discharge curve with the ohmic drop excluded. EIS measurements over a frequency range from 0.01 Hz to 100 kHz were performed at the open-circuit potential by applying an AC voltage of 5 mV in amplitude. The energy density (E, in W h kg^{-1}) and power density (P, in W kg^{-1}) were calculated as follows:[223]

$$E = \frac{1}{2} C_{sp} V^2 \frac{1}{4 \times 3.6} \tag{5}$$

$$P = \frac{E}{t} \tag{6}$$

where t is the discharge time (in h), and V is the cell voltage with the ohmic drop deducted.

5.3 Results and Discussion

5.3.1 Characterizations

In the present study, the hyperbranched polyethylene ionomer, briefly I containing 2.87 mol% tetraalkylammonium ions, was employed. Ionomer was synthesized by Pd—diimine-catalyzed direct copolymerization of ethylene with AETMA$^+$BF$_4^-$as the ionic liquid co-monomer. The copolymerization conditions and detailed characterization results of synthesized ionomers are presented in our previous work.[185] The hyperbranched architecture of the ionomer disrupts the formation of crystals and thus renders the ionomer with good dispersibility/solubility in non-polar and low-polarity solvents. Multi-layered $Ti_3C_2T_x$ MXene particles and delaminated flakes were prepared according to the synthesis process given in the experimental section. The schematic for fabricating the ionomer@MXenes composite by an electrostatic self-assembly approach is illustrated in Scheme 1. MXene nanosheets are negatively charged due to their surface terminations (–O, –OH, and –F). The ionomer containing multiple quaternary ammonium groups per chain was attracted to the surface of MXene nanosheets through electrostatic interaction and the ionic binding of their positive quaternary ammonium groups to the negatively charged surface of MXene. This successful self-assembly between MXenes and ionomer is a simple strategy without the usage of temperatures and energy. The resulting mixture was centrifugated at 10,000 rpm for 20 min, and the precipitate was thoroughly washed three times with excess fresh THF to remove unused ionomers and then dried, rendering the ionomer-modified MXenes (I@ML-Mxene and I@DL-MXene) solid black powders to prepare the composite electrodes. Additionally, the modification of DL-MXene has also been performed with CTAB, as a small-molecular analogue of the ionomers to render C@DL-MXene.

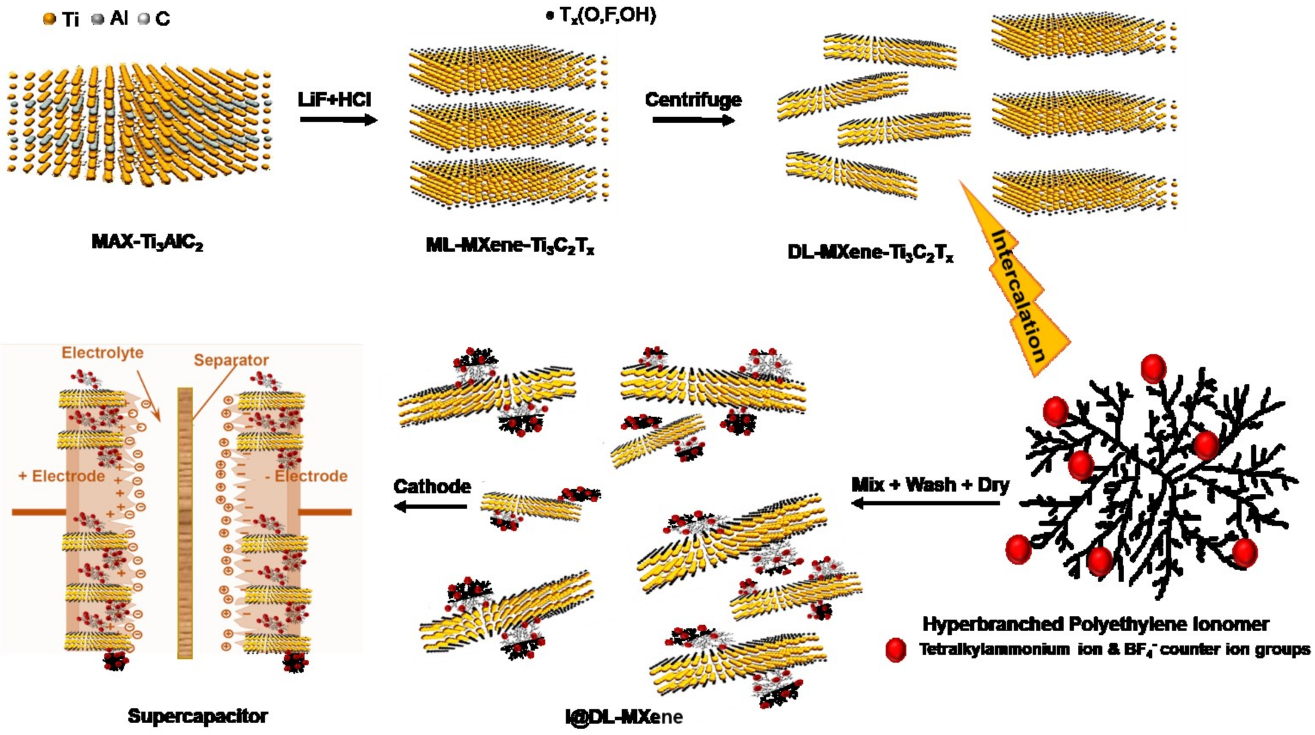

Scheme 5.1 Schematic illustration of the preparation of I@DL-MXene as electrodes for supercapacitor.

TGA characterization was performed on the modified MXenes to evaluate their thermal behaviour and quantify their ionomer and CTAB content. All TGA experiments are accomplished under N_2 atmosphere. Figure 5.1a shows the TGA curves of the I-modified DL-MXene and I-modified ML-MXene at $(m_{ionomer}/m_{MXene})_0$ ratio 2, along with those of pure ionomer, dried unmodified, and virgin ML- and DL-MXene, pure CTAB, and CTAB modified DL-MXene obtained at $(m_{CTAB}/m_{MXene})_0$ ratio 2 for comparison. Ionomer starts decomposition at 280 °C with a nearly complete weight loss at 480 °C. Dried unmodified ML-MXene and DL-MXene exhibit stability without considerable weight loss within this temperature range (T_{room} to 600°C). Both the Ionomer-modified MXenes (ML- and DL-) exhibit a one-step weight loss, within 280 ─ 480 °C (ΔW), attributable solely to the decomposition of the ionomer. So, the mass contents of the ionomer and CTAB in the modified DL-MXenes have thus been quantified from ΔW and are summarized in Table S5.1.

The initial stage was the confirmation of the structural quality of the commercial MAX phase, which was intended to be utilized as the precursor material for the MXene. This verification was performed using X-ray diffraction (XRD) analysis. The main phase was confirmed to be Ti_3AlC_2, as represented in our previous paper.[7] The *d*-spacing of multi-layer MXene (ML-MXene) and I@ML-MXene are 10.8 A° and 13.6 A°, respectively. The characteristic (002) peak in ionomer-modified DL-MXene (Figure 5.1b,c) is broadened and obviously shifted to a much lower diffraction angle direction, 2θ =4.7°, indicating the increase of interlayer distance. Indeed, the larger *d*-spacing of 6 A° additional than unmodified DL-MXene (*d*-spacing of 13A°) and 4.5 A° than C@DL-MXene are created. The *d*-spacing increase by CTABs is about 2 A◦ more than unmodified DL-MXene, which has been demonstrated before.[181] Ionomer with numerous quaternary ammonium groups per chain aggressively adsorbs onto MXene sheets by electrostatic interaction and ionic adsorption of their positive quaternary ammonium groups to the negatively charged MXene surface. This is additionally due to the hyperbranched morphology and topology of polyethylene branches, which expand the layer's space. The individual structure resembles an enlarged interlayer spacing; this may facilitate the transport of ions in the channel during charge/discharge cycle testing.

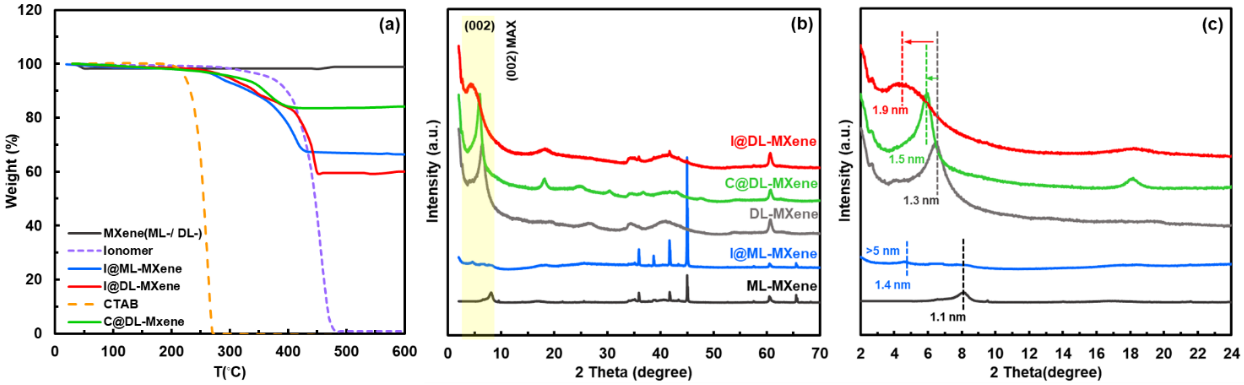

Figure 5.1 (a) TGA curves of unmodified ML-/DL-MXene, Ionomer, I@ML-MXene, and I@DL-MXene at Ionomer/ML- or DL-MXene mass ratio 2, pure CTAB, and CTAB modified DL-MXene (C@DL-MXene) with mass ratio 2; (b) XRD patterns of unmodified ML-MXene, DL-MXene,

I@ML-MXene, I@DL-MXene, and CTAB@dl-MXene; (c) magnified image of the selected region in figure b.

Figure 2 shows TEM images of unmodified ML-MXene and DL-MXene, I@ML-MXene, and I@DL-MXene. Layered 2D-sheet structures with an interplanar spacing of *ca.* 1 nm are observed in the unmodified ML-MXene (Figure 5.2a). The selected area electron diffraction (SAED) (inset in Figure 5.2a) shows that the basal planes' atomic arrangement is identical to that in the parent MAX phase.[224] 2D sheets are observed in I@ML-MXene (Figure 5.2b) but with a significantly enlarged interplanar spacing of 9.2 nm, confirming the successful exfoliation of the ML-MXene into large interplanar spacings upon the intercalation with the ionomer at a high content. Relative to ML-MXene, DL-MXene shows decreased number of layers (Figure 5.2c). The TEM images of I@DL-MXene show many few-layered structures, including mono- and bi-layers and aggregated flakes (Figure 5.2d) due to the cross-linking effect of the multidentate ionomer. From its SAED images, the hexagonal atomic structure is well retained in I@DL-MXene. Consistent with the XRD results, the TEM images provide additional evidence supporting the effective intercalation of the ionomer into the nanosheets, which results in the entire exfoliation for some of them. The strong ionic interactions between the quaternary ammonium ions on the ionomer and the negatively charged MXene layer surface are reasoned to contribute to the high efficiency of intercalation and subsequent exfoliation of the nanosheets.

Previous TEM elemental mapping of C, F, O, and Ti in Figure 4.2 j in the previous chapter showed qualitative changes in functional group distribution on DL-MXene before and after ionomer intercalation. It displayed a higher ratio of O to F groups in I@DL-MXene compared to DL-MXene.

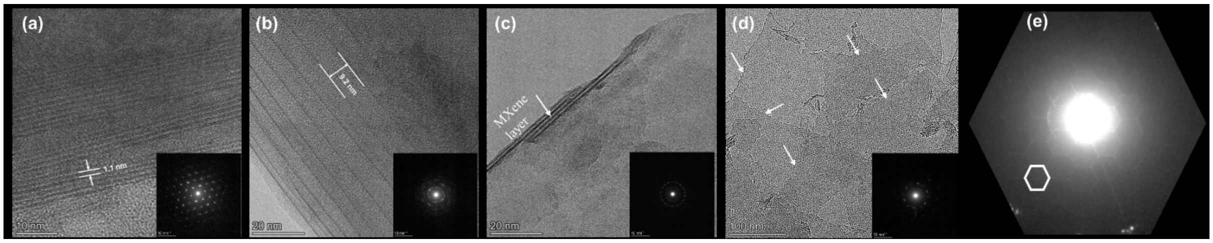

Figure 5.2 (a) TEM images of virgin unmodified Ti3C2Tx ML-MXene; (b) I@ML-MXene; (c) DL-MXene; and (d) I@DL-MXene; the insets in (a),(d),(c) and (d) are the SAED patterns in 10 nm-1; (e) magnification of (d).

5.3.2 Electrochemical Measurements

The selection of the electrolyte significantly affects the electrochemical performance of $Ti_3C_2T_x$ electrodes.[225] The pristine MXenes and modified MXenes electrodes were evaluated in two distinct aqueous and organic electrolyte solutions. This process was carried out to acquire a more profound knowledge of the influence of the electrolyte's composition and the electrode surface chemistry on the electrochemical performance of the MXene. The electrochemical characterization of the fabricated ML-/DL- MXene and I@DL-MXene electrodes was performed using a three-electrode setup with carbon current collectors in 1 M H2SO4 solution as the electrolyte. Figure 5.3 shows the cyclic voltammetry (CV) curves of ML-/DL- MXene and I@DL-MXene electrodes in a 1M H_2SO_4 electrolyte solution, with scan rates being varied from 2 to 200 mV s^{-1} in the positive potential window.[226] Both the treated and untreated samples exhibited a characteristic cyclic voltammetry (CV) response. ML-MXene commonly demonstrates a pseudocapacitive behaviour by a capacity value of about 80 mAh g^{-1} at a scan rate of 2 m Vs^{-1} in aqueous acidic electrolyte solutions.[225] Here, ML-MXene and DL-MXene at scan rate 2 m Vs^{-1} in H_2SO_4 electrolyts demonstrated the specific capacity of 109 and 270 F g^{-1}, respectively, although the performance of I@DL-MXene is suboptimal (53 F g^{-1}). The obtained specific capacity for both ML- and DL -MXene is even better compatible with aqueous electrolytes than other works, which does not apply to polyethylene ionomer-modified MXene as predicted. The upper and lower layers of the I@DL-MXene electrode are hydrophobe amorphous polymers, with the middle layer of the electrode shows layered microstructure, which is mainly crystalline $Ti_3C_2T_x$. Water contact angle measurements were performed on the films (see Figure S5.1 in Supporting Information). The unmodified MXene film shows a water contact angle of 27.5°, which suggests its high hydrophilicity. On the contrary, due to the strong ionic bonding of the ionomer with a hydrophobic hyperbranched polyethylene shell, I-MXene exhibits a high water contact angle of 125°, indicative of its strong hydrophobicity. This also confirms that the intercalation of the ionomer leads to the successful surface modification of the MXene sheets with the hydrophobic hyperbranched polyethylene segments. Consequently, by acting as a barrier against the aqueous electrolyte, the ionomer prevents it from penetrating the gaps between the $Ti_3C_2T_x$ layers.[227] Figure S4.2 in Supporting Information shows the N_2 adsorption−desorption isotherms for DL-MXene and I@DL-MXene, along with the surface area and pore volume data summarized in Table S4.2. While unmodified DL-MXene shows an appreciable surface area of 55.3 m^2 g^{-1} and pore volume of 0.15 cm^3 g^{-1}, I@DL-MXene is nearly nonporous with negligible surface area or pore volume. This also suggests the successful intercalation of the ionomer, with the voids within DL-MXene almost fully filled with the ionomer. Meanwhile, by acting as a hydrophobe barrier against the aqueous electrolyte, the ionomer prevents it from penetrating the gaps between the $Ti_3C_2T_x$ layers.[227] In contrast of hydrophilic and conductive polymers, here diffusion-limited contributions control the total capacitance. [226] It is well demonstrated that polymers like PPy (polypyrrole) with advanced conducting properties with beneficial electrical conductivity and high redox and capacitive current are able to enhance the MXene supercapacity behaviour.[228]

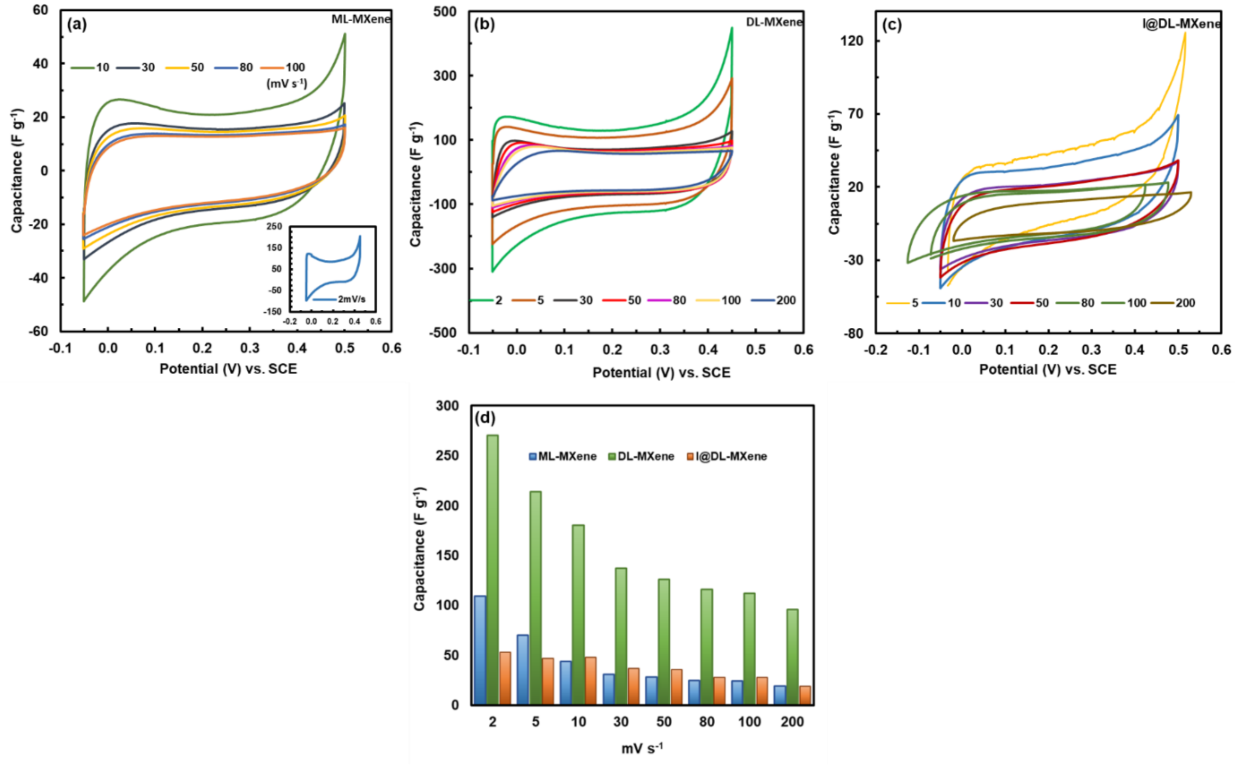

Figure 5.3 CV curves in different scan rates of (a) ML-MXene, (b) DL-MXene, and (c) I@DL-MXene electrodes in 1M H_2SO_4, measured in a 3-electrode cell configuration using carbon paper loaded with active material; (d) comparing the capacitance of ML-MXene, DL-MXene and I@DL-MXene in different scan rates.

Interest in the use of ionic liquids (ILs) in high-performance supercapacitor devices has increased exponentially among an abundance of liquid electrolytes. This innovative and multifunctional electrolyte medium is distinguished by its exceptional ionic conductivity, low vapour pressure, and broad, stable potential windows.[229] In general, aqueous electrolytes exhibit a restricted-energy density due to their relatively narrow operative voltage window, whereas organic electrolytes possess high toxicity and thermal instability characteristics. Pleasantly, ILs could offer the opportunity to fabricate supercapacitors characterized by excellent energy density and intensified safety.[230, 231] In this regard, electrochemical performance measurements for ionomer-modified MXene were conducted using a LiTFSi electrolyte solution. The rate capability of the I@DL-MXene electrodes was greatly increased, as illustrated by the CV and GCD tests carried out at various charging rates and presented in Figure 5.4. Figure 5.4c illustrates the relationship between specific capacity with scan rate. I@DL-MXene showed a special capacity of 124 F g−1 at a scan rate of 2 m Vs-1 in LiTFSi electrolyte.

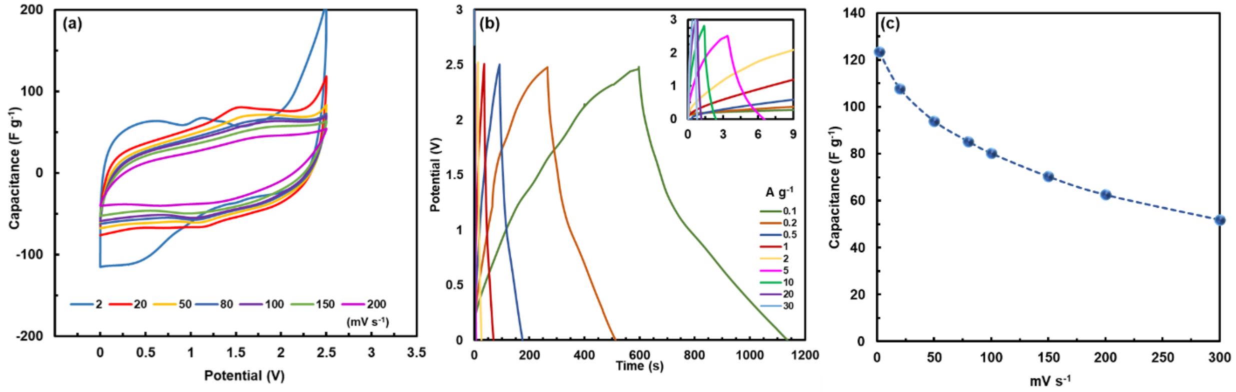

Figure 5.4 CV curves in different scan rates of I@DL-MXene electrodes in LiTFSi electrolyte; (b) GCD curves in different current densities of I@DL-MXene electrodes in LiTFSi electrolyte; (c) the relationship between specific capacity with scan rate.

Motivated by the enhanced results achieved in the ionic liquid electrolyte, an investigation was conducted to study and compare the electrochemical characteristics of the pristine ML-/DL-MXenes with ionomer and CTAB-modified MXene in another ionic liquid electrolyte solutions with a larger voltage window. So, the electrochemical behaviour of pure MXenes (ML-MXene and DL-MXene) and MXene nanocomposites (C@DL-MXene and I@DL-MXene) were fully assessed in a two electrodes cell while $EMIM^{+}BF^{-}_{4}$ was used as the electrolyte.

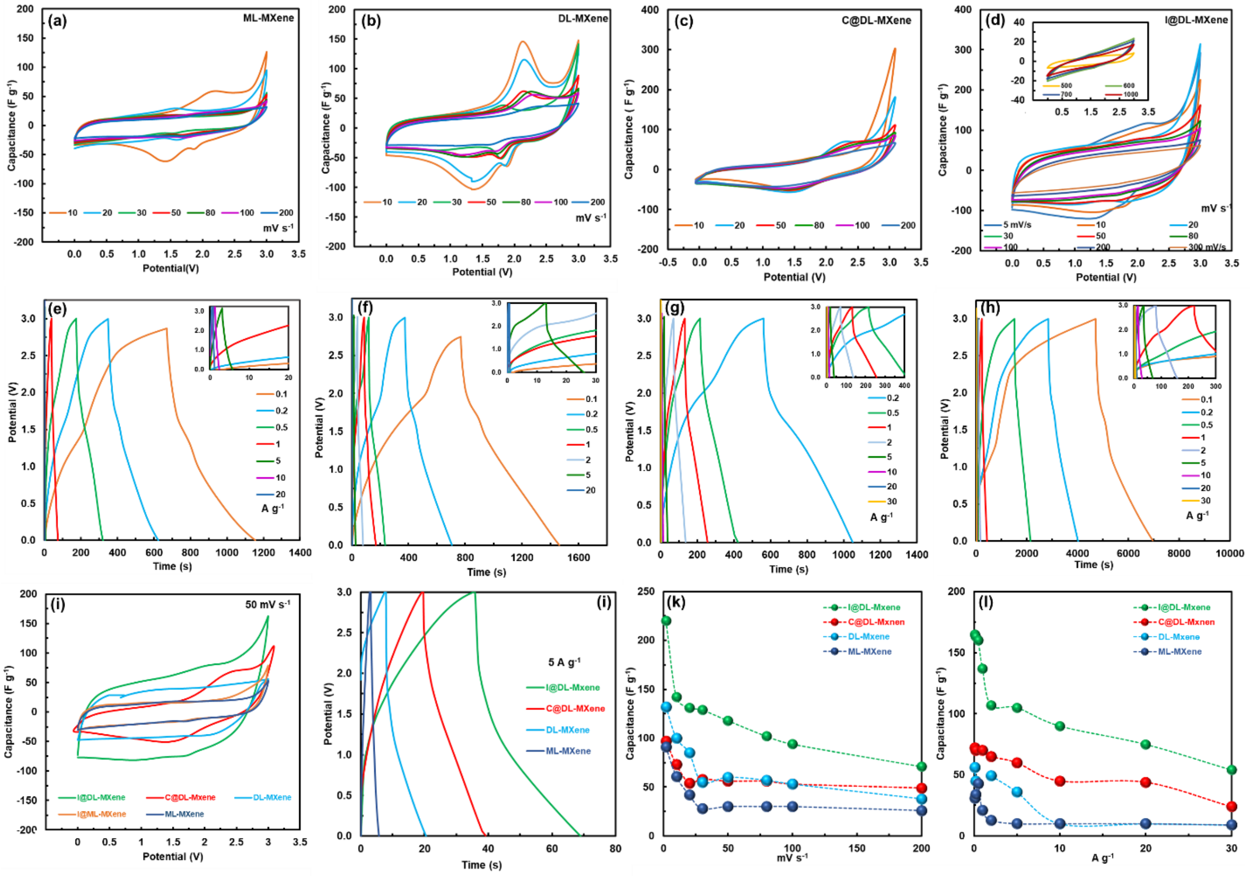

Figure 5.5 Electrochemical characteristics of ML-MXene, DL-MXene, C@DL-MXene and I@DL-MXene electrodes in $EMIM^{+}BF4^{-}$ electrolyte. (a-d) CV curves in different scan rates; (e-h) GCD curves in different current density; (i) comparing CV curves at scan rate 50 mV s^{-1}; (j) comparing GCD profiles at current density 5A g^{-1}; specific capacity of ML-MXene, DL-MXene, C@DL-MXene and I@DL-MXene electrodes based on (k) different scan rates and (l) different current densities.

The CV curves, Figure 5.5a-d, were recorded at different scan rates within a voltage window of 0.01 to 3 V, and the corresponding specific capacitance were 91, 132, 97, and 220 F g^{-1} for ML-MXene, DL-MXene, C@DL-MXene and I @DL-MXene respectively at scan rate 2 mV s^{-1}. In nearly all cycles (Figure 5.5d), broad reversible peaks are observed at around 1.3 and 2.0 V, corresponding to a combination of reversible intercalation and surface redox pseudocapacitance behaviour. I@DL-MXene demonstrated a much higher capacity than others. It is anticipated that the surface modification of the DL-MXene and the resulting increase in interlayer spacing will reduce the ion diffusion barrier and enhance the access of solvated ions into the MXene layers. The reduced quantity of fluorine terminations (based on elemental mapping from TEM results), results in decreased electrostatic interactions among the MXene sheets. [11]

The GCD profiles in Figure 5.5e-h clearly demonstrate the beneficial effect of the ionomer modification in $EMIM^{+}BF_4^{-}$ electrolyte solution. It is clearly observed that I@DL-MXene composite electrodes possessed a longer discharging time and larger capacitance retention. It’s suggested that the increased wettability of the electrolyte and the larger interlayer space would have a significant effect on the transport of electrolyte ions.[231] At lower current densities, 0.1 A g^{-1}, I@DL-MXene delivered a capacity of 165 F g^{-1}, whereas only 31, 56 and 72 F g^{-1} was obtained for the pristine ML-MXene,DL-MXene and C@DL-MXene electrode. Similarly, the I@DL-MXene exhibited a high capacity value of 90 F g^{-1} at a fast charging rate (10 A g^{-1}), whereas only 10, 10 and 44 F g^{-1} were obtained for ML-MXene, DL-MXene and C@DL-MXene due to diffusion limitations. Nevertheless, the capacitance achieved with I@DL-MXene is much higher than that with other electrodes at any given current density.

The CV curves for half-cell supercapacitors at scan rates of 50 mV S^{-1} with a potential window of 0.01–3 V for both virgin ML-/DL- MXene and modified MXene with CTAB and ionomer are shown in Figure 5.5i**.** The ionomer-modified MXene-based device shows a larger enclosed area than that of virgin and CTAB MXene-based devices, signifying increased capacitance with the former. This outcome is also confirmed by the GCD curves (Figure 5.5j).

Figure 5.5k plots the capacitance as a function of the scan rate. The I@DL-MXene electrode displays capacitances of 220, 147, 142, 131, 118, 102, 94, 71 and 57 F g^{-1} at 2, 5, 10, 20, 50, 80, 100, 200 and 300 mV s^{-1}, respectively, which are significantly higher than the corresponding values for the other MXene electrodes.

While all fresh devices except ML-MXene show nearly overlapping EIS curves, the I@DL-MXene device after 100 GCD cycles at 1 A g-1 displays a linear line of a larger slope in the low-frequency range than other MXene devices (Figure 5.6), reflecting the enhanced capacitive behaviour and improved ion dynamics with the former.[221] These results demonstrate that ionomer intercalation with expanded interlayer spacing offers a higher ion-accessible surface area with reduced ion migration resistances and thereby significantly increases the capacitance of electrochemically active MXene materials.[221, 225]

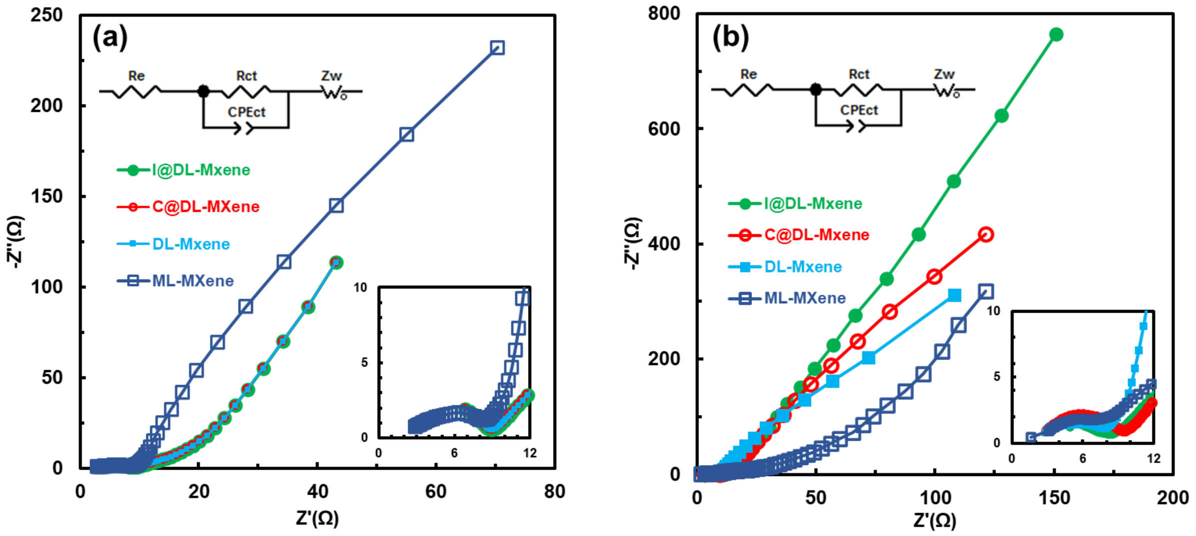

Figure 5.6 Nyquist plots of ML-MXene, DL-MXene, C@DL-MXene and I@DL-MXene electrodes in EMIM$^+$BF4$^-$ electrolyte with (a) fresh cells and (b) cells after 100 GCD cycles at 1 A g^{-1}.

Table 5.1 compares the capacitance results obtained in prior studies on $Ti_3C_2T_x$ in ionic liquid electrolytes. The capacitance values obtained herein with I@DL-MXene are comparable or even better than those reported in the literature.

Table 5.1 Electrochemical Parameters and Capacitances for MXene-based Electrodes

Material(s)	**Electrolyte**	**Potential Window ΔV (V)**	**Capacitance**	**Reference**
I@DL-MXene	$EMIMBF_4$	0 ─ 3	220 F g^{-1}@ 2 mV s^{-1}	This work
$Ti_3C_2T_X$ film	$EMIMBF_4$	0 ─ 3	96 F cm^{-3}@ 50 mV s^{-1}	[221]
CNT-Ti_3C_2 T_X	1M EMIMTFSI/ACN	-0.8 ─ 1	85 F g^{-1}@ 2 mV s^{-1}	[232]
$Ti_3C_2T_X$ film	1M $EMIMBF_4$/ACN	0 ─ 2.2	244.5 F cm^{-3}@ 2 mV s^{-1}	[233]

5.4 Conclusions

In summary, via sophisticated material design approaches, we were able to successfully fabricate a functionalized Ti3C2-MXene composite through the use of both hydrophobic ionomers and ionic liquid electrolytes. The utilization of ionomer was critical in the development of efficient electron/ion transport channels within the I@DL-MXene. The ionomer functions as a spacer, addressing both the issues of aggregation and restacking while additionally resulting in a favourable capacitance for the hybrid materials. Consequently, this led to a greater expansion of the ion-accessible area, thereby facilitating faster ion diffusion kinetics. Hence, the incorporation of these characteristics and properties in the ionomer-modified MXene is expected to result in a considerable enhancement in supercapacitor performances. This study presents the initial findings on the utilization of non-conductive polymer as spacers between MXene materials in an ionic liquid (IL) electrolyte. This novel approach offers an innovative framework for improving the electrochemical performance of MXenes in various IL electrolytes and other sorts of polymers for supercapacitors.

Chapter 6 Contributions and Significance of Thesis Research and Suggestions for Future Work

6.1 Contributions and Significance of Thesis Research

For the first time, a $Ti_3C_2T_x$ (MXene) is intercalated, delaminated, functionalized, and surface-modified with hyperbranched polyethylene ionomers by simple mixing. This superior hybrid structure effectively prevents the restacking phenomenon in 2D MXene material and renders high charge storage capacity, high dispersion stability in organic solvents, and minimized oxidation of MXene in aqueous suspensions. Furthermore, it is anticipated that these nanocomposite materials exhibit excellent electrochemical properties.

i) *Preparation of stable high-concentration MXene dispersions in low-polarity/ non-polar conventional organic solvents*

Delaminated $Ti_3C_2T_x$ shows as few- and single-layer flakes similar to graphene and other 2D materials. However, unlike graphene, these flakes are hydrophilic and have a highly negative ζ potential in the range of −39.5 to −63 mV. Herein, the set of I-MXenes obtained with different ionomers shows the increased ζ potential within 30 to 48 mV. The hyperbranched polyethylene ionomers, as the hydrophobe surfactants, adsorb onto the exfoliated MXene sheets through ionic interactions. The ionomer modification prevents MXene sheets from restacking and renders them stable dispersion in non-polar organic solvents. We have demonstrated the successful high-concentration dispersions of modified MXene flakes in a range of nonpolar/low-polarity solvents (benzene, toluene, xylene, hexane, cyclohexane, THF, chloroform, ethyl acetate), as well as some polar solvents (acetonitrile, DMSO, DMF, acetone). In these solvents, the dispersions of ionomer-modified MXenes with moderate ionic contents were stable for 100 days. With THF as the solvent, the dispersions of I-MXene at a concentration as high as 31.1 mg mL^{-1} were achieved. The ranges of Hildebrand and Hansen parameters of the solvents where I-MXene was well dispersed showed the broader range of nonpolar/low-polarity organic solvents where I-MXene could well disperse relative to other modified-MXenes reported in the literature. The UV-Vis extinction coefficients of I-MXene in four nonpolar/low-polarity solvents (chloroform, toluene, xylene, and THF) with the best dispersion stability have been measured.

In addition to our above procedure for the synthesis of ionomer-modified MXenes, we have also conducted an alternative interfacial modification/phase transfer strategy that further expands the toolbox of ionomer-functionalized MXenes.

ii) *Modification of MXene to mitigate oxidation in aqueous colloidal suspensions*

One way to prevent oxidation of MXene is to store it in organic solvents. Dispersions in organic solvents can provide a route to mitigate or prevent oxidation and extend the shelf life of MXene in solution. However, the fact that MXenes form less stable suspensions in the organic solvents compared to water is a major disadvantage. Intercalated water may lead to the degradation of organic electrolytes in electrochemical applications of MXenes. It has been demonstrated that the ionomer modification can effectively suppress MXene oxidation over a long time (at least 100 days *vs*. 10 days for virgin MXene) in water and exposed to air at room temperature.

iii) Application of MXene nanocomposites in energy storage (MIBs and Supercapacitors)

Ionomer modification effectively prevents the restacking phenomenon of 2D MXene and creates an ultra-large d-spacing between MXene sheets, presumably enabling faster transport of ions and electrons. The ionomer thus acts as the pillar in the pillared MXene, which renders the layers open and endows the pillared MXene with extra capacity for magnesium-ion storage. The ionomer also acts as a surfactant and modifies the surface of DL-MXene sheets by reducing the fluorine-to-oxygen ratio and enhancing the wettability with electrolytes. Our results have shown that I@DL-MXene cathode demonstrates enhanced magnesium-ion storage capacities (e.g., 213 mAh g^{-1} vs about 3 mAh g^{-1} for ML-MXene and 80 mAh g^{-1} for DL-MXene at 0.02 A g^{-1}). The I@DL-MXene cathode is also distinctly featured with the improved electrode/electrolyte interface charge transfer, which effectively overcomes the sluggish solid-state kinetics of Mg^{2+} in MIBs. It shows promising cycling stability with a capacity retention of 86% after 400 cycles and 71% after 1000 cycles at 200 mA g^{-1}.

A two-electrode supercapacitor made with an ionomer-modified MXene exhibits a capacitance of 220 F g^{-1} at a scan rate of 2 mV s^{-1} in $EMIM^{+}BF4^{-}$ electrolyte, which is comparable to or even better than those reported in the literature.

It has been demonstrated in this thesis that MXene can be easily modified with the hyperbranched ionomer to achieve lightweight, high efficiency, strong corrosion resistance, excellent mechanical properties, versatile property tune-ability, and excellent processibility for different applications, particularly energy storage devices.

6.2 Suggestions for future work

- Scalability and cost-effectiveness: The scalability and cost-effectiveness of polymer/MXene nanocomposites are important factors for their commercial viability. Currently, the synthesis of MXenes involves complex and time-consuming processes requiring chemical treatments. Developing cost-effective and large-scale synthesis methods that do not compromise the properties of MXenes is essential for their widespread use. Additionally, the cost of MXenes and polymers should be taken into consideration to ensure the economic feasibility of the nanocomposites.

- Augmented Multifunctionality: A compelling avenue for the future development of polymer/MXene nanocomposites resides in the augmentation of their multifunctionality. Precision tailoring of the properties inherent in both MXenes and polymers can yield nanocomposites possessing an amalgamation of highly coveted characteristics curated for specific applications. For instance, simultaneous enhancements in electrical conductivity, mechanical robustness, and thermal stability have the potential to underpin the creation of exceptionally efficient energy storage devices.
- Pioneering Processing Techniques: A pivotal trajectory for advancing the potential of polymer/MXene nanocomposites lies in the exploration of cutting-edge processing techniques. Methods such as electrospinning, 3D printing, and layer-by-layer assembly furnish opportunities to craft intricate hierarchical structures imbued with heightened performance attributes. Notably, these techniques confer the invaluable advantage of meticulous control over the composition and morphology of the nanocomposites, thereby facilitating the bespoke tailoring of their properties to cater to specific applications.
- Uncharted Applications: The utility of polymer/MXene nanocomposites extends well beyond the confines of energy storage systems. Their exceptional mechanical and electrical properties render them alluring prospects for diverse domains, including sensors, actuators, electromagnetic shielding, and water purification. Venturing into these uncharted realms of application unfolds the promise of exhilarating prospects for polymer/MXene nanocomposites, presenting novel solutions and innovative horizons in this evolving field.

References

1. Sangian, D.; Naficy, S.; Dehghani, F.; Yamauchi, Y., A review on layered mineral nanosheets intercalated with hydrophobic/hydrophilic polymers and their applications. *Macromolecular Chemistry and Physics* **2018,** *219* (13), 1800142.

2. Anasori, B.; Lukatskaya, M. R.; Gogotsi, Y., 2D metal carbides and nitrides (MXenes) for energy storage. *Nature Reviews Materials* **2017,** *2* (2), 1-17.

3. Pang, J.; Mendes, R. G.; Bachmatiuk, A.; Zhao, L.; Ta, H. Q.; Gemming, T.; Liu, H.; Liu, Z.; Rummeli, M. H., Applications of 2D MXenes in energy conversion and storage systems. *Chemical Society Reviews* **2019,** *48* (1), 72-133.

4. Niu, L.; Coleman, J. N.; Zhang, H.; Shin, H.; Chhowalla, M.; Zheng, Z., Production of two‐dimensional nanomaterials via liquid‐based direct exfoliation. *Small* **2016,** *12* (3), 272-293.

5. Gogotsi, Y.; Anasori, B., The rise of MXenes. ACS Publications: **2019**; Vol. 13, pp 8491-8494.

6. Lipatov, A.; Alhabeb, M.; Lukatskaya, M. R.; Boson, A.; Gogotsi, Y.; Sinitskii, A., Effect of synthesis on quality, electronic properties and environmental stability of individual monolayer Ti3C2 MXene flakes. *Advanced Electronic Materials* **2016,** *2* (12), 1600255.

7. Xiao, X.; Wang, H.; Urbankowski, P.; Gogotsi, Y., Topochemical synthesis of 2D materials. *Chemical Society Reviews* **2018,** *47* (23), 8744-8765.

8. Ghidiu, M.; Lukatskaya, M. R.; Zhao, M.-Q.; Gogotsi, Y.; Barsoum, M. W., Conductive two-dimensional titanium carbide 'clay'with high volumetric capacitance. *Nature* **2014,** *516* (7529), 78-81.

9. Lukatskaya, M. R.; Mashtalir, O.; Ren, C. E.; Dall'Agnese, Y.; Rozier, P.; Taberna, P. L.; Naguib, M.; Simon, P.; Barsoum, M. W.; Gogotsi, Y., Cation intercalation and high volumetric capacitance of two-dimensional titanium carbide. *Science* **2013,** *341* (6153), 1502-1505.

10. Dusastre, V., *Materials for sustainable energy: a collection of peer-reviewed research and review articles from Nature Publishing Group*. World Scientific: **2010.**

11. Simon, P., Two-dimensional MXene with controlled interlayer spacing for electrochemical energy storage. *ACS nano* **2017,** *11* (3), 2393-2396.

12. Anasori, B.; Gogotsi, Y., MXenes: Trends, growth, and future directions. *Graphene and 2D Materials* **2022,** *7* (3-4), 75-79.

13. Sang, X.; Xie, Y.; Lin, M.-W.; Alhabeb, M.; Van Aken, K. L.; Gogotsi, Y.; Kent, P. R.; Xiao, K.; Unocic, R. R., Atomic defects in monolayer titanium carbide (Ti3C2T x) MXene. *ACS nano* **2016,** *10* (10), 9193-9200.

14. Naguib, M.; Mochalin, V. N.; Barsoum, M. W.; Gogotsi, Y., 25th anniversary article: MXenes: a new family of two‐dimensional materials. *Advanced materials* **2014,** *26* (7), 992-1005.

15. Johnson, D.; Qiao, Z.; Uwadiunor, E.; Djire, A., Holdups in nitride MXene's development and limitations in advancing the field of MXene. *Small* **2022,** *18* (17), 2106129.

16. Lei, J.-C.; Zhang, X.; Zhou, Z., Recent advances in MXene: Preparation, properties, and applications. *Frontiers of Physics* **2015,** *10*, 276-286.

17. Natu, V.; Hart, J. L.; Sokol, M.; Chiang, H.; Taheri, M. L.; Barsoum, M. W., Edge capping of 2D‐MXene sheets with polyanionic salts to mitigate oxidation in aqueous colloidal suspensions. *Angewandte Chemie* **2019,** *131* (36), 12785-12790.

18. Li, X.; Huang, Z.; Shuck, C. E.; Liang, G.; Gogotsi, Y.; Zhi, C., MXene chemistry, electrochemistry and energy storage applications. *Nature Reviews Chemistry* **2022,** *6* (6), 389-404.

19. Sun, R.; Zhang, H. B.; Liu, J.; Xie, X.; Yang, R.; Li, Y.; Hong, S.; Yu, Z. Z., Highly conductive transition metal carbide/carbonitride (MXene)@ polystyrene nanocomposites fabricated by electrostatic assembly for highly efficient electromagnetic interference shielding. *Advanced Functional Materials* **2017,** *27* (45), 1702807.

20. Franssen, N. M.; Reek, J. N.; de Bruin, B., Synthesis of functional ‘polyolefins’: state of the art and remaining challenges. *Chemical Society Reviews* **2013,** *42* (13), 5809-5832.

21. Zhang, L.; Brostowitz, N. R.; Cavicchi, K. A.; Weiss, R., Perspective: Ionomer research and applications. *Macromolecular Reaction Engineering* **2014,** *8* (2), 81-99.

22. Marx, C. L.; Caulfield, D. F.; Cooper, S. L., Morphology of ionomers. *Macromolecules* **1973,** *6* (3), 344-353.

23. Khazaei, M.; Mishra, A.; Venkataramanan, N. S.; Singh, A. K.; Yunoki, S., Recent advances in MXenes: From fundamentals to applications. *Current Opinion in Solid State and Materials Science* **2019,** *23* (3), 164-178.

24. Deshmukh, K.; Muzaffar, A.; Kovářík, T.; Ahamed, M. B.; Pasha, S. K., Introduction to 2D MXenes: fundamental aspects, MAX phases and MXene derivatives, current challenges, and future prospects. *Mxenes and their Composites* **2022**, 1-47.

25. Wu, X.; Ma, P.; Sun, Y.; Du, F.; Song, D.; Xu, G., Application of MXene in electrochemical sensors: a review. *Electroanalysis* **2021,** *33* (8), 1827-1851.

26. Liu, C.; Han, X.; Cao, Y.; Zhang, S.; Zhang, Y.; Sun, J., Topological construction of phosphorus and carbon composite and its application in energy storage. *Energy Storage Materials* **2019,** *20*, 343-372.

27. Lim, K. R. G.; Shekhirev, M.; Wyatt, B. C.; Anasori, B.; Gogotsi, Y.; Seh, Z. W., Fundamentals of MXene synthesis. *Nature Synthesis* **2022,** *1* (8), 601-614.

28. Nehra, S.; Sharma, R.; Kumar, D., Remediation of Hazardous Pollutants via MXenes - Based Smart Materials. In *Age of MXenes, Volume 2. Applications in Diagnostics, Therapeutics, and Environmental Remediation*, ACS Publications: **2023**; pp 169-191.

29. Song, J.; Su, D.; Xie, X.; Guo, X.; Bao, W.; Shao, G.; Wang, G., Immobilizing polysulfides with MXene-functionalized separators for stable lithium–sulfur batteries. *ACS applied materials & interfaces* **2016,** *8* (43), 29427-29433.

30. Shuck, C. E.; Han, M.; Maleski, K.; Hantanasirisakul, K.; Kim, S. J.; Choi, J.; Reil, W. E.; Gogotsi, Y., Effect of Ti3AlC2 MAX phase on structure and properties of resultant Ti3C2T x MXene. *ACS Applied Nano Materials* **2019,** *2* (6), 3368-3376.

31. Ajmal, Z.; Qadeer, A.; Khan, U.; Hussain, M. B.; Irfan, M.; Mehmood, R.; Abid, M.; Djellabi, R.; Kumar, A.; Ali, H., Current progresses in two-dimensional MXene-based framework: prospects from superficial synthesis to energy conversion and storage applications. *Materials Today Chemistry* **2023,** *27*, 101238.

32. Khaledialidusti, R.; Khazaei, M.; Khazaei, S.; Ohno, K., High-throughput computational discovery of ternary-layered MAX phases and prediction of their exfoliation for formation of 2D MXenes. *Nanoscale* **2021,** *13* (15), 7294-7307.

33. Fang, H.; Wang, S.; Chen, R.; Xu, Q.; Yan, Y.; Su, Y.; Guo, J., The effects of the formation of a multi-scale reinforcing phase on the microstructure evolution and mechanical properties of a Ti 2 AlC/TiAl alloy. *Nanoscale* **2021,** *13* (29), 12565-12576.

34. Zhang, R., *Exfoliation of Bilayered Vanadium Oxide and Oxide/MXene Heterostructures for Energy Storage*. Drexel University: **2022.**

35. Seok, S.-H.; Sim, Y.; Han, J.-H.; Jin, Y. H.; Chae, Y.; Park, J.; Kwon, S.-Y., Synthesis and processing of two-dimensional nitride MXenes for electrocatalysis and energy storage. *Cell Reports Physical Science* **2023**.

36. Khan, K.; Tareen, A. K.; Iqbal, M.; Hussain, I.; Mahmood, A.; Khan, U.; Khan, M. F.; Zhang, H.; Xie, Z., Recent advances in MXenes: A future of nanotechnologies. *Journal of Materials Chemistry A* **2023**.

37. Chen, H.; Ma, H.; Li, C., Host–guest intercalation chemistry in MXenes and its implications for practical applications. *ACS nano* **2021,** *15* (10), 15502-15537.

38. Cockreham, C. B. Thermochemistry of MXenes Synthesized by CoF x/HCl Etching. Washington State University, **2022.**

39. Wei, Y.; Zhang, P.; Soomro, R. A.; Zhu, Q.; Xu, B., Advances in the synthesis of 2D MXenes. *Advanced materials* **2021,** *33* (39), 2103148.

40. Wong, A. J. Y.; Lim, K. R. G.; Seh, Z. W., Fluoride-free synthesis and long-term stabilization of MXenes. *Journal of Materials Research* **2022,** *37* (22), 3988-3997.

41. Sui, J.; Chen, X.; Li, Y.; Peng, W.; Zhang, F.; Fan, X., MXene derivatives: synthesis and applications in energy convention and storage. *RSC advances* **2021,** *11* (26), 16065-16082.

42. Kharissova, O. V.; Oliva González, C. s. M. x.; Kharisov, B. I., Solubilization and dispersion of carbon allotropes in water and non-aqueous solvents. *Industrial & Engineering Chemistry Research* **2018,** *57* (38), 12624-12645.

43. Mutalib, A. A. A.; Jaafar, N. F., Potential of deep eutectic solvent in photocatalyst fabrication methods for water pollutant degradation: A review. *Journal of Environmental Chemical Engineering* **2022,** *10* (3), 107422.

44. Liu, Y.; Yu, J.; Guo, D.; Li, Z.; Su, Y., Ti3C2Tx MXene/graphene nanocomposites: Synthesis and application in electrochemical energy storage. *Journal of Alloys and Compounds* **2020,** *815*, 152403.

45. Xia, J.; Guo, H.; Yu, G.; Chen, Q.; Liu, Y.; Liu, Q.; Luo, Y.; Li, T.; Traversa, E., 2D vanadium carbide (MXene) for electrochemical synthesis of ammonia under ambient conditions. *Catalysis Letters* **2021**, 1-7.

46. Yin, T.; Li, Y.; Wang, R.; Al-Hartomy, O. A.; Al-Ghamdi, A.; Wageh, S.; Luo, X.; Tang, X.; Zhang, H., Synthesis of Ti3C2Fx MXene with controllable fluorination by electrochemical etching for lithium-ion batteries applications. *Ceramics International* **2021,** *47* (20), 28642-28649.

47. Malaki, M.; Varma, R. S., Mechanotribological aspects of MXene‐reinforced nanocomposites. *Advanced Materials* **2020,** *32* (38), 2003154.

48. Levitt, A.; Zhang, J.; Dion, G.; Gogotsi, Y.; Razal, J. M., MXene‐based fibers, yarns, and fabrics for wearable energy storage devices. *Advanced Functional Materials* **2020,** *30* (47), 2000739.

49. Verger, L.; Xu, C.; Natu, V.; Cheng, H.-M.; Ren, W.; Barsoum, M. W., Overview of the synthesis of MXenes and other ultrathin 2D transition metal carbides and nitrides. *Current Opinion in Solid State and Materials Science* **2019,** *23* (3), 149-163.

50. He, S.; Sun, X.; Zhang, H.; Yuan, C.; Wei, Y.; Li, J., Preparation strategies and applications of MXene‐polymer composites: a review. *Macromolecular Rapid Communications* **2021,** *42* (19), 2100324.

51. Saha, D.; Dalmieda, J.; Patel, V., Surface-Modified MXenes: Simulation to Potential Applications. *ACS Applied Electronic Materials* **2023**.

52. Lu, Q.; Liu, C.; Zhao, Y.; Pan, W.; Xie, K.; Yue, P.; Zhang, G.; Omar, A.; Liu, L.; Yu, M., Freestanding MXene‐based macroforms for electrochemical energy storage applications. *SusMat* **2023,** *3* (4), 471-497.

53. Zhao, D.; Dang, L.-Y.; Wang, G.-G.; Sun, N.; Deng, X.; Han, J.-C.; Zhu, J.-Q.; Yang, Y., Multifunctional, superhydrophobic and highly elastic MXene/bacterial cellulose hybrid aerogels enabled via silylation. *Journal of Materials Chemistry A* **2022,** *10* (46), 24772-24782.

54. Janica, I.; Montes‐García, V.; Urban, F.; Hashemi, P.; Nia, A. S.; Feng, X.; Samorì, P.; Ciesielski, A., Covalently Functionalized MXenes for Highly Sensitive Humidity Sensors. *Small Methods* **2023**, 2201651.

55. Ayodhya, D., A review of recent progress in 2D MXenes: Synthesis, properties, and applications. *Diamond and Related Materials* **2022**, 109634.

56. Ding, B.; Ong, W.-J.; Jiang, J.; Chen, X.; Li, N., Uncovering the electrochemical mechanisms for hydrogen evolution reaction of heteroatom doped M2C MXene (M= Ti, Mo). *Applied Surface Science* **2020,** *500*, 143987.

57. Qu, G.; Zhou, Y.; Wu, T.; Zhao, G.; Li, F.; Kang, Y.; Xu, C., Phosphorized MXene-phase molybdenum carbide as an earth-abundant hydrogen evolution electrocatalyst. *ACS Applied Energy Materials* **2018,** *1* (12), 7206-7212.

58. Le, T. A.; Bui, Q. V.; Tran, N. Q.; Cho, Y.; Hong, Y.; Kawazoe, Y.; Lee, H., Synergistic effects of nitrogen doping on MXene for enhancement of hydrogen evolution reaction. *ACS Sustainable Chemistry & Engineering* **2019,** *7* (19), 16879-16888.

59. Chen, L.; Lin, Y.; Fu, J.; Xie, J.; Chen, R.; Zhang, H., Hybridization of binary non‐precious‐metal nanoparticles with d‐Ti3C2 MXene for catalyzing the oxygen reduction reaction. *ChemElectroChem* **2018,** *5* (21), 3307-3314.

60. Kong, W.; Deng, J.; Li, L., Recent advances in noble metal MXene-based catalysts for electrocatalysis. *Journal of Materials Chemistry A* **2022,** *10* (28), 14674-14691.

61. Ruan, X.; Li, S.; Huang, C.; Zheng, W.; Cui, X.; Ravi, S. K., Catalyzing Artificial Photosynthesis with TiO2 Heterostructures and Hybrids–Emerging Trends in a Classical yet Contemporary Photocatalyst. *Advanced Materials* **2023**, 2305285.

62. Naguib, M.; Barsoum, M. W.; Gogotsi, Y., Ten years of progress in the synthesis and development of MXenes. *Advanced Materials* **2021,** *33* (39), 2103393.

63. Bjork, J.; Rosen, J., Functionalizing MXenes by tailoring surface terminations in different chemical environments. *Chemistry of Materials* **2021,** *33* (23), 9108-9118.

64. Li, J.; Wang, S.; Du, Y.; Liao, W., Enhanced photocatalytic performance of TiO2@ C nanosheets derived from two-dimensional Ti2CTx. *Ceramics International* **2018,** *44* (6), 7042-7046.

65. Rafieerad, M.; Rafieerad, A.; Mehmandoust, B.; Dhingra, S.; Shanbedi, M., New water-based fluorescent nanofluid containing 2D titanium carbide MXene sheets: a comparative study of its thermophysical, electrical and optical properties with amine and carboxyl covalently functionalized graphene nanoplatelets. *Journal of Thermal Analysis and Calorimetry* **2021,** *146*, 1491-1504.

66. Altan, A.; Namvari, M., Multifunctional, flexible, and mechanically robust polyimide-MXene nanocomposites: a review. *2D Materials* **2023**.

67. Li, G.; Wyatt, B. C.; Song, F.; Yu, C.; Wu, Z.; Xie, X.; Anasori, B.; Zhang, N., 2D titanium carbide (MXene) based films: expanding the frontier of functional film materials. *Advanced Functional Materials* **2021,** *31* (46), 2105043.

68. Fakharuddin, A.; Li, H.; Di Giacomo, F.; Zhang, T.; Gasparini, N.; Elezzabi, A. Y.; Mohanty, A.; Ramadoss, A.; Ling, J.; Soultati, A., Fiber‐shaped electronic devices. *Advanced Energy Materials* **2021,** *11* (34), 2101443.

69. Tran, L.; Haase, M. F., Templating interfacial nanoparticle assemblies via in situ techniques. *Langmuir* **2019,** *35* (26), 8584-8602.

70. Peng, C.; Zhou, T.; Wei, P.; Xu, W.; Pan, H.; Peng, F.; Jia, J.; Zhang, K.; Yu, H., Photocatalysis over MXene-based hybrids: Synthesis, surface chemistry, and interfacial charge kinetics. *Apl Materials* **2021,** *9* (7).

71. Rizi, K. S.; Hatamluyi, B.; Darroudi, M.; Meshkat, Z.; Aryan, E.; Soleimanpour, S.; Rezayi, M., PCR-free electrochemical genosensor for Mycobacterium tuberculosis complex detection based on two-dimensional Ti3C2 Mxene-polypyrrole signal amplification. *Microchemical Journal* **2022,** *179*, 107467.

72. Zhou, X.; Guo, Y.; Wang, D.; Xu, Q., Nano friction and adhesion properties on Ti3C2 and Nb2C MXene studied by AFM. *Tribology International* **2021,** *153*, 106646.

73. Liu, L.; Raymundo-Piñero, E.; Taberna, P.-L.; Simon, P., Electrochemical characterization of Ti3C2Tx MXene prepared via a molten salt etching route in an acetonitrile-based electrolyte. *Electrochemistry Communications* **2023,** *148*, 107453.

74. Liu, L.; Orbay, M.; Luo, S.; Duluard, S.; Shao, H.; Harmel, J.; Rozier, P.; Taberna, P.-L.; Simon, P., Exfoliation and delamination of Ti3C2T x MXene prepared via molten salt etching route. *ACS nano* **2021,** *16* (1), 111-118.

75. Jasim, S. A.; Hadi, J. M.; Opulencia, M. J. C.; Karim, Y. S.; Mahdi, A. B.; Kadhim, M. M.; Bokov, D.; Jalil, A. T.; Mustafa, Y. F.; Falih, K. T., MXene/metal and polymer nanocomposites: preparation, properties, and applications. *Journal of Alloys and Compounds* **2022,** *917*, 165404.

76. Chen, X.; Zhao, Y.; Li, L.; Wang, Y.; Wang, J.; Xiong, J.; Du, S.; Zhang, P.; Shi, X.; Yu, J., MXene/polymer nanocomposites: preparation, properties, and applications. *Polymer Reviews* **2021,** *61* (1), 80-115.

77. Meng, W.; Liu, X.; Song, H.; Xie, Y.; Shi, X.; Dargusch, M.; Chen, Z.-G.; Tang, Z.; Lu, S., Advances and challenges in 2D MXenes: From structures to energy storage and conversions. *Nano Today* **2021,** *40*, 101273.

78. Orangi, J.; Beidaghi, M., A review of the effects of electrode fabrication and assembly processes on the structure and electrochemical performance of 2D MXenes. *Advanced Functional Materials* **2020,** *30* (47), 2005305.

79. Kshetri, T.; Tran, D. T.; Le, H. T.; Nguyen, D. C.; Van Hoa, H.; Kim, N. H.; Lee, J. H., Recent advances in MXene-based nanocomposites for electrochemical energy storage applications. *Progress in Materials Science* **2021,** *117*, 100733.

80. Boota, M.; Pasini, M.; Galeotti, F.; Porzio, W.; Zhao, M.-Q.; Halim, J.; Gogotsi, Y., Interaction of polar and nonpolar polyfluorenes with layers of two-dimensional titanium carbide (MXene): intercalation and pseudocapacitance. *Chemistry of Materials* **2017,** *29* (7), 2731-2738.

81. Ling, Z.; Ren, C. E.; Zhao, M.-Q.; Yang, J.; Giammarco, J. M.; Qiu, J.; Barsoum, M. W.; Gogotsi, Y., Flexible and conductive MXene films and nanocomposites with high capacitance. *Proceedings of the National Academy of Sciences* **2014,** *111* (47), 16676-16681.

82. Boota, M.; Anasori, B.; Voigt, C.; Zhao, M. Q.; Barsoum, M. W.; Gogotsi, Y., Pseudocapacitive electrodes produced by oxidant ‐ free polymerization of pyrrole between the layers of 2D titanium carbide (MXene). *Advanced Materials* **2016,** *28* (7), 1517-1522.

83. Zhang, H.; Wang, L.; Chen, Q.; Li, P.; Zhou, A.; Cao, X.; Hu, Q., Preparation, mechanical and anti-friction performance of MXene/polymer composites. *Materials & Design* **2016,** *92*, 682-689.

84. Naguib, M.; Saito, T.; Lai, S.; Rager, M. S.; Aytug, T.; Paranthaman, M. P.; Zhao, M.-Q.; Gogotsi, Y., Ti 3 C 2 T x (MXene)–polyacrylamide nanocomposite films. *RSC Advances* **2016,** *6* (76), 72069-72073.

85. Wu, X.; Hao, L.; Zhang, J.; Zhang, X.; Wang, J.; Liu, J., Polymer-Ti3C2Tx composite membranes to overcome the trade-off in solvent resistant nanofiltration for alcohol-based system. *Journal of membrane science* **2016,** *515*, 175-188.

86. Cao, Y.; Deng, Q.; Liu, Z.; Shen, D.; Wang, T.; Huang, Q.; Du, S.; Jiang, N.; Lin, C.-T.; Yu, J., Enhanced thermal properties of poly (vinylidene fluoride) composites with ultrathin nanosheets of MXene. *RSC advances* **2017,** *7* (33), 20494-20501.

87. Han, R.; Ma, X.; Xie, Y.; Teng, D.; Zhang, S., Preparation of a new 2D MXene/PES composite membrane with excellent hydrophilicity and high flux. *Rsc Advances* **2017,** *7* (89), 56204-56210.

88. Wu, Y.; Hu, H.; Yuan, C.; Song, J.; Wu, M., Electrons/ions dual transport channels design: Concurrently tuning interlayer conductivity and space within re-stacked few-layered MXenes film electrodes for high-areal-capacitance stretchable micro-supercapacitor-arrays. *Nano Energy* **2020,** *74*, 104812.

89. Chen, S.; Xiang, Y.; Banks, M. K.; Peng, C.; Xu, W.; Wu, R., Polyoxometalate-coupled MXene nanohybrid via poly (ionic liquid) linkers and its electrode for enhanced supercapacitive performance. *Nanoscale* **2018,** *10* (42), 20043-20052.

90. Yan, J.; Ma, Y.; Zhang, C.; Li, X.; Liu, W.; Yao, X.; Yao, S.; Luo, S., Polypyrrole–MXene coated textile-based flexible energy storage device. *RSC advances* **2018,** *8* (69), 39742-39748.

91. Qin, L.; Tao, Q.; Liu, X.; Fahlman, M.; Halim, J.; Persson, P. O.; Rosen, J.; Zhang, F., Polymer-MXene composite films formed by MXene-facilitated electrochemical polymerization for flexible solid-state microsupercapacitors. *Nano Energy* **2019,** *60*, 734-742.

92. McDaniel, R. M.; Carey, M. S.; Wilson, O. R.; Barsoum, M. W.; Magenau, A. J., Well-dispersed nanocomposites using covalently modified, multilayer, 2D titanium carbide (MXene) and in-situ “Click” polymerization. *Chemistry of Materials* **2021,** *33* (5), 1648-1656.

93. VahidMohammadi, A.; Moncada, J.; Chen, H.; Kayali, E.; Orangi, J.; Carrero, C. A.; Beidaghi, M., Thick and freestanding MXene/PANI pseudocapacitive electrodes with ultrahigh specific capacitance. *Journal of Materials Chemistry A* **2018,** *6* (44), 22123-22133.

94. Carey, M.; Hinton, Z.; Sokol, M.; Alvarez, N. J.; Barsoum, M. W., Nylon-6/Ti3C2T z MXene Nanocomposites Synthesized by in Situ Ring Opening Polymerization of ε-Caprolactam and Their Water Transport Properties. *ACS applied materials & interfaces* **2019,** *11* (22), 20425-20436.

95. Khosla, A.; Sonu; Awan, H. T. A.; Singh, K.; Gaurav; Walvekar, R.; Zhao, Z.; Kaushik, A.; Khalid, M.; Chaudhary, V., Emergence of MXene and MXene ‐ Polymer Hybrid Membranes as Future ‐ Environmental Remediation Strategies. *Advanced Science* **2022,** *9* (36), 2203527.

96. Feng, Y.; Deng, Q.; Peng, C.; Hu, J.; Li, Y.; Wu, Q.; Xu, Z., An ultrahigh discharged energy density achieved in an inhomogeneous PVDF dielectric composite filled with 2D MXene nanosheets via interface engineering. *Journal of Materials Chemistry C* **2018,** *6* (48), 13283-13292.

97. Liu, R.; Miao, M.; Li, Y.; Zhang, J.; Cao, S.; Feng, X., Ultrathin biomimetic polymeric Ti3C2T x MXene composite films for electromagnetic interference shielding. *ACS applied materials & interfaces* **2018,** *10* (51), 44787-44795.

98. Ghaffarkhah, A.; Kamkar, M.; Riazi, H.; Hosseini, E.; Dijvejin, Z. A.; Golovin, K.; Soroush, M.; Arjmand, M., Scalable manufacturing of flexible and highly conductive Ti 3 C 2 T x/PEDOT: PSS thin films for electromagnetic interference shielding. *New Journal of Chemistry* **2021,** *45* (44), 20787-20799.

99. Gund, G. S.; Park, J. H.; Harpalsinh, R.; Kota, M.; Shin, J. H.; Kim, T.-i.; Gogotsi, Y.; Park, H. S., MXene/polymer hybrid materials for flexible AC-filtering electrochemical capacitors. *Joule* **2019,** *3* (1), 164-176.

100. Xu, H.; Yin, X.; Li, X.; Li, M.; Liang, S.; Zhang, L.; Cheng, L., Lightweight Ti2CT x MXene/poly (vinyl alcohol) composite foams for electromagnetic wave shielding with absorption-dominated feature. *ACS applied materials & interfaces* **2019,** *11* (10), 10198-10207.

101. Pan, Q.; Zheng, Y.; Kota, S.; Huang, W.; Wang, S.; Qi, H.; Kim, S.; Tu, Y.; Barsoum, M. W.; Li, C. Y., 2D MXene-containing polymer electrolytes for all-solid-state lithium metal batteries. *Nanoscale Advances* **2019,** *1* (1), 395-402.

102. Babar, Z. U. D.; Della Ventura, B.; Velotta, R.; Iannotti, V., Advances and emerging challenges in MXenes and their nanocomposites for biosensing applications. *RSC advances* **2022,** *12* (30), 19590-19610.

103. Shuck, C. E.; Sarycheva, A.; Anayee, M.; Levitt, A.; Zhu, Y.; Uzun, S.; Balitskiy, V.; Zahorodna, V.; Gogotsi, O.; Gogotsi, Y., Scalable synthesis of Ti3C2Tx mxene. *Advanced Engineering Materials* **2020,** *22* (3), 1901241.

104. Sun, J.; Liu, B.; Zhao, Q.; Kirk, C. H.; Wang, J., MAX, MXene, or MX: What Are They and Which One Is Better? *Advanced Materials* **2023**, 2306072.

105. Fleischmann, S.; Mitchell, J. B.; Wang, R.; Zhan, C.; Jiang, D.-e.; Presser, V.; Augustyn, V., Pseudocapacitance: from fundamental understanding to high power energy storage materials. *Chemical Reviews* **2020,** *120* (14), 6738-6782.

106. Liu, Y.; Jiang, S. P.; Shao, Z., Intercalation pseudocapacitance in electrochemical energy storage: recent advances in fundamental understanding and materials development. *Materials Today Advances* **2020,** *7*, 100072.

107. Boffa, L. S.; Novak, B. M., Copolymerization of polar monomers with olefins using transition-metal complexes. *Chemical reviews* **2000,** *100* (4), 1479-1494.

108. Zhang, L.; Brostowitz, N.; Cavicchi, K.; Weiss, R., Perspective: Ionomer research and applications. Macromol React Eng 8 (2): 81–99, **2014**.

109. Xiang, P.; Ye, Z., Hyperbranched polyethylene ionomers containing cationic tetralkylammonium ions synthesized by Pd–diimine-catalyzed direct ethylene copolymerization with ionic liquid comonomers. *Macromolecules* **2015,** *48* (17), 6096-6107.

110. Johnson, L. K.; Mecking, S.; Brookhart, M., Copolymerization of ethylene and propylene with functionalized vinyl monomers by palladium (II) catalysts. *Journal of the American Chemical Society* **1996,** *118* (1), 267-268.

111. Guan, Z., Z. Guan, Control of polymer topology through late ‐ transition ‐ metal catalysis, J Polym Sci Part A: Polym Chem (2003), 41 (22), 3680 – 3692. *Journal of Polymer Science Part A: Polymer Chemistry* **2004,** *42* (1), 213-213.

112. Svejda, S. A.; Brookhart, M., Ethylene oligomerization and propylene dimerization using cationic (α-diimine) nickel (II) catalysts. *Organometallics* **1999,** *18* (1), 65-74.

113. Naguib, M.; Kurtoglu, M.; Presser, V.; Lu, J.; Niu, J.; Heon, M.; Hultman, L.; Gogotsi, Y.; Barsoum, M. W., Two ‐ dimensional nanocrystals produced by exfoliation of Ti3AlC2. *Advanced materials* **2011,** *23* (37), 4248-4253.

114. Naguib, M.; Mashtalir, O.; Carle, J.; Presser, V.; Lu, J.; Hultman, L.; Gogotsi, Y.; Barsoum, M. W., Two-dimensional transition metal carbides. *ACS nano* **2012,** *6* (2), 1322-1331.

115. Naguib, M.; Unocic, R. R.; Armstrong, B. L.; Nanda, J., Large-scale delamination of multi-layers transition metal carbides and carbonitrides "MXenes". *Dalton transactions* **2015,** *44* (20), 9353-9358.

116. Ding, L.; Wei, Y.; Li, L.; Zhang, T.; Wang, H.; Xue, J.; Ding, L.-X.; Wang, S.; Caro, J.; Gogotsi, Y., MXene molecular sieving membranes for highly efficient gas separation. *Nature communications* **2018,** *9* (1), 155.

117. Morales-Garcia, A.; Calle-Vallejo, F.; Illas, F., MXenes: new horizons in catalysis. *ACS Catalysis* **2020,** *10* (22), 13487-13503.

118. Shahzad, F.; Alhabeb, M.; Hatter, C. B.; Anasori, B.; Man Hong, S.; Koo, C. M.; Gogotsi, Y., Electromagnetic interference shielding with 2D transition metal carbides (MXenes). *Science* **2016,** *353* (6304), 1137-1140.

119. Soleymaniha, M.; Shahbazi, M. A.; Rafieerad, A. R.; Maleki, A.; Amiri, A., Promoting role of MXene nanosheets in biomedical sciences: therapeutic and biosensing innovations. *Advanced healthcare materials* **2019,** *8* (1), 1801137.

120. Mashtalir, O.; Naguib, M.; Mochalin, V. N.; Dall'Agnese, Y.; Heon, M.; Barsoum, M. W.; Gogotsi, Y., Intercalation and delamination of layered carbides and carbonitrides. *Nature communications* **2013,** *4* (1), 1716.

121. Zhang, Q.; Lai, H.; Fan, R.; Ji, P.; Fu, X.; Li, H., High concentration of Ti3C2T x MXene in organic solvent. *ACS nano* **2021,** *15* (3), 5249-5262.

122. Bian, R.; Lin, R.; Wang, G.; Lu, G.; Zhi, W.; Xiang, S.; Wang, T.; Clegg, P. S.; Cai, D.; Huang, W., 3D assembly of Ti 3 C 2-MXene directed by water/oil interfaces. *Nanoscale* **2018,** *10* (8), 3621-3625.

123. Wang, H.; Zhang, J.; Wu, Y.; Huang, H.; Li, G.; Zhang, X.; Wang, Z., Surface modified MXene Ti3C2 multilayers by aryl diazonium salts leading to large-scale delamination. *Applied Surface Science* **2016,** *384*, 287-293.

124. Riazi, H.; Nemani, S. K.; Grady, M. C.; Anasori, B.; Soroush, M., Ti 3 C 2 MXene–polymer nanocomposites and their applications. *Journal of Materials Chemistry A* **2021,** *9* (13), 8051-8098.

125. Maleski, K.; Mochalin, V. N.; Gogotsi, Y., Dispersions of two-dimensional titanium carbide MXene in organic solvents. *Chemistry of Materials* **2017,** *29* (4), 1632-1640.

126. Carey, M.; Hinton, Z.; Natu, V.; Pai, R.; Sokol, M.; Alvarez, N. J.; Kalra, V.; Barsoum, M. W., Dispersion and stabilization of alkylated 2D MXene in nonpolar solvents and their pseudocapacitive behavior. *Cell Reports Physical Science* **2020,** *1* (4).

127. Naguib, M.; Mashtalir, O.; Lukatskaya, M. R.; Dyatkin, B.; Zhang, C.; Presser, V.; Gogotsi, Y.; Barsoum, M. W., One-step synthesis of nanocrystalline transition metal oxides on thin sheets of disordered graphitic carbon by oxidation of MXenes. *Chemical communications* **2014,** *50* (56), 7420-7423.

128. Li, Z.; Wang, L.; Sun, D.; Zhang, Y.; Liu, B.; Hu, Q.; Zhou, A., Synthesis and thermal stability of two-dimensional carbide MXene Ti3C2. *Materials Science and Engineering: B* **2015,** *191*, 33-40.

129. Li, J.; Du, Y.; Huo, C.; Wang, S.; Cui, C., Thermal stability of two-dimensional Ti2C nanosheets. *Ceramics International* **2015,** *41* (2), 2631-2635.

130. Kim, D.; Ko, T. Y.; Kim, H.; Lee, G. H.; Cho, S.; Koo, C. M., Nonpolar organic dispersion of 2D Ti3C2T x MXene flakes via simultaneous interfacial chemical grafting and phase transfer method. *ACS nano* **2019,** *13* (12), 13818-13828.

131. Mecking, S.; Johnson, L. K.; Wang, L.; Brookhart, M., Mechanistic studies of the palladium-catalyzed copolymerization of ethylene and α-olefins with methyl acrylate. *Journal of the American Chemical Society* **1998,** *120* (5), 888-899.

132. Alhabeb, M.; Maleski, K.; Anasori, B.; Lelyukh, P.; Clark, L.; Sin, S.; Gogotsi, Y., Guidelines for synthesis and processing of two-dimensional titanium carbide (Ti3C2T x MXene). *Chemistry of Materials* **2017,** *29* (18), 7633-7644.

133. Dong, Z.; Ye, Z., Hyperbranched polyethylenes by chain walking polymerization: synthesis, properties, functionalization, and applications. *Polymer Chemistry* **2012,** *3* (2), 286-301.

134. Ye, Z.; Xu, L.; Dong, Z.; Xiang, P., Designing polyethylenes of complex chain architectures via Pd–diimine-catalyzed "living" ethylene polymerization. *Chemical Communications* **2013,** *49* (56), 6235-6255.

135. Huang, L.; Ye, Z.; Berry, R., Modification of cellulose nanocrystals with quaternary ammonium-containing hyperbranched polyethylene ionomers by ionic assembly. *ACS Sustainable Chemistry & Engineering* **2016,** *4* (9), 4937-4950.

136. Dong, Z.; Xiang, P.; Huang, L.; Ye, Z., Efficient, robust surface functionalization and stabilization of gold nanorods with quaternary ammonium-containing ionomers as multidentate macromolecular ligands. *RSC advances* **2016,** *6* (49), 43574-43590.

137. Ye, Z.; Zhu, S., Newtonian Flow Behavior of Hyperbranched High-Molecular-Weight Polyethylenes Produced with a Pd− Diimine Catalyst and Its Dependence on Chain Topology. *Macromolecules* **2003,** *36* (7), 2194-2197.

138. Xiang, P., Tuning polyethylene chain topology via ring incorporation in chain walking ethylene polymerization. *Macromolecules* **2009,** *42*, 4946-4949.

139. Xu, L.; Ye, Z.; Cui, Q.; Gu, Z., Noncovalent Nonspecific Functionalization and Solubilization of Multi‐Walled Carbon Nanotubes at High Concentrations with a Hyperbranched Polyethylene. *Macromolecular chemistry and physics* **2009,** *210* (24), 2194-2202.

140. Zhao, C.; Wang, Q.; Zhang, H.; Passerini, S.; Qian, X., Two-dimensional titanium carbide/RGO composite for high-performance supercapacitors. *ACS applied materials & interfaces* **2016,** *8* (24), 15661-15667.

141. Scheibe, B.; Kupka, V.; Peplińska, B.; Jarek, M.; Tadyszak, K., The influence of oxygen concentration during max phases (Ti3ALC2) preparation on the α-Al2O3 microparticles content and specific surface area of multilayered mxenes (Ti3C2Tx). *Materials* **2019,** *12* (3), 353.

142. Lin, H.; Gao, S.; Dai, C.; Chen, Y.; Shi, J., A two-dimensional biodegradable niobium carbide (MXene) for photothermal tumor eradication in NIR-I and NIR-II biowindows. *Journal of the American Chemical Society* **2017,** *139* (45), 16235-16247.

143. Hansen, C. M., *Hansen solubility parameters: a user's handbook*. CRC press: **2007**.

144. Russel, W. B.; Russel, W.; Saville, D. A.; Schowalter, W. R., *Colloidal dispersions*. Cambridge university press: **1991**.

145. Delgado, Á. V.; González-Caballero, F.; Hunter, R.; Koopal, L.; Lyklema, J., Measurement and interpretation of electrokinetic phenomena. *Journal of colloid and interface science* **2007,** *309* (2), 194-224.

146. Hernandez, Y.; Nicolosi, V.; Lotya, M.; Blighe, F. M.; Sun, Z.; De, S.; McGovern, I. T.; Holland, B.; Byrne, M.; Gun'Ko, Y. K., High-yield production of graphene by liquid-phase exfoliation of graphite. *Nature nanotechnology* **2008,** *3* (9), 563-568.

147. O'Neill, A.; Khan, U.; Nirmalraj, P. N.; Boland, J.; Coleman, J. N., Graphene dispersion and exfoliation in low boiling point solvents. *The Journal of Physical Chemistry C* **2011,** *115* (13), 5422-5428.

148. Hernandez, Y.; Lotya, M.; Rickard, D.; Bergin, S. D.; Coleman, J. N., Measurement of multicomponent solubility parameters for graphene facilitates solvent discovery. *Langmuir* **2010,** *26* (5), 3208-3213.

149. Konios, D.; Stylianakis, M. M.; Stratakis, E.; Kymakis, E., Dispersion behaviour of graphene oxide and reduced graphene oxide. *Journal of colloid and interface science* **2014,** *430*, 108-112.

150. Cunningham, G.; Lotya, M.; Cucinotta, C. S.; Sanvito, S.; Bergin, S. D.; Menzel, R.; Shaffer, M. S.; Coleman, J. N., Solvent exfoliation of transition metal dichalcogenides: dispersibility of exfoliated nanosheets varies only weakly between compounds. *ACS nano* **2012,** *6* (4), 3468-3480.

151. Bergin, S. D.; Sun, Z.; Rickard, D.; Streich, P. V.; Hamilton, J. P.; Coleman, J. N., Multicomponent solubility parameters for single-walled carbon nanotube− solvent mixtures. *ACS nano* **2009,** *3* (8), 2340-2350.

152. Xu, L.; McGraw, J.-W.; Gao, F.; Grundy, M.; Ye, Z.; Gu, Z.; Shepherd, J. L., Production of high-concentration graphene dispersions in low-boiling-point organic solvents by liquid-phase noncovalent exfoliation of graphite with a hyperbranched polyethylene and formation of graphene/ethylene copolymer composites. *The Journal of Physical Chemistry C* **2013,** *117* (20), 10730-10742.

153. Xuan, J.; Wang, Z.; Chen, Y.; Liang, D.; Cheng, L.; Yang, X.; Liu, Z.; Ma, R.; Sasaki, T.; Geng, F., Organic ‐ base ‐ driven intercalation and delamination for the production of functionalized titanium carbide nanosheets with superior photothermal therapeutic performance. *Angewandte Chemie* **2016,** *128* (47), 14789-14794.

154. Hantanasirisakul, K.; Alhabeb, M.; Lipatov, A.; Maleski, K.; Anasori, B.; Salles, P.; Ieosakulrat, C.; Pakawatpanurut, P.; Sinitskii, A.; May, S. J., Effects of synthesis and processing on optoelectronic properties of titanium carbonitride MXene. *Chemistry of Materials* **2019,** *31* (8), 2941-2951.

155. Li, R.; Zhang, L.; Shi, L.; Wang, P., MXene Ti3C2: an effective 2D light-to-heat conversion material. *ACS nano* **2017,** *11* (4), 3752-3759.

156. Zhang, C. J.; Pinilla, S.; McEvoy, N.; Cullen, C. P.; Anasori, B.; Long, E.; Park, S.-H.; Seral-Ascaso, A.; Shmeliov, A.; Krishnan, D., Oxidation stability of colloidal two-dimensional titanium carbides (MXenes). *Chemistry of Materials* **2017,** *29* (11), 4848-4856.

157. Mashtalir, O.; Cook, K. M.; Mochalin, V. N.; Crowe, M.; Barsoum, M. W.; Gogotsi, Y., Dye adsorption and decomposition on two-dimensional titanium carbide in aqueous media. *Journal of Materials Chemistry A* **2014,** *2* (35), 14334-14338.

158. Ghassemi, H.; Harlow, W.; Mashtalir, O.; Beidaghi, M.; Lukatskaya, M.; Gogotsi, Y.; Taheri, M. L., In situ environmental transmission electron microscopy study of oxidation of two-dimensional Ti 3 C 2 and formation of carbon-supported TiO 2. *Journal of Materials Chemistry A* **2014,** *2* (35), 14339-14343.

159. Zhao, X.; Vashisth, A.; Prehn, E.; Sun, W.; Shah, S. A.; Habib, T.; Chen, Y.; Tan, Z.; Lutkenhaus, J. L.; Radovic, M., Antioxidants unlock shelf-stable Ti3C2Tx (MXene) nanosheet dispersions. *Matter* **2019,** *1* (2), 513-526.

160. Habib, T.; Zhao, X.; Shah, S. A.; Chen, Y.; Sun, W.; An, H.; Lutkenhaus, J. L.; Radovic, M.; Green, M. J., Oxidation stability of Ti3C2Tx MXene nanosheets in solvents and composite films. *npj 2D Materials and Applications* **2019,** *3* (1), 8.

161. Wu, X.; Wang, Z.; Yu, M.; Xiu, L.; Qiu, J., Stabilizing the MXenes by carbon nanoplating for developing hierarchical nanohybrids with efficient lithium storage and hydrogen evolution capability. *Advanced Materials* **2017,** *29* (24), 1607017.

162. Aslam, M. K.; Niu, Y.; Xu, M., MXenes for non‐lithium‐ion (Na, K, Ca, Mg, and Al) batteries and supercapacitors. *Advanced Energy Materials* **2021,** *11* (2), 2000681.

163. Dong, Y.; Shi, H.; Wu, Z. S., Recent advances and promise of MXene‐based nanostructures for high‐performance metal ion batteries. *Advanced Functional Materials* **2020,** *30* (47), 2000706.

164. Guo, Z.; Zhao, S.; Li, T.; Su, D.; Guo, S.; Wang, G., Recent advances in rechargeable magnesium‐based batteries for high‐efficiency energy storage. *Advanced Energy Materials* **2020,** *10* (21), 1903591.

165. Yoo, H. D.; Shterenberg, I.; Gofer, Y.; Gershinsky, G.; Pour, N.; Aurbach, D., Mg rechargeable batteries: an on-going challenge. *Energy & Environmental Science* **2013,** *6* (8), 2265-2279.

166. Aurbach, D.; Lu, Z.; Schechter, A.; Gofer, Y.; Gizbar, H.; Turgeman, R.; Cohen, Y.; Moshkovich, M.; Levi, E., Prototype systems for rechargeable magnesium batteries. *Nature* **2000,** *407* (6805), 724-727.

167. Liu, F.; Wang, T.; Liu, X.; Fan, L. Z., Challenges and recent progress on key materials for rechargeable magnesium batteries. *Advanced Energy Materials* **2021,** *11* (2), 2000787.

168. Zhang, J.; Chang, Z.; Zhang, Z.; Du, A.; Dong, S.; Li, Z.; Li, G.; Cui, G., Current design strategies for rechargeable magnesium-based batteries. *ACS nano* **2021,** *15* (10), 15594-15624.

169. Zhang, Y.; Geng, H.; Wei, W.; Ma, J.; Chen, L.; Li, C. C., Challenges and recent progress in the design of advanced electrode materials for rechargeable Mg batteries. *Energy Storage Materials* **2019,** *20*, 118-138.

170. Mao, Y.; Soleymanabadi, H., Graphyne as an anode material for Mg-ion batteries: A computational study. *Journal of Molecular Liquids* **2020,** *308*, 113009.

171. Kannan, K.; Sadasivuni, K. K.; Abdullah, A. M.; Kumar, B., Current trends in MXene-based nanomaterials for energy storage and conversion system: a mini review. *Catalysts* **2020,** *10* (5), 495.

172. Ming, F.; Liang, H.; Huang, G.; Bayhan, Z.; Alshareef, H. N., MXenes for rechargeable batteries beyond the lithium‐ion. *Advanced Materials* **2021,** *33* (1), 2004039.

173. Son, S.-B.; Gao, T.; Harvey, S. P.; Steirer, K. X.; Stokes, A.; Norman, A.; Wang, C.; Cresce, A.; Xu, K.; Ban, C., An artificial interphase enables reversible magnesium chemistry in carbonate electrolytes. *Nature Chemistry* **2018,** *10* (5), 532-539.

174. You, C.; Wu, X.; Yuan, X.; Chen, Y.; Liu, L.; Zhu, Y.; Fu, L.; Wu, Y.; Guo, Y.-G.; van Ree, T., Advances in rechargeable Mg batteries. *Journal of Materials Chemistry A* **2020,** *8* (48), 25601-25625.

175. Er, D.; Li, J.; Naguib, M.; Gogotsi, Y.; Shenoy, V. B., Ti3C2 MXene as a high capacity electrode material for metal (Li, Na, K, Ca) ion batteries. *ACS applied materials & interfaces* **2014,** *6* (14), 11173-11179.

176. Rashad, M.; Asif, M.; Wang, Y.; He, Z.; Ahmed, I., Recent advances in electrolytes and cathode materials for magnesium and hybrid-ion batteries. *Energy Storage Materials* **2020,** *25*, 342-375.

177. Garg, R.; Agarwal, A.; Agarwal, M., A review on MXene for energy storage application: effect of interlayer distance. *Materials Research Express* **2020,** *7* (2), 022001.

178. Byeon, A.; Zhao, M.-Q.; Ren, C. E.; Halim, J.; Kota, S.; Urbankowski, P.; Anasori, B.; Barsoum, M. W.; Gogotsi, Y., Two-dimensional titanium carbide MXene as a cathode material for hybrid magnesium/lithium-ion batteries. *ACS Applied Materials & Interfaces* **2017,** *9* (5), 4296-4300.

179. Kaland, H.; Hadler-Jacobsen, J.; Fagerli, F. H.; Wagner, N. P.; Wang, Z.; Selbach, S. M.; Vullum-Bruer, F.; Wiik, K.; Schnell, S. K., Are MXenes suitable as cathode materials for rechargeable Mg batteries? *Sustainable Energy & Fuels* **2020,** *4* (6), 2956-2966.

180. Zhao, M.-Q.; Ren, C. E.; Alhabeb, M.; Anasori, B.; Barsoum, M. W.; Gogotsi, Y., Magnesium-ion storage capability of MXenes. *ACS Applied Energy Materials* **2019,** *2* (2), 1572-1578.

181. Xu, M.; Lei, S.; Qi, J.; Dou, Q.; Liu, L.; Lu, Y.; Huang, Q.; Shi, S.; Yan, X., Opening magnesium storage capability of two-dimensional MXene by intercalation of cationic surfactant. *Acs Nano* **2018,** *12* (4), 3733-3740.

182. Liu, F.; Liu, Y.; Zhao, X.; Liu, X.; Fan, L.-Z., Pursuit of a high-capacity and long-life Mg-storage cathode by tailoring sandwich-structured MXene@ carbon nanosphere composites. *Journal of Materials Chemistry A* **2019,** *7* (28), 16712-16719.

183. Xu, M.; Bai, N.; Li, H.-X.; Hu, C.; Qi, J.; Yan, X.-B., Synthesis of MXene-supported layered MoS2 with enhanced electrochemical performance for Mg batteries. *Chinese Chemical Letters* **2018,** *29* (8), 1313-1316.

184. Zhang, R.; Liu, Q.; Wang, Z.; Yang, X.; Guo, Y., Conductive polymer doped two-dimensional MXene materials: opening the channel of magnesium ion transport. *RSC advances* **2022,** *12* (7), 4329-4335.

185. Raisi, B.; Huang, L.; Ye, Z., Modification of Ti 3 C 2 T x MXene with hyperbranched polyethylene ionomers: stable dispersions in nonpolar/low-polarity organic solvents, oxidation protection, and potential application in supercapacitors. *Journal of Materials Chemistry A* **2023,** *11* (32), 17167-17187.

186. Luo, J.; Zhang, W.; Yuan, H.; Jin, C.; Zhang, L.; Huang, H.; Liang, C.; Xia, Y.; Zhang, J.; Gan, Y., Pillared structure design of MXene with ultralarge interlayer spacing for high-performance lithium-ion capacitors. *ACS nano* **2017,** *11* (3), 2459-2469.

187. Gao, X.; Du, X.; Mathis, T. S.; Zhang, M.; Wang, X.; Shui, J.; Gogotsi, Y.; Xu, M., Maximizing ion accessibility in MXene-knotted carbon nanotube composite electrodes for high-rate electrochemical energy storage. *Nature communications* **2020,** *11* (1), 6160.

188. Wang, X.; Mathis, T. S.; Li, K.; Lin, Z.; Vlcek, L.; Torita, T.; Osti, N. C.; Hatter, C.; Urbankowski, P.; Sarycheva, A., Influences from solvents on charge storage in titanium carbide MXenes. *Nature Energy* **2019,** *4* (3), 241-248.

189. Shterenberg, I.; Salama, M.; Gofer, Y.; Levi, E.; Aurbach, D., The challenge of developing rechargeable magnesium batteries. *Mrs Bulletin* **2014,** *39* (5), 453-460.

190. Hadler-Jacobsen, J.; Fagerli, F. H.; Kaland, H.; Schnell, S. K., Stacking sequence, interlayer bonding, termination group stability and Li/Na/Mg diffusion in MXenes. *ACS Materials Letters* **2021,** *3* (9), 1369-1376.

191. Wang, Y.; Xue, X.; Liu, P.; Wang, C.; Yi, X.; Hu, Y.; Ma, L.; Zhu, G.; Chen, R.; Chen, T., Atomic substitution enabled synthesis of vacancy-rich two-dimensional black TiO2–x nanoflakes for high-performance rechargeable magnesium batteries. *ACS nano* **2018,** *12* (12), 12492-12502.

192. Lai, S.; Jeon, J.; Jang, S. K.; Xu, J.; Choi, Y. J.; Park, J.-H.; Hwang, E.; Lee, S., Surface group modification and carrier transport properties of layered transition metal carbides (Ti 2 CT x, T:–OH,–F and–O). *Nanoscale* **2015,** *7* (46), 19390-19396.

193. Xie, Y.; Dall'Agnese, Y.; Naguib, M.; Gogotsi, Y.; Barsoum, M. W.; Zhuang, H. L.; Kent, P. R., Prediction and characterization of MXene nanosheet anodes for non-lithium-ion batteries. *ACS nano* **2014,** *8* (9), 9606-9615.

194. Xue, X.; Chen, R.; Yan, C.; Zhao, P.; Hu, Y.; Kong, W.; Lin, H.; Wang, L.; Jin, Z., One - step synthesis of 2 - ethylhexylamine pillared vanadium disulfide nanoflowers with ultralarge interlayer spacing for high - performance magnesium storage. *Advanced Energy Materials* **2019,** *9* (22), 1900145.

195. Wang, J.; Polleux, J.; Lim, J.; Dunn, B., Pseudocapacitive contributions to electrochemical energy storage in TiO2 (anatase) nanoparticles. *The Journal of Physical Chemistry C* **2007,** *111* (40), 14925-14931.

196. Wang, H.; Yao, T.; Li, C.; Meng, L.; Cheng, Y., Constructing three-dimensional ordered porous MoS2/C hierarchies for excellent high-rate long-life pseudocapacitive sodium storage. *Chemical Engineering Journal* **2020,** *397*, 125385.

197. Liu, Y.; Fan, L.-Z.; Jiao, L., Graphene intercalated in graphene-like MoS2: A promising cathode for rechargeable Mg batteries. *Journal of Power Sources* **2017,** *340*, 104-110.

198. Hadler‐Jacobsen, J.; Schnell, S. K., The Importance of Stacking and Coordination for Li, Na, and Mg Diffusion and Intercalation in Ti3C2T2 MXene. *Advanced Materials Interfaces* **2022**, 2200014.

199. Hadler‐Jacobsen, J.; Schnell, S. K., The Importance of Stacking and Coordination for Li, Na, and Mg Diffusion and Intercalation in Ti3C2T2 MXene. *Advanced Materials Interfaces* **2022,** *9* (17), 2200014.

200. Li, K.; Liang, M.; Wang, H.; Wang, X.; Huang, Y.; Coelho, J.; Pinilla, S.; Zhang, Y.; Qi, F.; Nicolosi, V., 3D MXene architectures for efficient energy storage and conversion. *Advanced Functional Materials* **2020,** *30* (47), 2000842.

201. Li, Y.; Xu, D.; Zhang, D.; Wei, Y.; Zhang, R.; Guo, Y., Study on MnO 2/MXene–Ti 3 C 2 composite materials as cathode materials for magnesium batteries. *RSC advances* **2019,** *9* (58), 33572-33577.

202. Sheberla, D.; Bachman, J. C.; Elias, J. S.; Sun, C.-J.; Shao-Horn, Y.; Dincă, M., Conductive MOF electrodes for stable supercapacitors with high areal capacitance. *Nature materials* **2017,** *16* (2), 220-224.

203. Zhang, L. L.; Zhao, X., Carbon-based materials as supercapacitor electrodes. *Chemical society reviews* **2009,** *38* (9), 2520-2531.

204. Forse, A. C.; Griffin, J. M.; Merlet, C.; Carretero-Gonzalez, J.; Raji, A.-R. O.; Trease, N. M.; Grey, C. P., Direct observation of ion dynamics in supercapacitor electrodes using in situ diffusion NMR spectroscopy. *Nature Energy* **2017,** *2* (3), 1-7.

205. Yu, M.; Lin, D.; Feng, H.; Zeng, Y.; Tong, Y.; Lu, X., Boosting the energy density of carbon‐based aqueous supercapacitors by optimizing the surface charge. *Angewandte Chemie* **2017,** *129* (20), 5546-5551.

206. Lukatskaya, M. R.; Kota, S.; Lin, Z.; Zhao, M.-Q.; Shpigel, N.; Levi, M. D.; Halim, J.; Taberna, P.-L.; Barsoum, M. W.; Simon, P., Ultra-high-rate pseudocapacitive energy storage in two-dimensional transition metal carbides. *Nature Energy* **2017,** *2* (8), 1-6.

207. Zhang, S.-W.; Yin, B.-S.; Liu, X.-X.; Gu, D.-M.; Gong, H.; Wang, Z.-B., A high energy density aqueous hybrid supercapacitor with widened potential window through multi approaches. *Nano Energy* **2019,** *59*, 41-49.

208. Zhang, S.-W.; Yin, B.-S.; Liu, C.; Wang, Z.-B.; Gu, D.-M., NiMoO4 nanowire arrays and carbon nanotubes film as advanced electrodes for high-performance supercapacitor. *Applied Surface Science* **2018,** *458*, 478-488.

209. Raza, W.; Ali, F.; Raza, N.; Luo, Y.; Kim, K.-H.; Yang, J.; Kumar, S.; Mehmood, A.; Kwon, E. E., Recent advancements in supercapacitor technology. *Nano Energy* **2018,** *52*, 441-473.

210. Vadiyar, M. M.; Liu, X.; Ye, Z., Macromolecular polyethynylbenzonitrile precursor-based porous covalent triazine frameworks for superior high-rate high-energy supercapacitors. *ACS applied materials & interfaces* **2019,** *11* (49), 45805-45817.

211. Augustyn, V.; Simon, P.; Dunn, B., Pseudocapacitive oxide materials for high-rate electrochemical energy storage. *Energy & Environmental Science* **2014,** *7* (5), 1597-1614.

212. Zhang, S.; Pan, N., Supercapacitors performance evaluation. *Advanced Energy Materials* **2015,** *5* (6), 1401401.

213. Kim, E.; Song, J.; Song, T.-E.; Kim, H.; Kim, Y.-J.; Oh, Y.-W.; Jung, S.; Kang, I.-S.; Gogotsi, Y.; Han, H., Scalable fabrication of MXene-based flexible micro-supercapacitor with outstanding volumetric capacitance. *Chemical Engineering Journal* **2022,** *450*, 138456.

214. Otgonbayar, Z.; Yang, S.; Kim, I.-J.; Oh, W.-C., Recent Advances in Two-Dimensional MXene for Supercapacitor Applications: Progress, Challenges, and Perspectives. *Nanomaterials* **2023,** *13* (5), 919.

215. Ando, Y.; Okubo, M.; Yamada, A.; Otani, M., Capacitive versus pseudocapacitive storage in MXene. *Advanced Functional Materials* **2020,** *30* (47), 2000820.

216. Huang, X.; Huang, J.; Yang, D.; Wu, P., A multi‐scale structural engineering strategy for high‐performance MXene hydrogel supercapacitor electrode. *Advanced Science* **2021,** *8* (18), 2101664.

217. Tian, W.; VahidMohammadi, A.; Wang, Z.; Ouyang, L.; Beidaghi, M.; Hamedi, M. M., Layer-by-layer self-assembly of pillared two-dimensional multilayers. *Nature Communications* **2019,** *10* (1), 2558.

218. Zhu, M.; Huang, Y.; Deng, Q.; Zhou, J.; Pei, Z.; Xue, Q.; Huang, Y.; Wang, Z.; Li, H.; Huang, Q., Highly flexible, freestanding supercapacitor electrode with enhanced performance obtained by hybridizing polypyrrole chains with MXene. *Advanced Energy Materials* **2016,** *6* (21), 1600969.

219. Wang, Z.; Zhu, M.; Pei, Z.; Xue, Q.; Li, H.; Huang, Y.; Zhi, C., Polymers for supercapacitors: Boosting the development of the flexible and wearable energy storage. *Materials Science and Engineering: R: Reports* **2020,** *139*, 100520.

220. Bhat, T.; Patil, P.; Rakhi, R., Recent trends in electrolytes for supercapacitors. *Journal of Energy Storage* **2022,** *50*, 104222.

221. Zheng, S.; Zhang, C. J.; Zhou, F.; Dong, Y.; Shi, X.; Nicolosi, V.; Wu, Z.-S.; Bao, X., Ionic liquid pre-intercalated MXene films for ionogel-based flexible micro-supercapacitors with high volumetric energy density. *Journal of Materials Chemistry A* **2019,** *7* (16), 9478-9485.

222. Grundy, M.; Ye, Z., Cross-linked polymers of diethynylbenzene and phenylacetylene as new polymer precursors for high-yield synthesis of high-performance nanoporous activated carbons for supercapacitors, hydrogen storage, and CO 2 capture. *Journal of Materials Chemistry A* **2014,** *2* (47), 20316-20330.

223. Liu, X.; Vadiyar, M. M.; Oh, J. K.; Ye, Z., Designing ultrasmall carbon nanospheres with tailored sizes and textural properties for high-rate high-energy supercapacitors. *ACS Applied Materials & Interfaces* **2021,** *13* (28), 32916-32929.

224. Naguib, M.; Mochalin, V. N.; Barsoum, M. W.; Gogotsi, Y., Two‐dimensional materials: 25th anniversary article: MXenes: a new family of two‐dimensional materials (Adv. Mater. 7/2014). *Advanced Materials* **2014,** *26* (7), 982-982.

225. Saha, A.; Shpigel, N.; Rosy; Leifer, N.; Taragin, S.; Sharabani, T.; Aviv, H.; Perelshtein, I.; Nessim, G. D.; Noked, M., Enhancing the energy storage capabilities of Ti3C2Tx MXene electrodes by atomic surface reduction. *Advanced Functional Materials* **2021,** *31* (52), 2106294.

226. Li, K.; Wang, X.; Li, S.; Urbankowski, P.; Li, J.; Xu, Y.; Gogotsi, Y., An ultrafast conducting polymer@ MXene positive electrode with high volumetric capacitance for advanced asymmetric supercapacitors. *Small* **2020,** *16* (4), 1906851.

227. Tong, L.; Jiang, C.; Cai, K.; Wei, P., High-performance and freestanding PPy/Ti3C2Tx composite film for flexible all-solid-state supercapacitors. *Journal of Power Sources* **2020,** *465*, 228267.

228. Wei, D.; Wu, W.; Zhu, J.; Wang, C.; Zhao, C.; Wang, L., A facile strategy of polypyrrole nanospheres grown on Ti3C2-MXene nanosheets as advanced supercapacitor electrodes. *Journal of Electroanalytical Chemistry* **2020,** *877*, 114538.

229. Shahzad, S.; Shah, A.; Kowsari, E.; Iftikhar, F. J.; Nawab, A.; Piro, B.; Akhter, M. S.; Rana, U. A.; Zou, Y., Ionic Liquids as Environmentally Benign Electrolytes for High‐Performance Supercapacitors. *Global Challenges* **2019,** *3* (1), 1800023.

230. Feng, J.; Wang, Y.; Xu, Y.; Sun, Y.; Tang, Y.; Yan, X., Ion regulation of ionic liquid electrolytes for supercapacitors. *Energy & Environmental Science* **2021,** *14* (5), 2859-2882.

231. Fan, Q.; Zhao, R.; Yi, M.; Qi, P.; Chai, C.; Ying, H.; Hao, J., Ti3C2-MXene composite films functionalized with polypyrrole and ionic liquid-based microemulsion particles for supercapacitor applications. *Chemical Engineering Journal* **2022,** *428*, 131107.

232. Dall'Agnese, Y.; Rozier, P.; Taberna, P.-L.; Gogotsi, Y.; Simon, P., Capacitance of two-dimensional titanium carbide (MXene) and MXene/carbon nanotube composites in organic electrolytes. *Journal of Power Sources* **2016,** *306*, 510-515.

233. Yang, C.; Tang, Y.; Tian, Y.; Luo, Y.; He, Y.; Yin, X.; Que, W., Achieving of flexible, free‐standing, ultracompact delaminated titanium carbide films for high volumetric performance and heat‐resistant symmetric supercapacitors. *Advanced Functional Materials* **2018,** *28* (15), 1705487.

Appendix

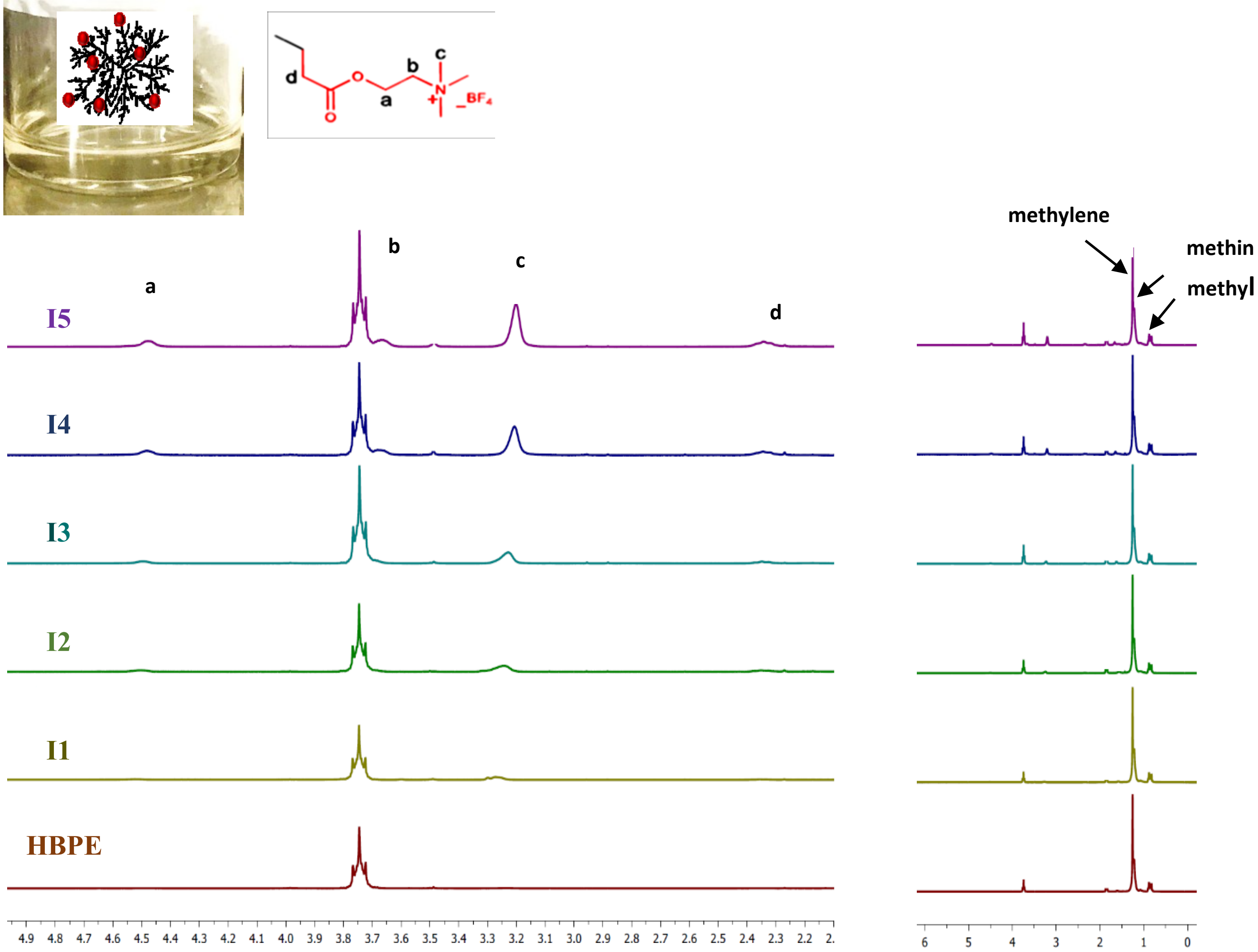

Figure S3.1 1H NMR spectra of the quaternary ammonium-containing hyperbranched polyethylene ionomers (I1 – I5) and a nonionic hyperbranched polyethylene homopolymer.

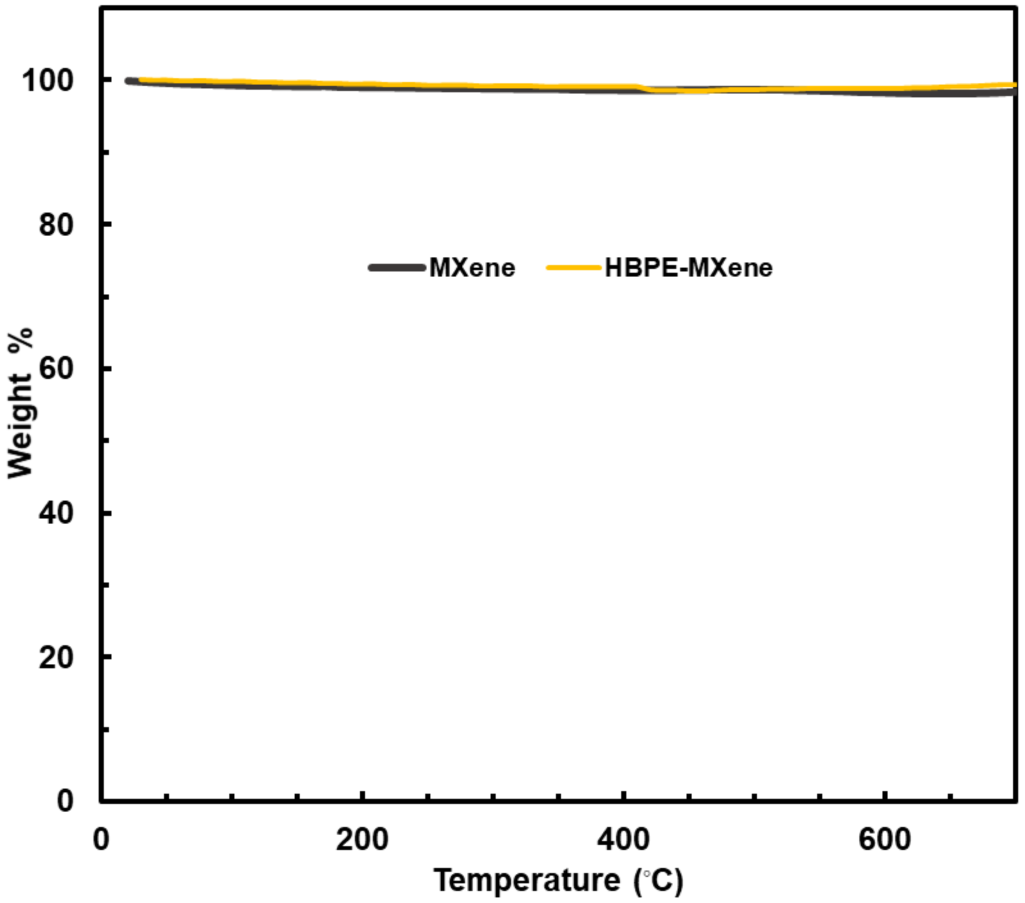

Figure S3.2 TGA curves of dried unmodified MXene and MXene modified with a nonionic hyperbranched ethylene homopolymer (HBPE).

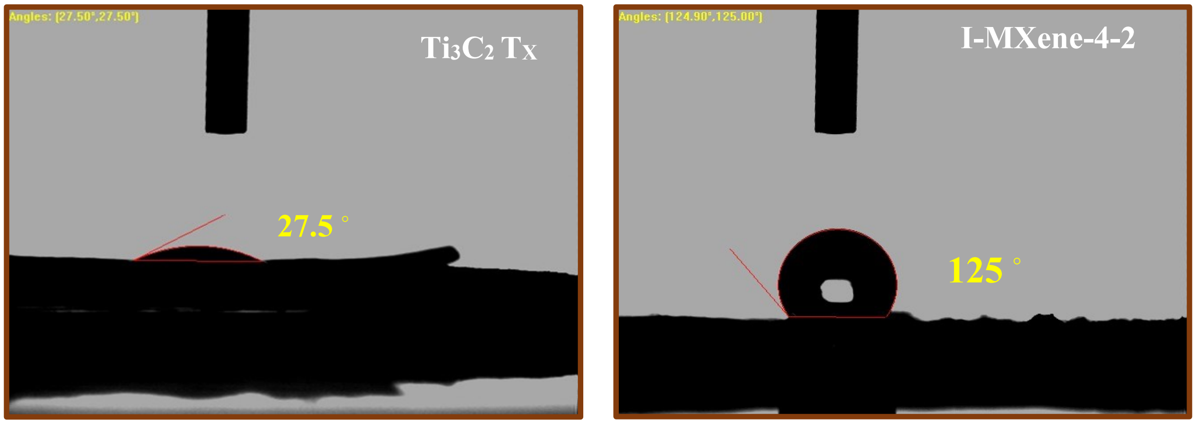

Figure S3.3 Water contact angle measurements on films of $Ti_3C_2T_x$ MXene and I-MXene-4-2.

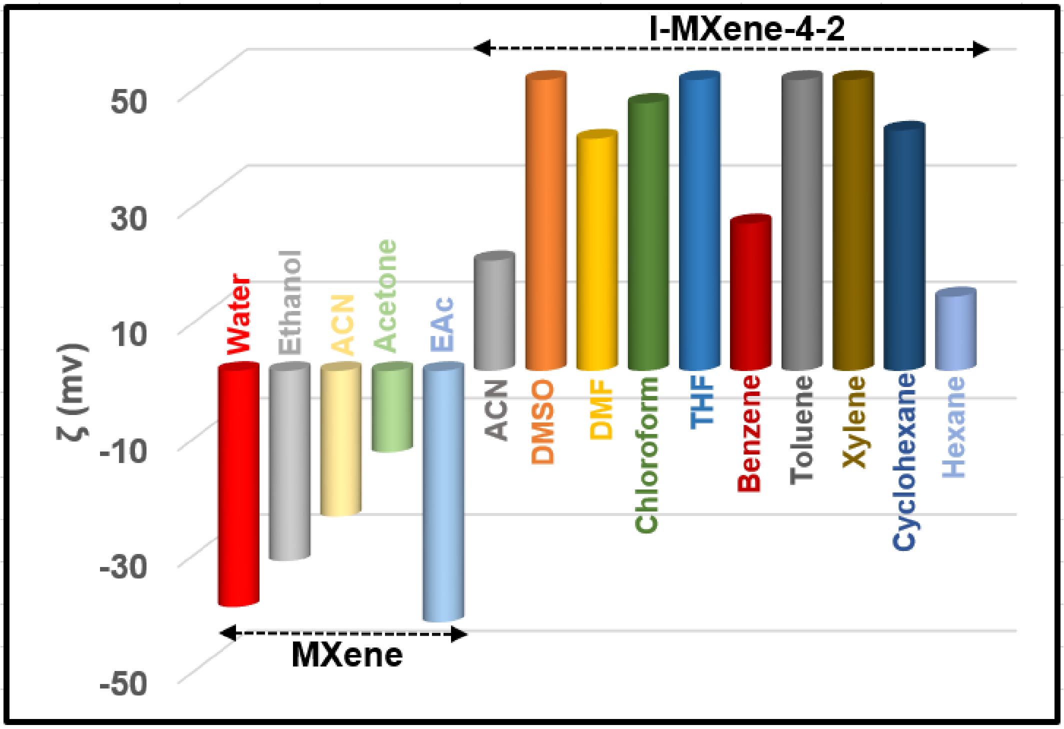

Figure S3.4 ζ potential results of MXene and I-MXene-4-2 in different solvents after 100 days.

Table S3.1 Physical-chemical properties of solvents used in this study

Solvent	Formula	Boiling Point (°C)	Density (g/mL) (at 20°C)	Solubility in H_2O^a (g/100mg)	**Relative Polarity**[b]	Refractive index (at 20°C)	Viscosity (cP) (at 25°C)	Dielectric Constant
Water	H_2O	100	0.998	M	**1**	1.333	0. 891	80.1
Methanol	CH_4O	64.6	0.791	M	**0.762**	1.329	0.544	32.7
Ethanol	C_2H_6O	78.5	0.789	M	**0.654**	1.36	1.04	24.5
Acetonitrile	C_2H_3N	81.6	0.786	M	**0.460**	1.344	0.369	36.64
DMSO	C_2H_6OS	189	1.092	M	**0.444**	1.479	1.987	47.24
DMF	C_3H_7NO	153	0.994	M	**0.386**	1.4305	0.92	36.7
Acetone	C_3H_6O	56.2	0.786	M	**0.355**	1.359	0.306	21.01
Pyridine	C_5H_5N	115.5	0.982	M	**0.302**	1.5093	0.88	12.4
Chloroform	$CHCl_3$	61.2	1.498	0.8	**0.259**	1.445	0.537	4.81
Ethyl acetate	$C_4H_8O_2$	77.1	0.902	8.7	**0.228**	1.372	0.423	6.08
THF	C_4H_8O	66	0.886	30	**0.207**	1.407	0.456	7.52
Benzene	C_6H_6	80.1	0.879	0.18	**0.111**	1.501	0.603	2.28
Toluene	C_7H_8	110.6	0.867	0.05	**0.099**	1.496	0.560	2.38
Xylene	C_8H_{10}	138.5	0.864	0.02	**0.074**	1.497	0.59	2.57
Hexane	C_6H_{14}	69	0.655	0.0014	**0.009**	1.375	0.300	1.89
Cyclohexane	C_6H_{12}	80.7	0.779	0.005	**0.006**	1.4262	0.9	2.02

[a] *M* indicates miscible.

[b] The values for relative polarity extracted from *Christian Reichardt, Solvents and Solvent Effects in Organic Chemistry*, Wiley-VCH Publishers, 3rd ed., **2003.**

Table S3.2 Hansen and Hildebrand solubility parameters of the solvents used in this study.

Solvent	Formula	Δd [a] (MPa $^{1/2}$)	δp [b]	δh [c]	Hildebrand (MPa $^{1/2}$)	Hydrogen-bonding capability
Water	H_2O	15.5	16	42.3	47.9	strong
Methanol	CH_4O	15.1	12.3	22.3	29.6	strong
Ethanol	C_2H_6O	15.8	8.8	19.4	26	strong
Acetonitrile	C_2H_3N	15.3	18	6.1	24.3	poor
DMSO	C_2H_6OS	18.4	16.4	10.2	24.5	moderate
DMF	C_3H_7NO	17.4	13.7	11.3	24.8	moderate
Acetone	C_3H_6O	15.5	10.4	7	20.2	moderate
Pyridine	C_5H_5N	19	8.8	5.9	21.9	strong
Chloroform	$CHCl_3$	17.8	3.1	5.7	19	poor
Ethyl acetate	$C_4H_8O_2$	15.8	5.3	7.2	18.1	moderate
THF	C_4H_8O	16.8	5.7	8	18.6	moderate
Benzene	C_6H_6	18.4	0	2	18.8	poor
Toluene	C_7H_8	18	1.4	2	18.2	poor
Xylene	C_8H_{10}	17.6	1	3.1	18	poor
Hexane	C_6H_{14}	14.9	0	0	14.9	poor
Cyclohexane	C_6H_{12}	16.8	0	0.2	16.8	poor

[a] Dispersive
[b] Polar
[c] H-bond

Polypropylene and polyethylene have δD=18, δP=0, δH=1, and δD=16.9, δP=0.8, δH=2.8 respectively. [3,4]

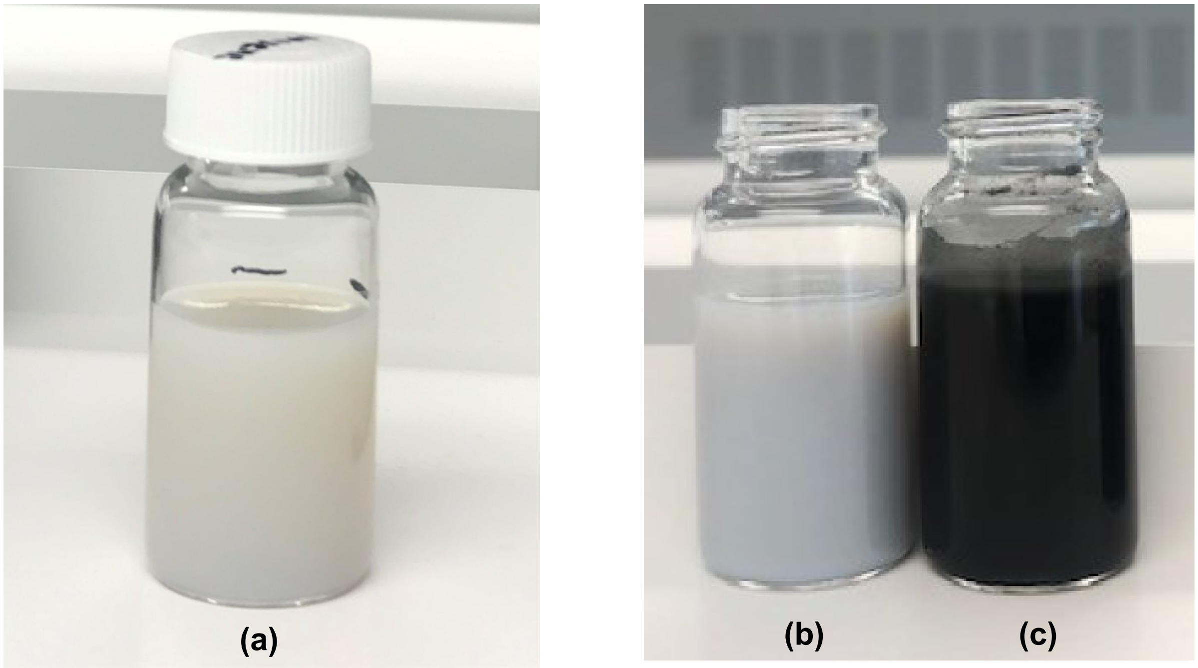

Figure S3.5 Photos of the dispersion of unmodified delaminated MXene in water in a closed vial after 30 days (a) and in an open vial after 20 days (b); (c) photo of a stable colloidal dispersion of delaminated I-MXene-4-2 in THF in an open vial after 30 days.

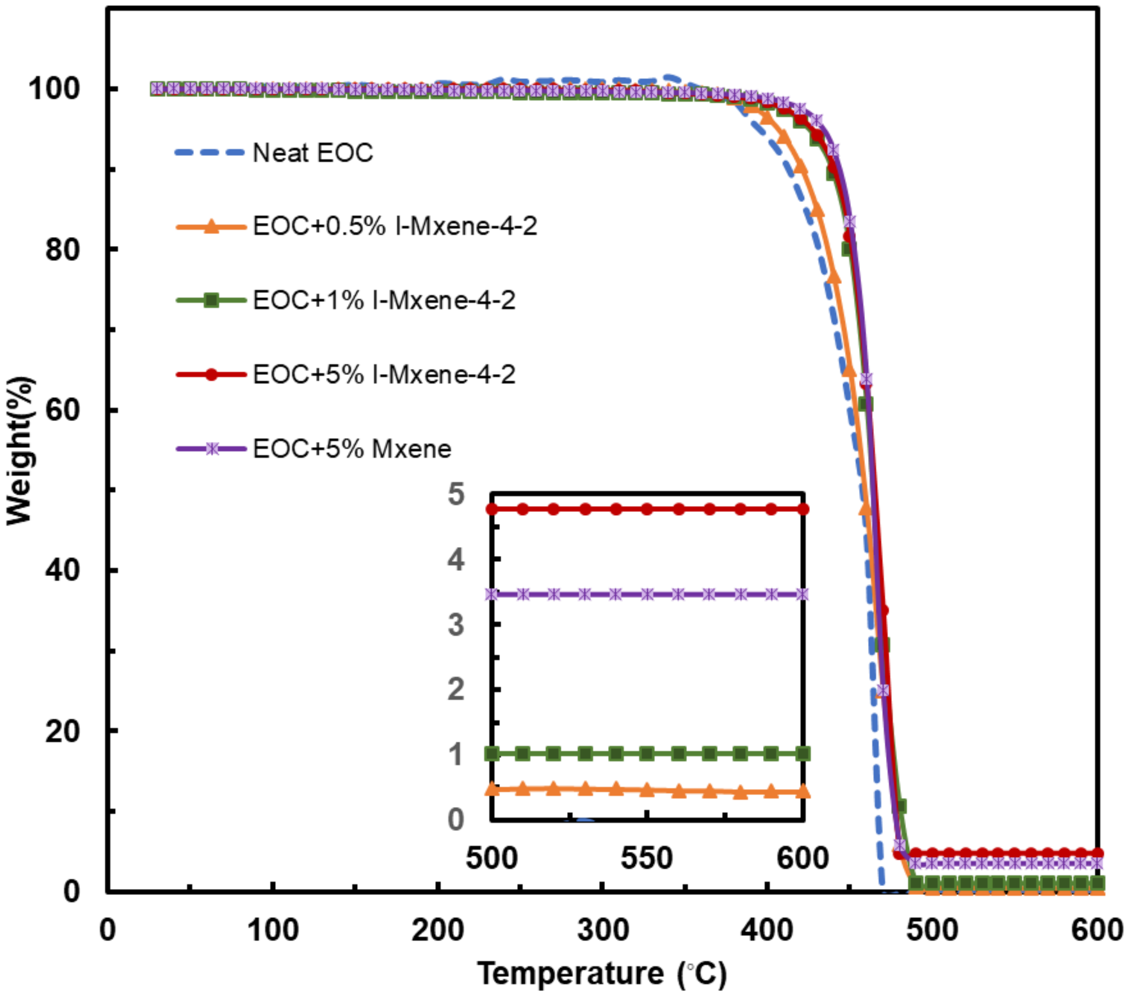

Figure S3.6 TGA curves of the EOC composites with MXene and I-MXene-4-2 and neat EOC. The measurements were undertaken at 10 ºC/min in N_2.

Table S4.1 Modified MXenes (ML- and DL-) prepared with two different ionomers and CTAB at varying ionomer or CTAB to MXene feed ratios

Modified Mxenes	**Modifier**	**$(m_{Modifier}/m_{Mxene})_0$**[a]	**Modifier Content**[b] **(wt%)**	**DLS Characterization**[c]			**XRD**	
				d_p (nm)	**PDI**	**ζ potential (mV)**	**2Θ(°) (002)**	**d(A°)**
ML-MXene	n.a.			288	0.2	-38	8.15	10.8
I@ML-MXene-5-2	I5	2	29	829	0.3	48	4.7 1.7	>50
DL-MXene	n.a.			133	0.3	-53	6.6	13
I@DL-MXene-3-3	I3	3	25	199	0.2	60	5.5	16
I@DL-MXene-5-2	I5	2	38	216	0.2	62	4.7	19
CTAB@DL-MXene-0.2	CTAB	0.2	9	-	-		6.1	14.5
CTAB@DL-MXene-2	CTAB	2	15	-	-	57	6.1	14.5

[a] Feed mass ratio of ionomer/CTAB to MXene employed in the synthesis of modified MXenes.

[b] Determined with TGA as the percentage weight loss within the temperature range of 280−480°C for ionomers and 200−400 °C for CTAB.

[c] Z-average hydrodynamic particle size (d_p), polydispersity index (PDI) of size distribution, and ζ potential determined with DLS on dilute dispersions in water (for unmodified MXenes and CTAB-modified DL-MXene) or THF (for I@DL-MXenes and I@ML-MXene-5-2).

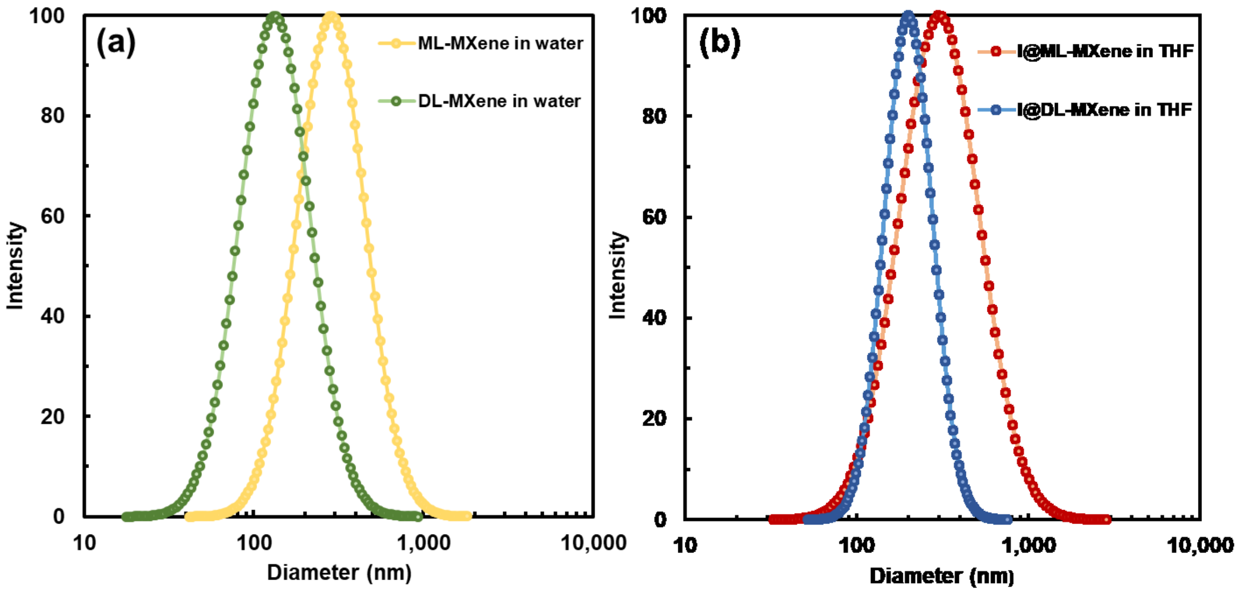

Figure S4.1 (a) DLS particle size distributions of ML- and DL-MXene in water; (b) DLS particle size distributions of I@ML-MXene and I@DL-MXene samples in THF.

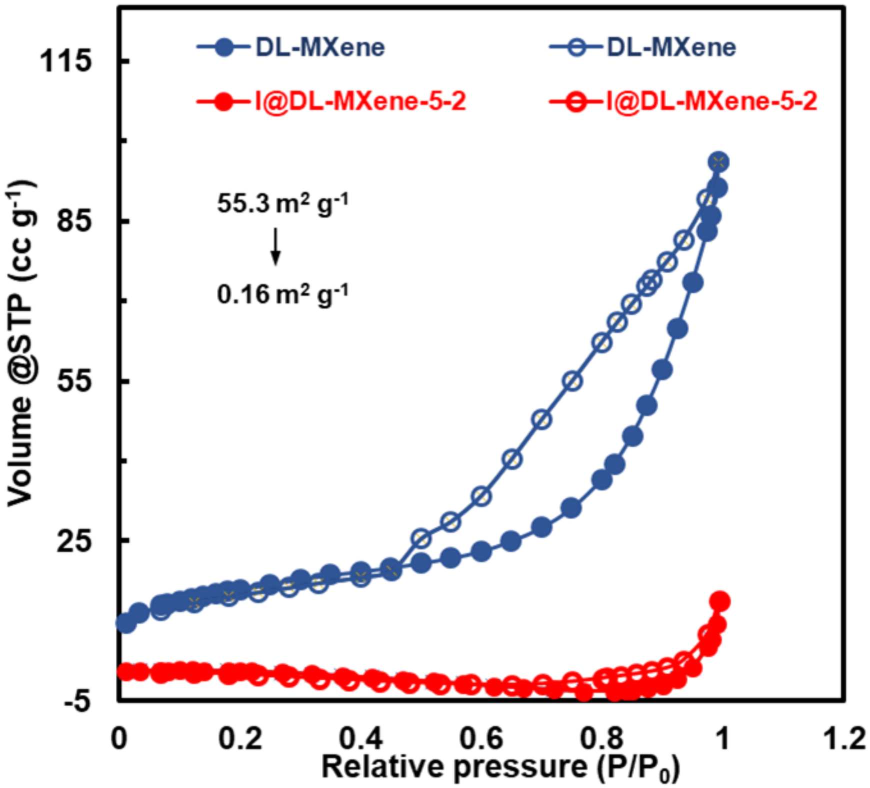

Figure S4.2 The N_2 adsorption−desorption isotherms for DL-MXene and I@DL-MXene-5-2.

Table S4.2 Surface area and pore volume data for DL-MXene and I@DL-MXene-5-2

	DL-MXene	**I@DL-MXene-5-2**
BET Surface Area (m^2 g^{-1})	55.3	0.16
Adsorption cumulative surface area of pores between 17A° and 3000 A° (m^2 g^{-1})	55.8	3.1
Desorption cumulative surface area of pores between 17A° and 3000 A° (m^2 g^{-1})	78.8	2.1
Pore volume (cm^3 g^{-1})	0.15	0.02
Adsorption cumulative volume of pores between 17A° and 3000 A° (m^3 g^{-1})	0.15	0.02
Desorption cumulative volume of pores between 17A° and 3000 A° (m^3 g^{-1})	0.15	0.02

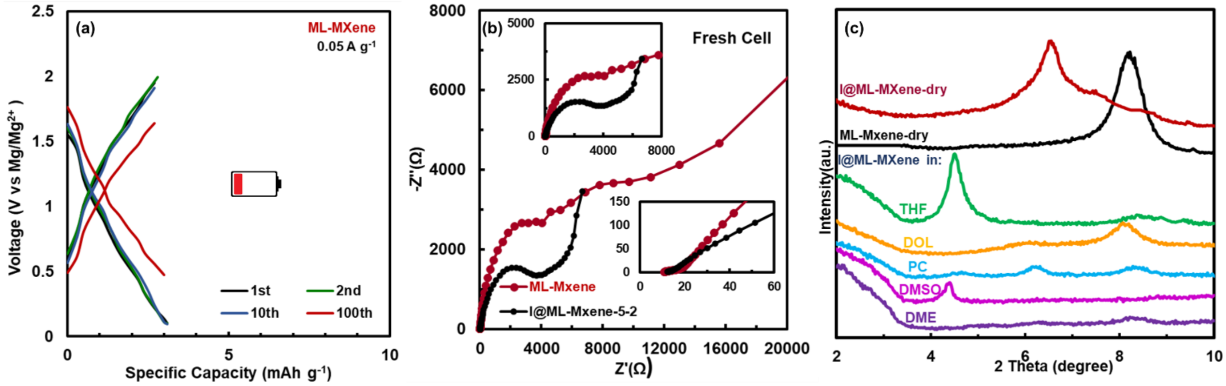

Figure S4.3 (a) GCD curves of virgin $Ti_3C_2T_x$ ML-MXene electrode at 50 mA g^{-1} ; (b) EIS data collected for ML-MXene and I-ML-MXene-5-2 electrodes fresh cell with the inset shows the magnified curves in the high-frequency range; (c) Low-angle XRD patterns of multi-layers MXene (ML-MXene) after etching, washing, and drying, dry ionomer modified MXene, and ionomer modified MXene suspensions in, THF, DOL, PC, DMSO and DME.

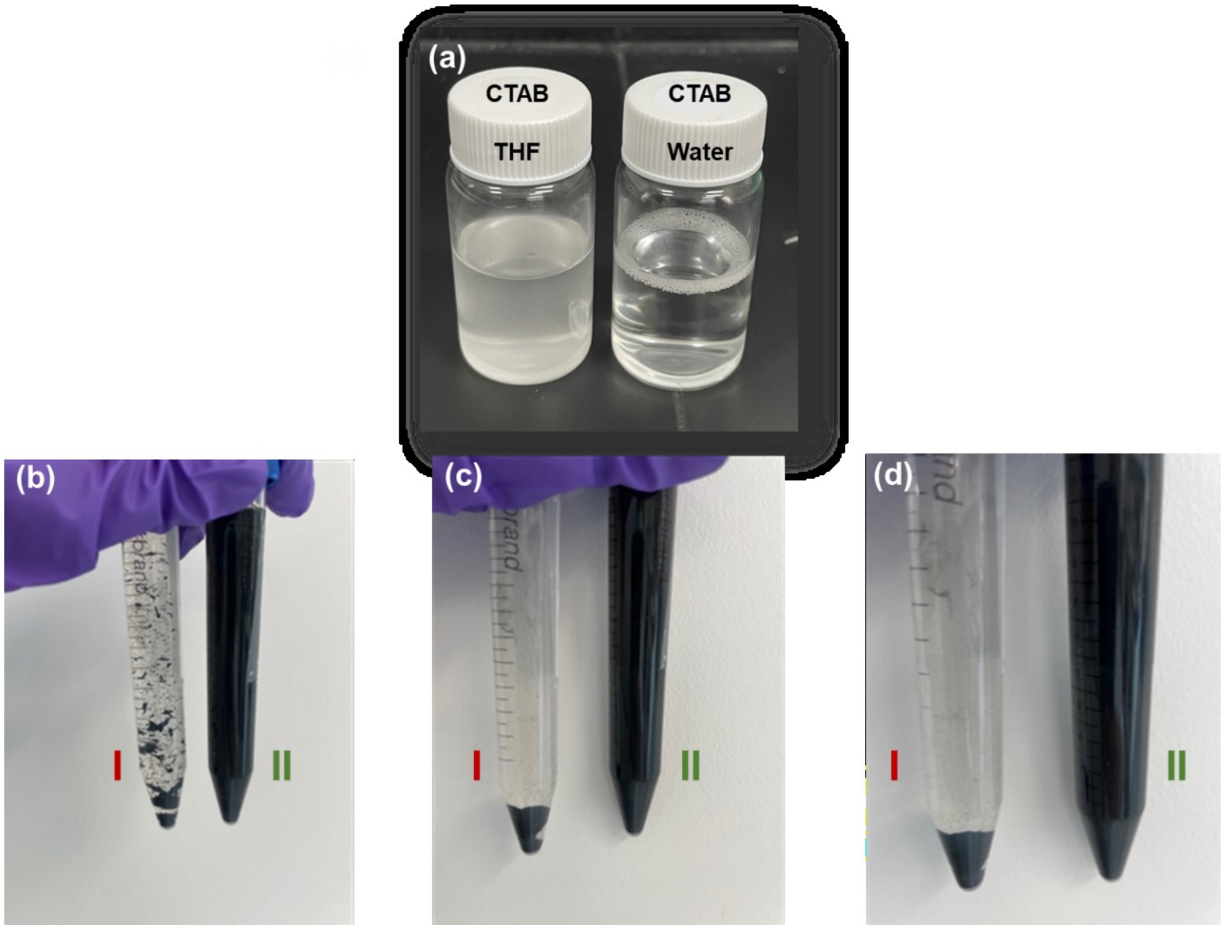

Figure S4.4 (a) Cetyltrimethylammonium Bromide (CTAB) powder solution in water and THF with the same concentration; (b) I) CTAB@dl-Mxene+Super P+PVDF(60:30:10) electrode and II) I@dl-Mxene-5-2+Super P+PVDF(60:30:10) electrode dispersion THF, respectively, immediately after shaking, (c) after one hour, and (d) after ten days.

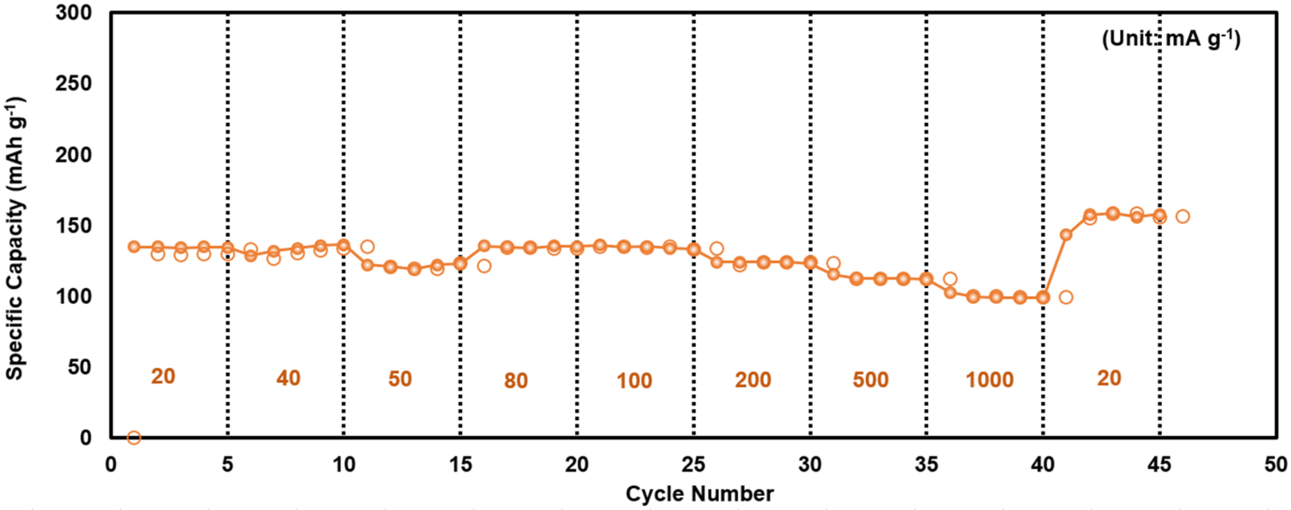

Figure S4.5 Gravimetric specific capacities of C@DL-MXene-2 at different current densities.

Table S5.1 Modified MXenes (ML- and dl-) prepared with ionomer and CTAB

Modified Mxenes	**Modifier**	**$(m_{Modifier}/m_{Mxene})_0$**[a]	**Modifier Content**[b] **(wt%)**	**DLS**[c]			**XRD**	
				d_p (nm)	**PDI**	**ζ potential (mV)**	**2Θ(°) (002)**	**d(A°)**
ML-MXene	na	0	0	288	0.2	-38	8.15	10.8
DL-MXene	na	0	0	133	0.3	-53	6.6	13
I@ML-MXene	I	2	10	1800	0.3	30	6.5	13.6
I@DL-MXene	I	2	38	216	0.2	62	4.7	19
C@DL-MXene	CTAB	2	15	-	-	57	6.1	14.5

[a] Feed mass ratio of ionomer to dl-MXene or CTAB to dl-MXene is employed in the synthesis of modified dl-MXenes.

[b] Determined from percentage weight loss within the temperature range of 280−480 °C for ionomer and 200−400 °C for CTAB from TGA characterization.

[c] Z-average hydrodynamic particle size (d_p), polydispersity index (PDI) for size distribution, and ζ potential determined by DLS from dilute dispersions in water (for unmodified MXenes and CTAB modified dl-MXene) or THF (for I@dl-MXenes).

Figure S5.1 Contact angle measurements on films of Ti3C2Tx MXene and I-MXene.